CHARACTERIZATION OF LSD COMPLEX FUNCTION, HISTONE EXCHANGE, AND REGULATION OF A TRYPTOPHAN CATABOLISM GENE PAIR IN *NEUROSPORA CRASSA*

by

WILLIAM K. STORCK

A DISSERTATION

Presented to the Department of Chemistry and Biochemistry
and the Graduate School of the University of Oregon
in partial fulfillment of the requirements
for the degree of
Doctor of Philosophy

March 2020

DISSERTATION APPROVAL PAGE

Student: William K. Storck

Title: Characterization of LSD Complex Function, Histone Exchange, and Regulation of a Tryptophan Catabolism Gene Pair in *Neurospora crassa*

This dissertation has been accepted and approved in partial fulfillment of the requirements for the Doctor of Philosophy degree in the Department of Chemistry and Biochemistry by:

Dr. Kenneth Prehoda	Chairperson
Dr. Eric Selker	Advisor
Dr. Bradley Nolen	Core Member
Dr. Kryn Stankunas	Institutional Representative

and

Kate Mondloch	Interim Vice Provost and Dean of the Graduate School

Original approval signatures are on file with the University of Oregon Graduate School.

Degree awarded March 2020

DISSERTATION ABSTRACT

William K. Storck

Doctor of Philosophy

Department of Chemistry and Biochemistry

March 2020

Title: Characterization of LSD Complex Function, Histone Exchange, and Regulation of a Tryptophan Catabolism Gene Pair in *Neurospora crassa*

Gene expression is regulated by a plethora of factors associated with chromatin, such as histone proteins. DNA can be methylated and histones can be marked with various chemical tags, which can influence expression of underlying DNA. Chromatin is organized into distinct domains: transcriptionally-active euchromatin and transcriptionally-silent heterochromatin. My dissertation involved investigating different aspects of chromatin regulation in the filamentous fungus *Neurospora crassa*.

I examined heterochromatin spreading in Neurospora mutants defective in lysine-specific demethylase 1 (LSD1). Loss of either LSD1 or its associated complex members, PHF1 or BDP-1, results in variable spreading of trimethylation of H3K9 (H3K9me3) and DNA methylation, and this spreading is dependent on DNA methylation, which is typically not involved in H3K9me3 establishment, and on the catalytic activity of the histone deacetylase complex, HCHC. Though there are gene expression changes present in Δ*lsd1* strains, these changes do not appear to be driven by spreading H3K9me3 and DNA methylation.

Though their relative positioning within chromatin appears to be regulated, histones are not static structures embedded within DNA, but are subject to constant

exchange. I characterized a light-inducible histone turnover reporter strain and used it to build a simple protocol for profiling DNA replication-independent histone turnover in Neurospora. I investigated how histone turnover correlates with gene expression, and observed similarities to other models in turnover profiles over genes. I also examined turnover at heterochromatin domains in heterochromatin mutants, which revealed that loss of H3K9me3 or its binder, HP1, or histone deacetylation by HCHC results in turnover increases.

Lastly, I investigated the regulation of a pair of genes involved in tryptophan catabolism, *kyn-1* and *iad-1*. I demonstrate that these genes are induced through the exposure of extracellular tryptophan. Though this locus is enriched for the conserved repressive mark, H3K27me3, loss of which does not appear to significantly affect the activity of this locus. Rather, I show that this locus is repressed by the H3K36 methyltransferase, ASH1, and chromatin remodelers, CRF4-1 and CRF6-1. Another H3K36 methyltransferase, SET-2, is required to overcome this repression.

This dissertation contains previously unpublished coauthored material.

CURRICULUM VITAE

NAME OF AUTHOR: William K. Storck

GRADUATE AND UNDERGRADUATE SCHOOLS ATTENDED:

University of Oregon, Eugene, Oregon
Western Michigan University, Kalamazoo, Michigan

DEGREES AWARDED:

Doctor of Philosophy, Chemistry, 2020, University of Oregon

Bachelor of Science, Chemistry, 2012, Western Michigan University

AREAS OF SPECIAL INTEREST:

Epigenetics
Chromatin Profiling
Genomics

PROFESSIONAL EXPERIENCE:

Graduate Student Researcher, Eric Selker Laboratory, University of Oregon, 2014-2020

Graduate Teaching Fellow, Department of Chemistry, University of Oregon, 2013-2015

Lab Purchasing & Library Assistant, Kalsec Inc., 2012-2013

Teaching Assistant, Western Michigan University, Department of Chemistry, 2010-2011

GRANTS, AWARDS, AND HONORS:

Genetics Training Grant, National Institutes of Health, 2015-2018

Summa cum Laude, Western Michigan University, 2012

PUBLICATIONS:

Storck, W.K., Bicocca, V.T., Rountree, M.R., Honda, S., Ormsby, T., and Selker, E.U. LSD1 prevents aberrant heterochromatin formation in *Neurospora crassa*. *Nucleic Acids Research. Submitted*

Storck, W.K., Bicocca, V.T., Rountree, M.R., and Selker, E.U. A light-inducible strain for genome-wide histone turnover profiling in *Neurospora crassa*. *In preparation*.

Klocko, A.D., Summers, C.A., Glover, M.L., Parrish, R., **Storck, W.K.**, McNaught, K.J., Moss, N., Gotting, K., Stewart, A., Morrison, A., Payne, L., Shiver, A., Hatakeyama, S., and Selker, E.U. Selection and characterization of mutants defective in DNA methylation in *Neurospora crassa*. *In preparation*.

ACKNOWLEDGMENTS

My sincerest and warmest thanks and appreciation to Dr. Eric Selker for the years of guidance and tutelage throughout my graduate career. I would also like to thank Drs. Andrew Klocko, Vincent Bicocca, and Jordan Gessaman for their mentorship in my formative years as well as the entire Selker Laboratory, both past and present, for fostering such a welcoming and conducive work environment and scientific community. I appreciate the advice and feedback provided by my dissertation advisory committee: Drs. Kenneth Prehoda, Kryn Stankunas, and Bradley Nolen. Finally, I would like to thank my family, who have been an unmovable pillar of support for me, and the friends I have made during my time in Eugene. I wish you all the best, with all my heart.

To my parents, Kurt and Kye, who are an everlasting source of love and comfort in my life, and to my brother, David, for all the laughs over the years.

TABLE OF CONTENTS

Chapter Page

Chapter Page

Chapter Page

LIST OF FIGURES

Figure Page

LIST OF TABLES

CHAPTER I

INTRODUCTION

Eukaryotes utilize histone proteins to package and organize extraordinary amounts of DNA into the relatively small volume of the nucleus. Two copies each of four different members of this protein family, H2A, H2B, H3, and H4, form a histone octamer complex. Approximately 146 base pairs of DNA is able to wrap around the histone octamer, creating a basic unit of chromatin called a nucleosome. Histones within nucleosomes possess long unstructured tails that are subject to various post-translational modifications. These modifications can reflect and/or influence the transcriptional state of the underlying DNA, and chromatin is segregated into distinct types, transcriptionally-active euchromatin or transcriptionally-silent heterochromatin, based on these histone marks[1].

Heterochromatin is typically considered to be a compacted "closed" form of chromatin that is refractory toward transcription and recombination, and is characterized by general hypoacetylation of histones H3 and H4, trimethylation of lysine 9 of histone H3 (H3K9me3), and cytosine methylation in DNA[1]. Heterochromatin also functions to prevent the deleterious activity of transposable elements and contributes to other cellular processes such as chromosome segregation[1]. Misregulation of heterochromatin has been implicated in human disease etiology, including cancer[2]. Thus, understanding how heterochromatin is regulated could be crucial towards therapeutic development.

The filamentous fungus *Neurospora crassa* is a well-suited model for studying heterochromatin. Easy to culture as well as genetically tractable, *N. crassa* possesses

heterochromatin features found in higher eukaryotes, such as DNA methylation, that are absent in other common model systems such as the budding yeast *Saccharomyces cerevisiae*, the fission yeast *Schizosaccharomyces pombe*, the fruit fly *Drosophila melanogaster*, and the round worm *Caenorhabditis elegans*[3]. *N. crassa* also features trimethylation of lysine 27 of histone H3 (H3K27me3), a conserved facultative heterochromatin mark that is absent in budding and fission yeasts[3], but essential for proper development in higher eukaryotes[4]. Furthermore, *N. crassa* has the added benefit in that DNA methylation, H3K9me3, H3K27me3 are all dispensable for viability, unlike other higher eukaryotes[4–10], facilitating loss-of-function studies.

This dissertation examines three different aspects of chromatin biology in *N. crassa* and includes previously unpublished co-authored material. Chapter II examines how constitutive heterochromatin is affected by the absence of a conserved histone demethylase, LSD1, and characterizes the resulting spreading of heterochromatin. Chapter III describes the validation of a histone turnover profiling strain of *N. crassa*. Using this strain, I examined histone turnover at constitutive heterochromatin domains in the absence of some heterochromatin-related factors and how level of histone turnover correlates at genes with respect to expression levels. Chapter IV describes work uncovering the regulation of a divergently-expressed gene pair involved in tryptophan catabolism marked with H3K27me3. This gene pair is normally silent, but is rapidly induced upon exposure to extracellular tryptophan.

CHAPTER II

LSD1 PREVENTS ABERRANT HETEROCHROMATIN FORMATION IN *NEUROSPORA CRASSA*

This work was performed in collaboration with Vincent Bicocca, Michael Rountree, Shinji Honda, and Tereza Ormsby. I generated most of *Neurospora crassa* strains in this study, performed all H3K9me3 ChIP-seq experiments, performed all qPCR experiments, performed all the Southern hybridizations, performed all linear growth rate assays, performed all western immunoblots, and carried out some of the bisulfite-seq experiments. Vincent Bicocca carried out some of the bisulfite-seq experiments, assisted in early exploratory experiments, and assisted in data analysis. Michael Rountree carried out some of the bisulfite-seq experiments. Shinji Honda conducted the protein purification and sample preparation for mass spectrometry, and carried out the yeast two-hybrid analyses. Tereza Ormsby performed the RNA-seq analysis. Eric Selker was the principal investigator for this work.

Introduction

One of the defining characteristics of heterochromatin is its capability to propagate along the chromosome, often guided through feedback of histone marks. Some "writers" of heterochromatin marks such as the H3K9-specific methyltransferase Clr4 of *S. pombe* and the mammalian H3K9 methyltransferase Suv39 are also "readers" capable of binding to their own mark, which in turn promotes further methylation on adjacent

nucleosomes[11,12]. If left unchecked, heterochromatin tends to "spread" into neighboring gene-rich euchromatin, with potentially negative consequences, such as down-regulation of important genes[1]. Thus, mechanisms to prevent inappropriate expansion of heterochromatin are necessary. Natural barriers include nucleosome-depleted regions[13,14], high levels of nucleosome turnover[15], and genetic elements such as tRNA genes[16,17]. In addition, factors antagonistic to the spreading of heterochromatin can be directed to the boundaries of heterochromatin domains. In *S. pombe*, the JmjC domain protein, Epe1, a putative H3K9 demethylase, localizes to the edges of heterochromatin in a Swi6/HP1-dependent manner[18]. Similarly in *N. crassa*, the JmjC domain protein, DMM-1, is part of a complex recruited to borders of some heterochromatin domains in an HP1-dependent manner, where it limits spreading presumably by demethylating trimethylation of lysine 9 of histone H3 (H3K9me3)[19].

Previous work has uncovered lysine-specific demethylase 1 (LSD1) as another important regulator of heterochromatin spreading, prompting us to examine its function in *N. crassa*. LSD1 is highly conserved in eukaryotes from yeasts to humans, and regulates heterochromatin propagation, apparently by removing mono- or di-methylation from either H3K4 or H3K9[20–23]. *S. pombe* has two LSD1 paralogs and two associated PHD-domain proteins, Phf1 and Phf2, whose specific functions have yet to be determined but are essential for viability. The LSD complexes in *S. pombe* appear to function as dedicated H3K9 demethylases, and localize to the edges of pericentromeric heterochromatin and promoters of certain genes, all of which display hyper H3K9 trimethylation when one or both of the LSD1 homologs are compromised[21]. The *Drosophila* homolog of LSD1, SU(VAR)3-3, plays an important role in promoting

heterochromatin formation during embryogenesis. *In vitro,* SU(VAR)3-3 was shown to eliminate the inhibitory effect of H3K4me1 or H3K4me2 on H3K9 methyltransferase activity of SU(VAR)3-9[22]. *In vivo,* SU(VAR)3-3 colocalizes with, and demethylates, H3K4me2 in inter-band regions, facilitating the formation of H3K9me-marked heterochromatin.

In humans, LSD1 appears to be able to act both as a transcriptional repressor and as an activator by removing mono- and di-methylation from either H3K4 or H3K9, depending on its binding partners or splicing isoforms[20,23]. LSD1 removes H3K4me2 from targeted promoters and is a member of the Co-REST complex, which functions to silence neuron-specific genes in non-neuronal cells[24]. LSD1 is also essential for proper neuron maturation and a neuron-specific isoform (LSD1+8a) possesses intrinsic demethylation activity towards H3K9 but not H3K4. LSD1+8a localizes to target genes during neuronal differentiation and removes H3K9me to promote transcription[23]. LSD1 was also found to associate with androgen receptor (AR) in androgen-sensitive tissues leading its recruitment to AR target genes and changing the specificity of LSD1 from H3K4 to H3K9, resulting in the loss of H3K9me and increased expression[20].

The fact that LSD1 homologs and isoforms have different roles in heterochromatin regulation in different organisms provided motivation for our investigation of the possible role of Neurospora's single LSD1 homolog in control of heterochromatin. Here we report the identification of the Neurospora LSD complex (LSDC), including an LSD1 homolog, a PHD-domain protein homologous to *S. pombe* Phf1, and the bromodomain protein, BDP-1. Loss of any LSDC members, or of LSD1 catalytic activity, increases heterochromatin spreading and results in the appearance of new heterochromatin loci

throughout the genome. The spreading is variable and dependent on the presence of DNA methylation as well as HCHC-catalyzed histone deacetylation. We conclude LSD1 functions to prevent heterochromatin expansion and to restrict heterochromatin to its normal chromosomal locations in Neurospora.

Results

Loss of LSD1 Results in Heterochromatin Spreading

As one approach to identify factors involved in regulating constitutive heterochromatin, we screened strains with knockouts of putative histone demethylases for defects in H3K9 methylation or DNA methylation. LSD1 was a likely candidate given previous studies on its function as a histone lysine demethylase, its importance in regulating heterochromatin in yeasts, flies, and humans, and its overall conservation in eukaryotes examined previously[20–23,25,26]. Neurospora possesses one gene, *NCU09120*, that is homologous to genes encoding LSD1 in other eukaryotes. The predicted Neurospora LSD1 contains the conserved **Swi**3p, **R**sc8p and **M**oira (SWIRM) and amine oxidase domains typical of LSD1 homologs, as well as a C-terminal HMG domain that is present in both *S. pombe* paralogs but absent in human LSD1 (Fig. 1).

In Neurospora, DNA methylation is directed to heterochromatin via trimethylation of lysine 9 on histone H3 (H3K9me3) and therefore can serve as a proxy for the presence of H3K9me3[5,27,28]. To test whether LSD1 plays a role in regulating heterochromatin in Neurospora, we performed whole genome bisulfite sequencing (WGBS) on DNA from an LSD1 knockout strain (FGSC# 11964)[29,30]. The Δ*lsd1* strain exhibited extensive

spreading of DNA methylation at select loci as well as the appearance of about 200 new regions of DNA methylation distributed throughout the genome (Fig. 2A and Fig. 3). The hypermethylation, whether expanding from a normal domain or in a new region, typically spread over 2-5 kb, with the largest hypermethylation spreading covering over 8 kb. The spreading did not preferentially affect specific genic elements (e.g. promoters); it appeared to indiscriminately cover chromatin in a contiguous manner (Fig. 2A and Fig. 3). Despite extensive spreading of DNA methylation, total H3K9me3 levels in the Δ*lsd1* strain appeared similar to wild type by western blot analysis (Fig. 4, right), implying Δ*lsd1*-dependent spreading of H3K9me3 has a negligible effect on bulk histones.

Identification of Members of the Neurospora LSD Complex

To identify potential LSD1 complex (LSDC) members in Neurospora, we generated strains with C-terminal 3xFLAG-tagged LSD1 expressed at its endogenous locus, immuno-purified the bait and associated proteins, and analyzed the material by mass spectrometry. We identified peptides covering 46% of a PHD finger domain-containing protein previously identified in *S. pombe* as an LSD complex member called PHF1 (*PH*D *F*inger 1)[21] and 13% of a bromodomain-containing protein named BDP-1 (*B*romo*d*omain *P*rotein 1) (Table 1). A reciprocal pull-down with PHF1-3xFLAG yielded peptides covering 42.1% of LSD1 and 15% of BDP-1, supporting its interaction with LSD1 and BDP-1 (Table 2). Immunoprecipitation of BDP-1-3xFLAG did not yield LSD1 or PHF1 peptides, however (Table 3). To further test these interactions, we performed co-immunoprecipitation experiments in strains with PHF1-3xFLAG or BDP-1-3xFLAG, and LSD1-HA, in which we immunoprecipitated the FLAG-tagged protein and then assayed

both epitopes by western blotting. Consistent with the mass spectrometric analyses, PHF1-3xFLAG readily pulled down LSD1-HA, but BDP-1-3xFLAG did not (Fig. 5A). To examine further the potential interaction between LSDC members, we utilized yeast two-hybrid assays. We observed no interaction between LSD1 and PHF1 or LSD1 and BDP-1, potentially resulting from disruptions from the tag moieties. However, bait constructs containing either the N-terminus (amino acids and 2 to 140) or the C-terminus (amino acids 401 to 605) in front of or behind the PHF1 PHD domain with full length BDP-1 as prey allowed for growth on selection nutritional medium. We also examined potential interaction of full length PHF1 with BDP-1 fragments. BDP-1 fragments containing the N-terminal BTB domain (amino acids 45 to 236) but not the C-terminal Bromo domain (amino acids 198 to 480) supported growth, suggesting it may be important for stable interaction with the rest of the complex (Fig. 5B). Altogether, these results indicate PHF1 and BDP-1 directly interact. We conclude LSDC in *N. crassa* includes LSD1, PHF1, and BDP-1 (Fig. 2B).

To investigate whether strains with knockout mutations for members of LSDC exhibit a phenotype similar to that of Δ*lsd1,* we digested genomic DNA from knockout strains for the complex members with the 5-methylcytosine-sensitive restriction endonuclease AvaII, and performed Southern hybridizations probing for regions that we found hypermethylated in the Δ*lsd1* strain. We found that knockouts of all three members exhibited more high-molecular mass bands than the wild-type control, with Δ*phf1* and Δ*bdp-1* phenocopying Δ*lsd1* (Fig. 2C). These results support the idea that LSD1, PHF1, and BDP-1 form a complex and function in the same pathway.

Variability of DNA Hypermethylation in LSDC Knockout Strains

Curiously, we found that Δ*lsd1* siblings from sexual crosses exhibited different extents of DNA hypermethylation. Similarly, independently generated Δ*lsd1* knockout strains also exhibited variable DNA hypermethylation. This phenotype was also observed with Δ*phf1* and Δ*bdp-1* siblings as well as independently generated knockouts of these genes (Fig. 2C). In contrast, normally methylated regions exhibit consistent levels of DNA methylation in wild-type strains. The variable nature of Δ*lsd1* hypermethylation is not consistent genome-wide as some strains exhibit less hypermethylation at some loci and more hypermethylation at others (Fig. 6A; Fig. 7A). Double knockouts of any combination between the three complex members did not present an additive phenotype, but rather one similar to a Δ*lsd1* or Δ*phf1* single knockout (Fig. 7B), further supporting the hypothesis that LSD1, PHF1, and BDP-1 function in the same pathway by forming the LSDC.

To test whether variability of hypermethylation also occurred in asexually propagated strains, we isolated and tested strains generated from microconidia, which are generally mononucleate[31] unlike macroconidia, which possess multiple, potentially variably hypermethylated nuclei. Results of Southern hybridizations on genomic DNA digested with AvaII showed that the asexually-propagated isolates also exhibited variable levels of DNA hypermethylation, and that further propagation continued to yield isolates with variable hypermethylation (Fig. 6A and Fig. 7A). Replicate WGBS experiments with the same isolate revealed slight differences at hypermethylated regions. Perhaps not surprisingly, less variability was observed in a strain propagated with a bulk transfer of macroconidia (Fig. 7A).

We were curious whether variably hypermethylated Δ*lsd1* strains would show other variable phenotypes. In *S. pombe*, deletion of *lsd1* results in reduced growth rate and *lsd2* is essential for viability, highlighting the importance of these two enzymes[21]. To test the importance of each identified member of LSDC for Neurospora growth, we measured the linear growth rates of two independent knockouts of each complex member with "race tubes". All knockouts exhibited a modest reduction in growth rate (Fig. 6B). We then assayed the growth rate of the single-microconidium-propagated strains illustrated in Figure 6A by race tubes, in triplicate. Most of the strains grew at a slightly slower rate than wild type, though two grew at a much slower rate (Fig. 6C, strains 1 and 7). All the single-microconidium-propagated stains exhibited greater variance in growth rates between the replicates than wild type. It did not appear that the slower growing isolates exhibited noticeably higher degrees of hypermethylation than the faster growing isolates (Fig. 6A and Fig. 7A).

Δ*lsd1* Strains Exhibit DNA Methylation-Dependent Spreading of H3K9me3

In Neurospora, the establishment of DNA methylation at constitutive heterochromatin is dependent on the presence of H3K9me3, while H3K9me3 establishment is independent of DNA methylation[5,27,28]. However, loss of the heterochromatin limiting complex DMM results in DNA methylation-dependent spreading of H3K9me3 at some heterochromatin boundaries[19]. We therefore tested if the heterochromatin spreading resulting from loss of LSD1 is also dependent on DNA methylation. As a first step to explore the relationship of DNA methylation and H3K9 methylation in abnormal heterochromatin formed in the absence of LSD1, we performed

H3K9me3 chromatin immunoprecipitation followed by high-throughput DNA sequencing (ChIP-seq) to test for concomitant spreading of H3K9me3 with DNA methylation in a Δ*lsd1* strain. As expected, we observed H3K9 hypermethylation concomitant with DNA hypermethylation in the Δ*lsd1* strain (Fig. 8A). These results were confirmed in triplicate ChIP-qPCR experiments, which showed increased levels of H3K9me3 at Δ*lsd1*-sensitive loci (Fig. 9).

We next investigated whether Δ*lsd1*-induced spreading of H3K9me3 is dependent on DIM-2, as in *dmm* strains[19]. To do so, we performed H3K9me3 ChIP-seq on a Δ*lsd1; Δdim-2* strain as well as a strain with catalytically inactive DIM-2 (*dim-2*^{C926A})[32] in a Δ*lsd1* background. In both cases, the H3K9me3 spreading observed in Δ*lsd1* single knockouts was absent; instead, the distribution of H3K9me3 was equivalent to the distribution in *lsd1*$^{+}$ strains (Fig. 8A; confirmation by ChIP-qPCR presented in Fig. 9). This indicates that the abnormal H3K9me3 found in Δ*lsd1* strains depends on DNA methylation, like in DMM mutants and at disiRNA locus DNA methylation (DLDM) regions[19,33], in contrast to native constitutive heterochromatin domains.

Because loss of DNA methylation rescued the heterochromatin spreading phenotype observed in Δ*lsd1*, we asked if the reduction in growth rate observed in LSDC knockout strains would also be affected. Curiously, triplicate growth assays of Δ*lsd1; Δdim-2* and Δ*lsd1; dim-2*^{C926A} strains showed that both strains were actually slower than wild-type and Δ*lsd1* single knockout strains (Fig. 8B). This contrasts the situation with DMM mutants where loss of *dim-2* rescues the growth defect phenotype of Δ*dmm-1* strains, and was surprising given the modest growth defects observed in Δ*lsd1* and Δ*dim-2* single knockout strains[27].

Considering that LSD1 is a presumptive H3K9 demethylase, it was of interest to test if mutation of conserved residues of the putative catalytic domain would result in DNA hypermethylation, as in Δ*lsd1* strains. We therefore constructed a presumptive catalytic null 3xFLAG-tagged LSD1 strain by mutating a conserved lysine thought to be critical for catalytic activity in such proteins (Fig. 8C)[34]. Results of Southern hybridizations showed that wild-type 3xFLAG-tagged LSD1 strains had a modest hypermethylation phenotype (Fig. 10) while the presumptive catalytic null strains exhibited hypermethylation equivalent to that of the Δ*lsd1* strains. Given the role of H3K9 methylation in establishment of DNA methylation and the highly conserved nature of the LSD1 protein, these data support a model in which the H3K9 demethylase activity of LSDC is required to prevent heterochromatin spreading (Fig. 8C)[20,21,23].

H3K9me1 persists in Δ*dim-5* strains

The catalytic mechanism of LSD1 is thought to restrict it to demethylating mono- or di-methylated lysines; trimethylated residues should not be susceptible[24]. Since the principle form of histone methylation associated with constitutive heterochromatin in Neurospora is H3K9me3, it is not obvious how LSD1 affects heterochromatin spreading. Although ChIP-seq and western blotting experiments have not revealed H3K9me2 in Neurospora[5], low levels of this modification were detected by mass spectroscopy[35], consistent with the possibility that this could be a substrate for LSD1. Mass spectroscopy of Neurospora H3 also revealed H3K9me1, even though this modification has also not been detected by ChIP[35]. We obtained signal for H3K9me1 in western blots (Fig. 4, left panel) but curiously, nearly identical levels of H3K9me1 signals were found in wild-type,

Δ*lsd1*, and Δ*dim-5* strains, whereas control cell lysate from *S. cerevisiae,* which is thought to have no H3K9 methylation[36] did not yield a signal. These findings raised the possibility of an unknown H3K9 methyltransferase in Neurospora.

In an attempt to identify the hypothetical methyltransferase responsible for H3K9me1, we screened knockouts of every predicted SET domain protein as well as homologs of non-SET domain lysine methyltransferases, all in a Δ*dim-5* background. The apparent H3K9me1 signal persisted in every strain tested (for complete list of screened KOs, see Table 4). These findings are comparable to observations in *S. pombe clr4*Δ strains[37] and leave open the possibility of an unrecognized H3K9 methyltransferase in *N. crassa*.

Gene Expression in the Presence of H3K9me3 and DNA Methylation

Constitutive heterochromatin, such as that resulting from RIP operating on duplicated sequences, has been shown to cause gene silencing in Neurospora[38], at least in part because DNA methylation can inhibit transcriptional elongation[39]. Prior work also showed that heterochromatin spreading into neighboring euchromatin in Neurospora strains deficient for DMM causes down-regulation of underlying genes[19]. Considering that Δ*lsd1* strains also show spreading of heterochromatin over gene-rich euchromatin, we wished to test if this is associated with silencing. We therefore performed poly-A^+ RNA-seq on wild-type and Δ*lsd1* strains and compared their expression profiles. Setting a 4-fold difference threshold, we identified 118 downregulated and 17 upregulated genes in the Δ*lsd1* strain. Curiously, only five of the downregulated genes and none of the upregulated genes were observed to be hypermethylated, as assayed by WGBS of the

same Δ*lsd1* strain used in the RNA-seq analysis (Tables 5 and 6). To test directly whether Δ*lsd*1-induced hypermethylation silences genes, we examined four hypermethylated genes by RT-qPCR. All four genes (NCU00911: polysaccharide synthase, *cps-1*; NCU02455: FKBP-type peptidyl-prolyl cis-trans isomerase, *fkr-5*; NCU06512: methionine synthase, *met-8*; and NCU02437: histone H2A, *hH2A*) are within the top expression quartile in wild type. Surprisingly, no significant change in expression was detected for any of the four genes (Fig. 11), indicating that the spreading of H3K9me3 and DNA methylation resulting from the deletion of *lsd1* was insufficient to silence underlying sequences. This result also suggests that the observed expression changes in Δ*lsd1* are due to a LSD1 function besides its role regulating heterochromatin spreading. This finding is consistent with our observations that Δ*lsd1* strains are "healthier" than Δ*dmm-1* strains and that growth of Δ*lsd1* strains is not improved by loss of DNA methylation, unlike the case for *dmm* mutants[19].

Spreading of Heterochromatin in Δ*lsd1* Strains is Dependent on HCHC

The HCHC histone deacetylase complex is involved in promoting some heterochromatin spreading in Neurospora[40,41], and similarly in *S. pombe*, spreading requires the recruitment of the histone deacetylase (HDAC) Clr3[42,43]. We noticed considerable overlap (~55%) between regions that lose DNA methylation in HCHC-defective strains and those that gain DNA methylation in Δ*lsd1* strains (Fig. 12A). Moreover, previous findings with tethered heterochromatin components demonstrated the importance of HCHC activity in nucleation of ectopic DNA methylation[44]. We therefore tested whether HCHC catalytic activity is involved in Δ*lsd1*-induced heterochromatin

spreading. To do so, we generated Δ*lsd1* strains with catalytic null alleles of *hda-1* (*hda-1*^{D263N}), the catalytic subunit of HCHC[41], and performed DNA methylation-sensitive Southern hybridizations probing for Δ*lsd1*-sensitive regions. We observed loss of DNA methylation in *hda-1*^{D263N} at these regions to levels even below that of a wild-type strain, and the level of DNA methylation in Δ*lsd1; hda-1*^{D263N} strains was identical to that in the *hda-1*^{D263N} strain (Fig. 12B), suggesting that histone deacetylation by HCHC is necessary for Δ*lsd1*-induced hypermethylation.

DCDC Localization at Δ*lsd1*-Sensitive Regions

Because Δ*lsd1* strains exhibit increased levels of H3K9me3 at affected loci, it was of interest to determine if DCDC, the complex responsible for H3K9me3 in Neurospora[5], is enriched at these loci, even in a wild-type strain. DCDC localization has been successfully assessed by DamID but not ChIP[45,46]. A fusion of the *Escherichia coli* adenine methyltransferase (Dam) with DIM-5, resulted in specific methylation of adenines as detected by digestion with DpnI, which cuts GATC sites containing methylated adenines, followed by Southern hybridizations[45]. The Dam tag partially compromises DCDC activity, but DIM-5-Dam still localizes to normal regions of constitutive heterochromatin[40,46]. Although the partial loss of DIM-5 catalytic activity by the Dam tag prevents Δ*lsd1*-induced hypermethylation, robust digestion was observed in wild-type backgrounds, to the point of producing fully digested DpnI products, suggesting that DCDC localizes over Δ*lsd1*-sensitive loci; generic euchromatic loci only yielded modest levels of digestion (Fig. 13). These results suggest that DCDC is poised on regions that are subject to hypermethylation.

Discussion

LSDC-Mediated Demethylation in Neurospora

In Neurospora, H3K9me3 is the predominant form of H3K9 methylation associated with constitutive heterochromatin, presumably resulting from processive addition of methyl groups by DIM-5, which is thought to be responsible for all H3K9 methylation in Neurospora[5,46,47]. As LSD1 is thought to be only able to act on mono- or di-methylated substrates[24], it is puzzling how LSD1 affects heterochromatin spreading. It is notable that in *S. pombe*, loss of LSD1 catalytic activity results in a larger increase of H3K9me3 than H3K9me2, suggesting that LSD1 functions to balance the levels of these two marks[21]. Potentially, LSD1 actively removes H3K9me concurrently as it is catalyzed by DCDC, actively countering establishment of the mark at susceptible chromatin before it is trimethylated and "locked into place" by virtue of no longer being a substrate of LSD1. Other, not necessarily mutually exclusive, possibilities are that H3K9me is catalyzed by DIM-5 and an additional, hypothetical histone methyltransferase that catalyzes mono- or di-methylation of H3K9 (Fig. 14B), or that LSDC cooperates with a JmjC domain protein, which demethylates mono-, di-, and trimethylated lysines[48], in order to limit heterochromatin spreading. Neurospora LSD1 could also regulate heterochromatin through the direct demethylation of heterochromatin machinery proteins themselves. LSD1 has been shown to promote DNA methylation genome-wide in mouse embryonic stem cells by demethylating the maintenance DNA methyltransferase, Dmnt1, resulting in increased protein stability[26].

Though the exact mechanism of LSDC recruitment is unknown, it seems likely both PHD1 and BDP-1 play important roles as PHD and bromo domains are known readers of histone modifications, binding to lysine acetylation and methylation, respectively. These domains were also dispensable to support growth in our yeast two-hybrid assays, consistent with the possibility that they fulfill other roles outside of association (Fig. 7B)[49]. It is possible the SWIRM domain of LSD1 itself assists in localization as well. SWIRM domains are present in many chromatin remodeling or histone modifying proteins and have been shown to bind double-stranded DNA and dinucleosomes *in vitro*[50].

H3K9me1 in Neurospora

In *S. pombe*, H3K9me1 persists in *clr4*Δ strains, suggesting there is an additional enzyme catalyzing H3K9me[37]. We too observed, by western blotting, the persistence of H3K9me1 in Δ*dim-5* strains (Fig. 4, left). Consistent with this observation, a previous middle-down hybrid chromatography/tandem mass spectrometry (LC-MS/MS) analysis of wild-type Neurospora histones detected both H3K9me1 and H3K9me3[35]. Despite screening through knockouts strains for all SET domain proteins as well as non-SET domain lysine methyltransferases, all in a Δ*dim-5* background, we have yet to identify a hypothetical methyltransferase (for complete list of screened KOs, see Table 4). H3K9me1-specific histone methyltransferases have been previously shown to be critical for heterochromatin regulation. Indeed, work by Pinheiro and colleagues revealed the importance of H3K9me1 in heterochromatin establishment and integrity in mammals, where cytoplasmic hH3 is marked with H3K9me1 by the redundant H3K9me1-specific

methyltransferases Prdm3 & Prdm16[51]. Knock-downs of these enzymes prevent Suv39h-dependent H3K9me3 and induce the disintegration of heterochromatin foci that are largely maintained after loss of H3K9me3 in *Suv39h* and *Suv39h/Eset* knock-down experiments[51]. Neurospora does not show homologs of Prdm3 or Prdm16, but the observation of only modest Hi-C pattern changes in Δ*dim-5* strains, suggests that H3K9me3 is mostly dispensable for proper maintenance of genomic architecture[52]. Conceivably, H3K9me1 is more important for maintaining proper chromatin conformation in Neurospora, as it appears to be in mammalian contexts.

Variable Heterochromatin Spreading in Neurospora

The variable spreading of heterochromatin displayed by LSDC mutants is particularly interesting. Although enigmatic, it is reminiscent of the variability seen in classic "position-effect variegation" (PEV), first discovered in flies showing mottled eye color due to chromosomal rearrangements with breakpoints within heterochromatin[53]. Interestingly, PEV is partly alleviated by adding extra heterochromatin, e.g. in the form of additional Y chromosomes, consistent with the possibility that heterochromatin machinery can be "titrated away" by additional substrate[54]. This suggests spreading is partially driven by a "surplus" of heterochromatin elements, providing a need for regulation by factors such as LSD1[1].

LSDC might remove H3K9me at the edges of heterochromatin domains or in other regions susceptible to aberrant heterochromatin formation, potentially creating a local chromatin environment less conducive for heterochromatin establishment and spreading, leaving the heterochromatin machinery sequestered at its normal regions. In the absence

of LSD1, competition for factors might result between regions as heterochromatin reinforces itself via feedback mechanisms, stochastically leading to greater spreading at some regions than others, i.e. the observed variability. During the reestablishment of heterochromatin throughout cell divisions, this unstable balance of machinery may be tipped towards other, less methylated Δ*lsd1*-sensitive regions, and titrate away machinery from previously hypermethylated regions, causing the observed shifts in spreading throughout the genome.

DNA Methylation-Dependent H3K9me3

Our studies provide a new example of DNA methylation-dependent H3K9me3, which is uncommon in Neurospora[19,33]. We note that the DNA methylation-dependent H3K9me3 resulting from defects in LSDC, as well as that previously discovered associated with *dmm* mutants and at DLDM loci, occurs in chromatin with a higher GC-content than in natural constitutive heterochromatin, which is largely comprised of AT-rich relics of transposons altered by RIP[28,55]. Indeed, it appears that as heterochromatin spreads outside of the normal boundaries of heterochromatin associated with AT-rich DNA, additional heterochromatin-associated factors become necessary for propagation across chromatin. In wild-type Neurospora, both the H3K9 methyltransferase complex, DCDC, and the HDAC complex, HCHC, are recruited to AT-rich heterochromatin regions, where the respective activities of these complexes are able to further reinforce the recruitment of the other[40,41,44,46]. In HCHC mutants, DCDC is still recruited to heterochromatin via AT-rich DNA, but in the absence of HCHC activity, heterochromatin fails to spread out to the boundaries of these domains, which show

steeply decreasing AT-richness[41] (Fig. 14A, 14B left). HCHC can be directed to heterochromatin through the AT-hook domains of the CHAP subunit, as well as through binding of HP1 to H3K9me3, and subsequent deacetylation is able to recruit DCDC-mediated methylation, leading to further establishment of H3K9me3[44] (Fig. 14B middle). Through feedback between the respective activities of these two complexes, heterochromatin is able to propagate across domains. Interestingly, only in contexts where heterochromatin forms or spreads over non-RIP'd DNA in which the base composition is neutral (i.e. ~50%), such as in LSDC mutants, *dmm* mutants[19], and at DLDM loci[33], is DNA methylation required for H3K9me3 (Fig. 14B right). While the possible requirement of HCHC activity for spreading in a DMM mutant or for DLDM has not been tested, this would be consistent with what we found for Δ*lsd1*-induced heterochromatin spreading. In a study examining the sufficiency of tethered heterochromatin factors to induce H3K9 and DNA methylation at a euchromatic locus, it was observed that loss of DNA methylation resulted in ~50% less induced H3K9me3 with tethered HP1[44]. It is possible DNA methylation assists the localization of other heterochromatin machinery or contributes to a more conducive environment for its activity. How DNA methylation affects heterochromatin propagation remains unclear, however. No DNA methylation-binding factor that affects heterochromatin has been yet identified in Neurospora[5,27,28].

Concluding Remarks

Our investigation of LSD1 provides further evidence of its function as a regulator of heterochromatin and describes an example of variable heterochromatin spreading in *N.*

crassa. Though the target substrate of LSDC in Neurospora remains uncertain, our results indicate that LSD1 functions to prevent HCHC-driven heterochromatin expansion. Our data and previous studies on *S. pombe* suggest fungal LSD1 functions to limit heterochromatin spreading[21], contrasting with studies from mammalian models, which show LSD1 can promote or antagonize heterochromatin depending on splicing isoforms or associated factors. In the future, it would be of interest to investigate thoroughly the individual contributions of PHF1 and BDP-1 in LSDC function. Altogether, our results are in line with the conserved role of LSD1 and provide further insight on regulation of heterochromatin.

Materials and Methods

N. crassa Strains and General Methods

All *N. crassa* strains and primers used in this study are listed in Appendices C and D, respectively. Strains were cultured, crossed, and maintained according to standard procedures[56]. Linear growth was assayed with "race tubes" at 32˚C[57], except 25-mL plastic serological pipets (89130-912; VWR) were used instead of glass tubes. Deletion strains were obtained from the Neurospora knockout collection[29] or made by replacing the indicated gene with the *nat-1* marker as previously described[58]. Epitope-tagged strains were built as previously described[58].

Generation of 3xFLAG-Tagged Catalytic Null LSD1 Strain

To generate a catalytic mutant of LSD1 tagged with 3xFLAG, we amplified the

middle of the *lsd1* gene (NCU09120) with genomic DNA from strain N3752 using primers 6716 and 6717 to make a fragment with a 3' overhang harboring the target mutation and using primers 6718 and 6720 to generate a fragment with a 5' overhang harboring the target mutation and a 3' overhang complementary to the 10xGlycine linker sequence of plasmid *pZero::3×FLAG::nat-1::loxP*. These two fragments were then combined by "stitching-PCR". The 3' UTR region of *lsd1* was amplified using primers 6721 and 6722 to generate a fragment with a 5' overhang to the *loxP* site of *pZero::3×FLAG::nat-1::loxP*. The combined fragment bearing the target mutation and the *3xFLAG::nat-1* cassette was PCR-stitched using primers 6716 and 4883 to create a 5' split marker construct as described[59]. The 3' UTR fragment and the *3xFLAG::nat-1* cassette were PCR-stitched using primers 4884 and 6722 to create a 3' split marker construct as described[59]. These fragments were simultaneously transformed into strain N2930 and *nat-1*$^{+}$ transformants were verified by Southern hybridizations and crossed to strain N625 to generate homokaryotic progeny.

Nucleic Acid Manipulations and Molecular Analysis

DNA isolation, Southern hybridization, co-IP, western blotting and IP/MS analyses were performed as previously described[19,27,40,45,46]. DNA for methylation-sensitive Southern hybridizations was digested with AvaII unless noted otherwise. The following antibodies were used: anti-FLAG-HRP (A8592; Sigma), anti-HA (M180-3; MBL), anti-H3K9me1 (CS-065-100; Diagenode), and anti-hH3 (ab1791; Abcam). Co-IP experiments used anti-FLAG conjugated to agarose beads (A2220; Millipore). Secondary antibodies were used as previously described[27]. Chemiluminescence resulting from the

treatment with SuperSignal West Femto Substrate (34095; Thermo Fisher Scientific) for anti-FLAG-HRP, anti-HA, anti-H3K9me1, and anti-hH3 was imaged using a LI-COR Odyssey Fc imaging system. Yeast two-hybrid strains and assays were built and carried out as previously described[27].

ChIP-qPCR

ChIP was performed as previously indicated[35] using anti-H3K9me3 (39161; Active Motif). For quantitative ChIP, real-time qPCR experiments on independent experimental replicates were performed in triplicate using PerfeCTa SYBR Green Fastmix ROX (Quantabio) with the listed primers (Table S8) and were analyzed using a StepOnePlus Real-Time PCR system (Life Technologies). Relative enrichment of each modification was determined by measuring enrichment as a percent of the total input. The enrichment of the indicated loci was then scaled to relative enrichment at *hH4*.

ChIP-seq

H3K9me3 ChIP samples were prepared for sequencing as previously described[35]. Sequencing was performed using an Illumina NextSeq 500 using single-end 75 nucleotide reads or using an Illumina HiSeq 4000 using single-end 100 nucleotide reads. Manipulations of the sequencing data were performed on the Galaxy platform[60]. All sequences were mapped to the corrected *N. crassa* OR74A (NC12) genome[52] using Bowtie2[61]. For visualization, the mapped read enrichment was calculated over 25 bp bins and normalized by RPKM using bamCoverage from deepTools[62]. The sequencing tracks are displayed as 25-nt window bigWig files with the Integrative Genomics Viewer

(IGV)[63].

Bisulfite-seq

Bisulfite-sequencing sample preparation was performed using the NEBNext Ultra DNA Library Prep Kit for Illumina (E7370; NEB) and the EpiMark Bisulfite Conversion Kit (E3318; NEB). Data acquisition and processing were performed as previously described[59]. To display the bisulfite-sequencing data, the average 5mC level was calculated for 25 bp windows across the genome using the MethPipe program[64]. The resulting wig files were displayed on IGV.

RNA-seq

RNA-sequencing, data processing, and analyses were performed as previously described[65]. For qRT-PCR analyses, RNA from biological triplicates was isolated as previously described[39]. Equal levels of Qubit-RNA (Life Technologies) assayed RNA were DNase-treated (Invitrogen), and cDNA was synthesized using the Superscript III kit (Life Technologies) according to the manufacturer's protocol. 1:10 diluted cDNA was used for qRT-PCR experiments with PerfeCTa SYBR Green Fastmix ROX (Quantabio) and listed primers (Table S8), and were analyzed using a StepOnePlus Real-Time PCR system (Life Technologies). Enrichment for each gene was normalized to enrichment of the housekeeping gene *rpt-1* (NCU02840, primers 6271/6272; Table S8)[66].

DamID

Dam-ID was performed as previously described[45,67]. Briefly, genomic DNA of

indicated strains were incubated with or without DpnI, which cuts adenine-methylated GATC sites. Genomic DNA was also digested with the 5mC-insensitive isoschizomer DpnII for each strain as a control for complete digestion. Digested DNA was analyzed by Southern hybridizations with probes for the designated loci.

Bridge to Chapter III

During the time I performed the work for Chapter II, I also worked on a separate project characterizing a histone turnover reporter strain built by Michael Rountree and Vincent Bicocca. I built histone turnover reporter strains in heterochromatin mutant backgrounds and investigated how histone turnover at heterochromatin domains was affected. I also used the reporter strain to examine differences in histone turnover at Neurospora genes with respect to expression level.

CHAPTER III

A LIGHT INDUCIBLE STRAIN FOR GENOMIC-WIDE HISTONE TURNOVER PROFILING IN *NEUROSPORA CRASSA*

This work was performed in collaboration with Michael Rountree and Vincent Bicocca. I generated all homokaryotic strains used in this study. I performed western immunoblotting analysis characterizing the expression kinetics of the light-inducible 3xFLAG-tagged histone H3 used to profile histone turnover. I codeveloped the protocol for histone turnover profiling with Vincent Bicocca. I performed all ChIP experiments, all qPCR analyses, and all histone turnover meta-analyses. Vincent Bicocca designed the codon-optimized histone H3 gene plasmid and generated the primary transformants of the histone turnover strain. Michael Rountree built the plasmid used to place the histone H3 gene under the control of the *vvd* promoter, tag with 3xFLAG, and target to the *his-3* locus.

Introduction

Although the positions of nucleosomes within chromatin are typically regulated, histones are not static; they show significant and variable exchange[68]. Moreover, histone exchange can be independent of DNA replication, and higher rates of histone turnover are correlated with gene expression[68]. Histone turnover has implications with regard to chromatin regulation. High levels of turnover allow for greater accessibility to DNA for transcriptional machinery such as transcription factors and RNA polymerases, and is

important for regulating levels and distributions of histone marks and variants[68]. Histone turnover may also play a role as boundary elements to contain heterochromatin spreading[1]. Heterochromatin is generally thought of as a tightly compacted form of chromatin, rendering its DNA inaccessible to transcriptional factors and suppressing the deleterious activity of selfish genetic elements[1]. Consistent with this view, heterochromatin has been found to be refractory towards histone exchange, and disruption of heterochromatin leads to increases in turnover[15,69]. As such, suppression of histone turnover appears to be a feature of heterochromatin and likely contributes to its function and epigenetic inheritance.

In metazoans, replication-independent histone turnover such as during transcription causes the replacement of hH3.1 deposited during DNA replication with the closely related histone variant, hH3.3. This continual exchange is thought to assist in exposing DNA binding sites, and is crucial for development[68]. Some investigations of histone turnover have been performed in the yeasts *S. cerevisiae* and *S. pombe*, which offer a simpler complement of histone proteins; yeasts have only one isoform of hH3, a homolog of the histone variant hH3.3[68]. Like yeasts, the filamentous fungus *Neurospora crassa* possesses only one histone H3 isoform, which is also homologous to metazoan hH3.3. However, Neurospora possesses chromatin features more analogous to higher eukaryotes in complexity. For example, Neurospora possesses two dedicated methyltransferases for lysine 36 on histone H3 (H3K36), the methylation of which is implicated in regulating histone exchange in the wake of Pol II during its passage over gene bodies, while yeasts have only one[65]. Neurospora also sports DNA methylation at constitutive heterochromatin as well as the conserved facultative heterochromatin mark,

methylation of lysine 27 of histone H3 (H3K27me), both of which are absent in yeasts[3].

Here we report the construction and validation of a histone turnover reporter strain of *N. crassa*. Our strain utilizes 3xFLAG-tagged histone H3 under the control of a light-inducible promoter. Inducible tagged histones have been successfully used in the past to assay histone exchange in other models, but these systems have required the addition of an inducing agent - often through a change of growth medium - and a lengthy incubation period, typically on the order of hours[15,69–73]. Our reporter strain has the advantages of using light as the inducing signal, which is less disruptive than a change of medium and provides greater control, as well as a much more rapid induction. We have used our reporter system to initiate explorations of possible effects on histone turnover at heterochromatin domains resulting from loss of elements of heterochromatin machinery.

Results and Discussion

Expression of *hH3-3xFLAG* Under the Control of the *vvd* Promoter

In order to assay histone turnover genome-wide in Neurospora, we constructed a strain expressing 3xFLAG-tagged histone H3 at the *his-3* locus, regulated by the *vvd* promoter (Fig. 15A). *N. crassa* possesses a well-characterized circadian rhythm, and over 5% of its genes are expressed in response to light exposure[74]. The *vvd* promoter allows for light-inducible expression of genes; in dark conditions, *vvd* is weakly expressed but is rapidly induced by up to 300-fold within minutes of light exposure[75,76]. Indeed, the *vvd* promoter has already been successfully utilized for the inducible and tunable control of gene expression[77]. Since complete histone eviction requires the prior removal of H2A-

H2B dimers, and the H3-H4 tetramer is incorporated into chromatin prior to other histone proteins, the incorporation of H3-3xFLAG should represent turnover of the entire nucleosome[78].

To confirm light-inducible expression of H3-3xFLAG and to characterize its expression dynamics post induction, we grew cultures of the reporter strain in complete darkness for 18 hours, exposed them to a short period (two minutes) of blue light (465 nm; 30 μmole photons/m^2/s), and assessed H3-3xFLAG expression by immunoblotting in a time course experiment (Fig. 15B). Consistent with previous characterization of gene expression controlled by the *vvd* promoter, we observed a low basal level of H3-3xFLAG expression at the pre-induction time point (Fig. 15B, DD). By 20 minutes there was a marked accumulation of H3-3xFLAG, which appeared to culminate by 40 minutes (Fig. 15B). This level of H3-3xFLAG persisted for at least two hours after induction. As each slant used to inoculate the darkroom cultures was grown in light, it stands to reason that P_{vvd}*:hH3-3xFLAG* was active at the start of the incubation period. The low level of H3-3xFLAG observed in the uninduced strains suggests that high levels brought on by light induction is effectively reduced to this low basal level within 18 hours.

H3-3xFLAG is Incorporated into Chromatin

To verify incorporation of light-induced H3-3xFLAG into chromatin, we attempted to immunoprecipitate formaldehyde cross-linked FLAG-tagged histones after different periods of histone incorporation, and tested for association with DNA by quantitative PCR (qPCR). We expected that longer incorporation times would give greater enrichment of immunoprecipitated chromatin. To assess whether FLAG-tagged

histones are effectively incorporated in a replication-independent manner, we blocked DNA replication by treatment with hydroxyurea (HU)[79]. Cultures were spiked with 100 mM HU and incubated for three hours, a regimen previously shown to effectively arrest replication without compromising viability[79]. Strains were then exposed to a two-minute light pulse to induce H3-3xFLAG expression, and incubated for 20 minutes or two hours to allow for incorporation of FLAG-tagged histones before cross-linking, chromatin shearing, immunoprecipitation, and isolation of associated DNA (Fig. 16).

We performed qPCR using primers for different chromatin contexts: active genes (*actin*, *fkr-5*, and *csr-1*), constitutive heterochromatin (Cen IIIL, 8:A6, and 8:F10), and facultative heterochromatin (Tel VIIL). We observed similarly low levels of relative enrichment across all regions in our uninduced control. After 20 minutes of incorporation after induction, we observed increased relative enrichment at all regions, and further enrichment after two hours of incorporation (Fig. 17A, left panel). These results indicate light-induced H3-3xFLAG is readily incorporated into chromatin, and that longer incubation periods following induction result in increased incorporation of H3-3xFLAG.

Considering the rapid induction and magnitude of H3-3xFLAG expression, we were concerned about the possibility that this would lead to abnormal levels of histones within chromatin. We therefore immunoprecipitated total hH3 after each incorporation period, and compared relative enrichment of associated DNA from each region across all incorporation time points by qPCR. For all regions, we found similar levels of enrichment for both incorporation time points as our uninduced control, suggesting that nucleosome concentration within chromatin was unchanged for at least two hours after induced expression of H3-3xFLAG (Fig. 17A, right panel).

Replication-Independent Histone Turnover in Neurospora

We examined replication-independent histone turnover genome-wide in *N. crassa* by performing next generation sequencing on our H3-3xFLAG-associated chromatin. We were concerned that a lengthy incorporation time could lead to saturation of our FLAG-tagged histones within chromatin, and the resulting enrichment perhaps more representative of histone occupancy rather than rates of histone turnover. In order to assess the incorporation of a "pulse" of labeled histones, we allowed for only 30 minutes of incorporation (Fig. 16). Based on our qPCR results, increasing amounts of H3-3xFLAG are still incorporated between 20 minutes and two hours after induction (Fig. 17A). We reasoned that at this time point, the size of any observed peaks of enrichment would reflect relative histone turnover rates rather than occupancy.

We sequenced two replicate turnover experiments and observed reproducible H3-3xFLAG enrichment patterns genome-wide. The most prominent peaks were present over promoter regions of genes and typically adjacent to a region showing low turnover in the corresponding gene body, consistent with previous reports investigating replicating-independent histone turnover in budding yeast (Fig. 17B)[70,71,80,81]. Similarly, previous studies of replication-independent exchange of the histone H3 variant, hH3.3, in mouse and human cell cultures observed high levels of turnover at promoter regions, 5' UTRs, and the 3' ends of genes[72,82,83]. There was a noticeable lack of histone turnover at constitutive heterochromatin domains, as previously observed in fission yeast[15,69]. Altogether, the general correlations between histone turnover and chromatin contexts found in other models appear in *N. crassa* as well.

Histone Turnover in Neurospora Genes

To characterize histone turnover in Neurospora genes, we divided all genes by wild-type expression level into quartiles, aligned them relative to their putative transcriptional start and end sites, and averaged the relative signal across the promoter regions and gene bodies for each quartile. We found each expression quartile possesses a distinct turnover profile (Fig. 17C). Similar to observations in *S. cerevisiae*, *D. melanogaster*, *C. elegans*, mouse, and human cells, increased levels of histone turnover correlated with higher relative expression levels[70,71,73,81–88]. As in other model organisms, higher levels of histone turnover was found over promoter regions and in the 5' and 3' ends of genes[70,71,81–84,86,87] (Fig. 17C). Notably, the interior of gene bodies exhibited relatively low turnover, most likely due to SET-2-catalyzed H3K36me-mediated suppression of histone exchange[68]. Consistent with this possibility, previous work on H3K36me in Neurospora found SET-2-mediated H3K36me is mainly enriched over gene bodies, marking most (~80%) Neurospora genes, although not genes with low or no expression[65]. The level of turnover within gene bodies appeared lower in the top three expression quartiles than the basal turnover found at genes within the lowest quartile, perhaps highlighting this mechanism, which is dependent on Pol II elongation[68].

The low level of turnover within Neurospora gene bodies appears more similar to that in yeasts, and contrasts with the relatively high hH3.3 turnover levels within gene bodies of *C. elegans*, *D. melanogaster*, and humans. Indeed, even though general trends in replication-independent histone turnover are similar in all organisms examined, the relative amounts of incorporated hH3.3 appear higher compared to neighboring

chromatin than the amount of turnover within Neurospora gene bodies compared with their respective neighboring chromatin.

The overall shape of histone turnover profiles over genes in Neurospora appears to reflect additional conserved features of nucleosome organization in eukaryote gene bodies. Previous genome-wide studies uncovered dedicated nucleosome-free regions (NFRs) present immediately upstream of the transcriptional start sites in yeasts[89–93], worms[94,95], flies[96], medaka[97], and humans[98,99]. Though less studied, an NFR at the 3' end of genes has also been identified in yeasts[88,91] and flies[96]. Expressed genes in Neurospora, represented by the top three expression quartile profiles, appear to organize their nucleosomes at the end of gene bodies similarly as in other model systems. There are noticeable dips in H3-3xFLAG enrichment just upstream of the transcriptional start site and downstream of the transcriptional end sites, most likely due to the presence of NFRs (Fig. 17C). Overall, it appears the general associations between active transcription and histone turnover are present in Neurospora, suggesting Neurospora organizes chromatin at active genes in a similar fashion as other eukaryotes.

Histone Turnover in Neurospora Heterochromatin Mutants

Heterochromatin is generally thought to be compacted, largely transcriptionally silent chromatin that renders underlying DNA inaccessible to *trans*-acting factors[1]. Studies in *S. pombe* have shown heterochromatin to be refractory towards replication-independent histone turnover relative to transcriptionally active euchromatin[15,69]. Mutants deficient for heterochromatin-associated factors such as the histone deacetylase (HDAC) Clr3, the histone H3 lysine 9-specific methyltransferase Clr4, or the chromodomain

proteins that bind this histone mark, Swi6 and Chp2, exhibit increases in histone turnover at heterochromatin domains, suggesting destabilization of heterochromatin structure[15,69].

Constitutive heterochromatin in Neurospora sports distinct histone marks and conserved features typical of this category of chromatin. H3K9me3 is catalyzed by the histone methyltransferase, DIM-5[5,46]. This mark is recognized by the chromodomain protein HP1[100], which functions as a platform to recruit the DNA methyltransferase DIM-2 to methylate underlying cytosines[27]. HP1 also assists in directing the HDAC complex, HCHC, to heterochromatin, whose activity is dependent on its catalytic subunit, HDA-1[40,41]. To test how the loss of different heterochromatin factors may affect histone turnover in Neurospora, we built reporter strains in Δ*dim-2*, Δ*dim-5*, Δ*hpo*, and Δ*hda-1* backgrounds, and assayed for H3-3xFLAG incorporation by next generation sequencing.

In all mutant backgrounds tested, H3-3xFLAG patterns in euchromatin were nearly identical to that observed in wild type, suggesting that loss of heterochromatin machinery has little effect on histone turnover in euchromatin (Fig. 18A). However, as expected, there were differences in heterochromatin domains. In contrast to euchromatin, heterochromatin domains in wild-type strains exhibit relatively low levels of histone exchange and are flanked by short regions of rapid turnover (Fig. 18A and B). It is of note that high levels of histone exchange were also observed at heterochromatin boundaries in *S. pombe* and *D. melanogaster*, and that histone turnover has been previously suggested to limit heterochromatin spreading[15,71,87].

Histone turnover at heterochromatin in Δ*dim-2* strains appears largely normal in that turnover remained largely suppressed across heterochromatin domains. However, there was a modest increase of turnover at the edges of heterochromatin domains (Fig.

18A and B). These results suggest that DNA methylation has little influence on histone turnover in Neurospora. Loss of DIM-5, and thus H3K9me3, or the HDAC HDA-1 led to greater disruption of heterochromatin domains. In Δ*dim-5* strains, we observed reduced turnover at domain edges and increased turnover within the interior of heterochromatin domains (Fig. 18A and B). Similar increased turnover within the interior of heterochromatin domains was observed in Δ*hda-1* strains, but unlike Δ*dim-5* strains, there was concomitant increases in turnover at domain edges (Fig. 18A and B). Despite these increases, the general profile of histone turnover appears largely preserved in these mutants, perhaps reflecting redundant mechanism to maintain heterochromatin structure. These results are similar to observations at the *S. pombe* mating type locus, where loss of the HDAC Clr3 leads to greater increases of histone turnover than loss of Clr4 and heterochromatin-associated H3K9me[15]. Interestingly, the greatest increases in histone turnover were observed in Δ*hpo* strains. Similar to Δ*hda-1* strains, there is increased turnover at domain edges, but histone turnover is much higher overall throughout the entire domain (Fig. 18A and B). That loss of HP1 leads to greater destabilization of heterochromatin is puzzling as HP1 is dependent on H3K9me3, and thus DIM-5 catalytic activity, for localization to heterochromatin[100], and DIM-5 is responsible for all H3K9me3 in Neurospora[5]. However, this result is consistent with the observation that HP1 chromodomain mutants retain a low level of DNA methylation, which suggests that HP1 is still recruited to heterochromatin domains despite lacking the ability to bind H3K9me3[41].

A Simple Method to Profile Histone Turnover in *Neurospora crassa*

We have created a strain that expresses 3xFLAG-tagged histone H3 under the control of a light-inducible promoter to profile histone turnover genome-wide. Inducible tagged histones have been successfully used in the past in multiple organisms to profile histone turnover[15,69–73]. However, our reporter strain provides greater ease of use and magnitude of expression of H3-3xFLAG, all without compromising physiological levels of histone occupancy (Fig. 18A). Whereas reporter strains in yeasts, mice, and flies require a lengthy incubation period for induction, typically 1-2 hours[15,69–73], our strain expresses readily detectible H3-3xFLAG expression and chromatin incorporation as early as 20 minutes (Figs.15B and Fig. 17A). Induction in our strain does not requires a change of growth medium to one with an inducing agent. Rather, our strain merely requires a short period of exposure to light. Though we used blue light for induction, previous work characterizing the *vvd* promoter has shown that white light (400-700 nm) from conventional light bulbs are sufficient[77]. The rapid nature of induction of our strain should be useful for profiling histone exchange genome-wide in any context and amenable for chromatin profiling at regions with quick transcriptional kinetics as it can more rapidly "pulse" in tracible histones into chromatin.

Materials and Methods

N. crassa Strains and Molecular Analyses

N. crassa strains are listed in Appendix C, and were grown, crossed, and maintained according to standard procedures[56]. Primers used are listed in Appendix D. DNA isolation and western blotting were performed as previously described[27]. The

following antibodies were used in western blot analyses: anti-FLAG-conjugated peroxidase (FLAG-HRP) (A8592; Sigma) and anti-phosphoglycerate kinase 1 (PGK1) (ab113687; Abcam). Secondary antibodies were used as previously described[27]. Chemiluminescence from treatment with SuperSignal West Pico Substrate (34080; Thermo Fisher Scientific) for anti-PGK1 and anti-FLAG-HRP was imaged using a LI-COR Odyssey Fc imaging system.

Generation of *P_{vvd}::hH3-3xFLAG::his-3$^+$* Reporter Strain

The promoter region of the *vvd* gene was amplified by PCR using wild-type genomic DNA as template using primers *VVD-3000F_EcoRI\NotI* and *VVD-R1_XbaI* containing NotI and XbaI sites, respectively. The PCR product and pCCG::C-Gly::3xFLAG[58] were digested with NotI and XbaI, and ligated together to create pVVD::C-Gly::3xFLAG. pVVD::C-Gly::3xFLAG and pIDTSMART-AMP containing Neurospora codon-optimized *hH3* (NEB) were digested with XbaI and PacI and ligated together to yield pVVD:hH3::C-Gly::3xFLAG. The ligation product was verified by restriction digest. pVVD::hH3::C-Gly::3xFLAG was then linearized and transformed into strains N2930 and N3012. The resulting *his-3$^+$* strains (N6049 and N6054) were verified by Southern hybridization.

Histone Exchange Profiling and Analyses

Fresh conidia were inoculated in Vogel's minimal liquid medium supplemented with 1.5% sucrose at a concentration of $1x10^6$ conidia/mL, and grown for 18 hours at 32˚C with shaking (150 rpm) in a dark room. Low intensity red light was used during all

culturing steps to prevent light stimulation[101]. To block DNA replication, cultures were spiked with hydroxyurea to a final concentration of 100 mM, and incubated for 3 hours. We affixed five, 2 ft long strips of blue light LED lights (LEDs: EL-BVRIB12V, power supply: EL-12VADPT, dimmer switch: EL-SC12DIM, and DC 5-way splitter: EL-SJDCSPLIT; Elemental LED) to the bottom of the incubator lid. To induce H3-3xFLAG expression, the LED strips were activated to 100% power, and cultures were exposed to blue light (465 nm; 30 μmole photons/m^2/s) for 2 mins. Cultures were incubated for 30 mins (unless noted otherwise) to allow for H3-3xFLAG incorporation into chromatin and immediately harvested, washed with PBS buffer, and transferred to 125mL Erlenmeyer flasks with 10 mL PBS buffer. For chromatin fixation, formaldehyde to a final concentration of 0.5% was added, and incubated for 30 mins at room temperature. The crosslinking reaction was quenched by adding glycine to a final concentration of 0.2M, and incubating for 5 mins at room temperature. Tissue was lysed by sonication, and chromatin was sheared with a bioruptor (Diagenode) for 20 min with a 30 sec on/30 sec off cycle at high power. Subsequent chromatin immunoprecipitation (ChIP) was subsequently performed as previously described[5] using the following antibodies: anti-FLAG-conjugated agarose beads (A2220; Millipore) and anti-hH3 (Ab1791; Abcam).

For ChIP-qPCR analysis, experiments on independent experimental replicates were performed in triplicate using PerfeCTa SYBR Green Fastmix ROX (Quantabio) with the listed primers (Table S2), and analyzed using a StepOnePlus Real-Time PCR system (Life Technologies). Relative enrichment was determined by calculating enrichment as a percent of the total input.

H3-3xFLAG ChIP samples were prepared for sequencing as previously

described[35]. Sequencing was performed using an Illumina HiSeq 4000 system with single-end 75-nt or 100-nt reads. Sequencing data was processed and analyzed using the Galaxy platform (https://usegalaxy.org/)[60]. Sequences were aligned to the corrected *N. crassa* OR74A (NC12) genome[52] using Bowtie2[61]. For visualization, BedGraph files were generated from mapped read data using HOMER[102], converted into bigWig files using the Wig/BedGraph-to-bigWig program via Galaxy, and visualized with the Integrative Genomics Viewer (IGV)[63]. Meta analyses were carried out using the computeMatrix and plotProfile programs from deepTools[62] via Galaxy.

Light characterization

Light spectral range was measured using an ILT350 chroma meter (International Light Technologies) and intensity was measures using a MQ-200 quanta meter (Apogee Instruments).

Bridge to Chapter IV

I was also involved in another project investigating the regulation of a pair of divergently transcribed genes, *kyn-1* and *iad-1*, that are involved the highly conserved kynurenine pathway that converts tryptophan into various catabolites. *kyn-1* and *iad-1* are marked with H3K27me3 and ASH1-mediated H3K36me2, both marks associated with gene repression[4,65]. These genes are silent under normal conditions, but are rapidly induced by extracellular tryptophan. Expression of *kyn-1* and *iad-1* appears to be dependent on the transcription factor, TAH-2. By monitoring the fluorescent

accumulation of anthranilic acid, a by-product of the kynurenine pathway, I characterized the expression of *kyn-1* and *iad-1* in mutants defective in H3K27me or H3K36me as well as chromatin remodelers that were implicated in H3K27me- and H3K36me-mediated silencing. I found evidence that the expression of *kyn-1* and *iad-1* is largely unaffected by the loss of H3K27me3, but is regulated by ASH1-mediated H3K36me2, hypothetically effected through the chromatin remodelers ISWI and CHD1. I also found that another H3K36 methyltransferase, SET-2, is required to overcome ASH1-mediated repression of these genes, suggesting a paradigm where H3K36me both represses and activates this locus.

CHAPTER IV

REGULATION OF TRYPTOPHAN CATABOLISM GENES *KYN-1* AND *IAD-1* IN *NEUROSPORA CRASSA*

This chapter contains unpublished co-authored work investigating the regulation of a pair of genes involved in the kynurenine pathway, *kyn-1* and *iad-1*. Kevin McNaught performed some of the initial H3K27me3 ChIP characterizing the region and mapped a mutation in a classic kynurenine pathway Neurospora mutant, which he found to be in *tah-2*, a transcription factor essential for activation of this locus. I was responsible for generating relevant strains, the experimental design and execution of assaying anthranilic acid secretion, and performing ChIP-qPCR of H3K27me3 comparing the distribution of this mark in inducing conditions versus non-inducing conditions. Eric Selker was the principal investigator for this work.

Introduction

In addition to its indispensable role as an essential amino acid in protein synthesis, tryptophan is an important precursor for many bioactive molecules, including serotonin[103]. Most of tryptophan catabolism is carried out through the kynurenine pathway, which is conserved throughout prokaryotes and eukaryotes, and ultimately culminates in the production of nicotinamide adenine dinucleotide (NAD^+), an importance source of cellular energy[103]. The various metabolites resulting from this pathway are involved in a variety of physiological processes and neurological disorders

including inflammation, psychosis, schizophrenia, blood pressure, and immune response[103,104].

The kynurenine pathway has been extensively studied in the filamentous fungus *N. crassa*[105–108]. Neurospora possesses two kynureninase homologs, a crucial factor in this pathway, as identified by distinct enzymatic activities from cell lysates separated by chromatography. Though one kynureninase gene is constitutively active at a low basal level, expression of the second homolog is inducible. The kynurenine pathway is largely inactive during normal growth conditions, but is rapidly activated in response to exposure to extracellular tryptophan, kynurenine, or *N*-formyl-kynurenine[107,108].

Here we report an initial characterization of the regulation of inducible kynureninase in Neurospora. We identify a transcription factor, TAH-2, that is required for induction of the kynurenine pathway. The gene encoding inducible kynureninase, *kyn-1*, is located immediately upstream of a gene encoding indoleamine-2,3-dioxygenase, *iad-1*, which carries out the first catalytic step of the kynurenine pathway. These genes are divergently transcribed and are enriched in two chromatin marks implicated in gene silencing, SET-7-mediated methylation of lysine 27 of histone H3 (H3K27me) and ASH1-mediated methylation of lysine 36 of histone H3 (H3K36me)[4,65]. We explore how loss of H3K27me- and H3K36me-related machinery affects secretion of anthranilic acid, a by-product of the kynurenine pathway in response to tryptophan. Loss of H3K27me appears to have little or no effect on kynurenine pathway activity, but loss of ASH1-mediated H3K36me leads to increased anthranilic acid accumulation. Interestingly, another conserved H3K36 methyltransferase, SET-2, is required for effective anthranilic acid production, but only in the presence of ASH1 catalytic activity. Altogether, our

findings describe a paradigm where H3K36me is involved in the repression and activation of this pathway, in which ASH1-mediated H3K36me represses the activity of this pathway and SET-2 is required to overcome this suppression for effective induction.

Results and Discussion

kyn-1 and *iad-1* Expression is Induced by Extracellular Tryptophan

N. crassa possesses two kynureninase homologs that are involved in the kynurenine pathway[108]. Previous work revealed that one of these enzymes is constitutively active, while the other is inducible by exposing cultures to extracellular tryptophan, kynurenine, or *N*-formyl-kynurenine, increasing the enzymatic activity of crude extracts by as much as 600-fold[105]. Consistent with this, we found Neurospora possesses two genes predicted to be homologous to kynureninase, *NCU09183* and *NCU00463*. Interestingly, *NCU09183* is directly upstream from a divergently transcribed gene predicted to be an indoleamine-2,3-dioxygenase (*NCU09184*), which is responsible for the first catalytic step in the kynurenine pathway (Fig. 19A). Previous RNA expression sequencing experiments showed very little or no expression from *NCU09183*[4], so we hypothesized it was the previously described inducible kynureninase.

To test if *NCU09183* expression is inducible, I tagged the predicted protein at its C-terminus with 3xFLAG, and examined primary transformants by western blot in inducing (1mM Trp)[106] and non-inducing (no Trp) conditions. Given the upstream position of the predicted indoleamine-2,3-dioxygenase gene, its known involvement in the first step of the kynurenine pathway, and that it also appears to be silent by RNA-

seq[4], I hypothesized that its expression might be inducible as well and generated primary transformants bearing a C-terminal 3xFLAG tag on the predicted indoleamine-2,3-dioxygenase. I observed no FLAG signal from two primary transformants each for both *NCU09183* and *NCU09184* grown in non-inducing conditions (Fig. 19B, Trp -). However, I observed robust expression of both *NCU09183* and *NCU09184* in response to extracellular tryptophan exposure (Fig. 19B, Trp +). From here on, I will refer to *NCU09183* as *kyn-1* and *NCU09184* as *iad-1*.

TAH-2 is Essential for Kynurenine Pathway Activation

In the kynurenine pathway, extracellular tryptophan is rapidly converted into anthranilic acid by kynureninase[109]. Previous work revealed that inducible kynureninase activity in Neurospora preferentially acts on kynurenine[108], producing anthranilic acid, which is actively secreted into the surrounding growth medium and can be monitored by fluorescence[105]. As production of anthranilic acid from tryptophan also requires the activity of IAD-1, anthranilic acid fluorescence should represent the combined activities of these two enzymes[109].

Previous work by Schlitt et al. described an inducible kynureninase mutant with significantly reduced kynureninase activity[106]. To explore how the *kyn-1*/*iad-1* region is regulated, Kevin McNaught performed bulk-segregant analysis[110] on this mutant strain. He identified a G to A point mutation resulting in a premature stop codon in the *tah-2* transcription factor (*NCU02214*) (Fig. 20). To test whether loss of *tah-2* results in defects in the kynureninase pathway, I monitored anthranilic acid secretion from strains exposed to tryptophan.

I first characterized anthranilic acid accumulation from a wild-type strain. Cultures were spiked with 1mM tryptophan, and the growth medium was sampled every 20 minutes for three hours. There was steadily increasing concentrations of anthranilic acid across all time points (Fig. 19C). I wanted to test if the observed rate of anthranilic acid secretion would increase in response to additional tryptophan during the time course. Surprisingly, when I spiked in additional tryptophan every 20 minutes, I found the rate of anthranilic acid accumulation to be the same as cultures that were exposed to tryptophan only at the start of the time course, suggesting that exposure to 1 mM induces a maximum catalytic response from a wild-type strain. However, I observed no appreciable increase anthranilic acid fluorescence across the time course for the Δ*tah-2* strain, demonstrating that this transcription factor is necessary for the robust anthranilic acid accumulation observed in wild-type strains (Fig. 19C).

Loss of PRC2 Components does not Increase Anthranilic Acid Accumulation

Methylation of lysine 27 of histone H3 (H3K27me) is a conserved histone mark involved in gene silencing that is established by Polycomb Repressive Complex 2 (PRC2)[111]. This mark is present in *N. crassa*, and loss of PRC2 components results in the expression of some transcriptionally quiescent genes marked by H3K27me3[4]. The *kyn-1*/*iad-1* locus is enriched with this mark (Fig. 21B, lower panel), raising the question whether loss of PRC2 function would affect expression from the *kyn-1*/*iad-1* locus and thereby lead to changes in anthranilic acid accumulation. It is worth noting that expression of *kyn-1*/*iad-1* appears unchanged in Δ*set-7* strain under non-inducing

conditions[4]. However, we hypothesized H3K27me3 may play a role in the regulation of this gene pair during activation.

To account for potential differences in anthranilic acid secretion rates resulting from differences in mycelial mass due to growth defects of the mutants, we normalized anthranilic acid fluorescence by dry mass. I did not observe an increase in anthranilic acid accumulation in Δ*set-7*, Δ*eed*, or Δ*suz12* strains (Fig. 21A). Rather, the Δ*set-7* strain secreted anthranilic acid at the same rate as the wild type control, and Δ*eed* and Δ*suz12* strains exhibited a slightly dampened response (Fig. 21A), suggesting H3K27me3 does not negatively regulate this locus under inducing conditions.

Given the conserved role of H3K27me3 as a repressive mark, I hypothesized H3K27me3 enrichment might change at this locus upon the induction. It seemed feasible that this locus might require reduction of H3K27me3 for efficient activation, and genetic removal of the mark could create a chromatin environment at *kyn-1*/*iad-1* conducive for expression, but not significantly affect the maximum rate of anthranilic acid production. I performed H3K27me3 ChIP-qPCR, examining four regions within the *kyn-1*/*iad-1* locus (Fig. 21B). I observed the same level of H3K27me3 within both gene bodies in both the presence and absence of tryptophan but detected an approximately 50% reduction of H3K27me3 in the presumptive promoter region under inducing conditions. Altogether, my data suggest the presence or absence of H3K27me appears to have little effect on the activity of *kyn-1*/*iad-1*, begging the question of how this locus overcomes the repressive effect of this mark.

Loss of Chromatin Remodelers Increases Anthranilic Acid Secretion

Work by Tish Wiles and Kevin McNaught previously identified the conserved chromatin remodelers ISWI and CHD1 (known as CRF4-1 and CRF6-1, respectively, in Neurospora) as crucial factors involved in H3K27me-mediated silencing through a forward genetic selection mutant hunt (Wiles and McNaught et al., *in prep*). These chromatin remodelers have been shown to be directed to chromatin by H3K36me in budding yeast[112]. Interestingly, H3K36me2 catalyzed by ASH1 co-marks chromatin at nearly every H3K27me3-marked gene in *N. crassa* and has been found to be crucial for silencing many of these genes[65]. We wondered if the loss of these remodeling factors would affect anthranilic acid production.

I performed anthranilic acid secretion time course assays in wild-type, Δ*tah-2*, Δ*crf4-1*, and Δ*crf6-1* strains. Consistent with previous results, we observed steady anthranilic acid accumulation from wild type and no accumulation from the Δ*tah-2* strain (Fig. 22). Both Δ*crf4-1* and Δ*crf6-1*, however, yielded significantly more anthranilic acid than wild type, suggesting that these chromatin remodelers are involved in the downregulation of the *kyn-1*/*iad-1* locus.

SET-2 is Required to Overcome ASH1-Mediated Suppression of *kyn-1*/*iad-1*

The apparent involvement of CRF4-1 or CRF6-1 prompted me to investigate how loss of H3K36me might affect the locus as well. Neurospora sports two H3K36-specific methyltransferases, SET-2 and ASH1[65]. ASH1-mediated H3K36me appears largely enriched over lowly transcribed or silent genes, while SET-2 marks active genes through the conserved mechanism of recruitment by RNA Pol II[65]. To test whether loss of SET-2- or ASH1-mediated H3K36me affects the activity of the *kyn-1*/*iad-1* locus, we performed

anthranilic acid secretion time courses on Δ*set-2* and catalytic-null *ash1* (*ash1**) strains. It appears even with the loss of SET-2 or ASH1 catalytic activity, *kyn-1* and *iad-1* remains silent in non-inducing conditions[65]. Similar to the heightened rate of anthranilic acid production observed in Δ*crf4-1* and Δ*crf6-1* strains, I observed a comparable increased rate in *ash1** strains (Fig. 23A). Curiously, I observed a greatly reduced anthranilic acid response in Δ*set-2* strains (Fig. 23A). I wondered how anthranilic acid accumulation might be affected in strains bearing mutations in both H3K36 methyltransferases. I observed that Δ*set-2*; *ash1** strains accumulated anthranilic acid at rate comparable to *ash1** single mutants. As loss of ASH1 catalytic activity overcame the dampened anthranilic acid response phenotype of Δ*set-2* strains and chromatin remodeler mutants exhibit a heightened response similar to *ash1** strains, I wondered if loss of chromatin remodelers would also overcome the Δ*set-2* phenotype. I observed an increased anthranilic acid response in Δ*set-2*; Δ*crf4-1*, similar to that observed in *ash1** and Δ*set-2*; *ash1** strains (Fig. 23A).

kyn-1/*iad-1* Expression is Regulated by H3K36me

Altogether, our data suggest a model in which H3K36me both positively and negatively regulates the inducible activity of the *kyn-1*/*iad-1* locus. It appears this locus remains silent in non-inducing conditions as loss of H3K27me or H3K36me appears to have no effect on *kyn-1* or *iad-1* expression[4,65]. However, the expression of this locus is rapidly induced upon exposure to extracellular tryptophan, and this activation requires the transcription factor TAH-2, which is likely recruited to the shared promoter region between *kyn-1* and *iad-1* (Fig. 19C). Based on my results, I propose a "lock and key"

model of *kyn-1*/*iad-1* regulation upon induction. Efficient induction requires the H3K36-specific methyltransferase, SET-2 (Fig. 23A). Loss of ASH1 catalytic activity, another H3K36-specific methyltransferase, or either of the presumptive chromatin remodelers CRF4-1 (ISWI) or CRF6-1 (CHD1), results in increased anthranilic acid secretion, suggesting increased expression from the *kyn-1*/*iad-1* locus (Fig. 23A). However, the loss of SET-2 appears to have no effect on the increased anthranilic acid response observed in *ash1** and Δ*crf4-1* strains. As H3K36me has been shown to direct both ISWI and CHD1 in yeast[112], these results suggest this locus is actively suppressed by ASH1-catalyzed H3K36me mediated through chromatin remodeling activities, i.e. the "lock". Though the mechanism remains to be established, SET-2 is required to overcome ASH1-mediated suppression, i.e. the "key" (Fig. 23B). In the absence of the "lock" (ASH1 or key chromatin remodelers), the "key" (SET-2) becomes no longer necessary for rapid induction.

That the loss of H3K27me does not obviously affect anthranilic acid secretion is interesting, given the conserved role of this histone mark in mediating gene repression[111]. It is possible the observed H3K27me is a consequence of ASH1-mediated H3K36me. Previous work has shown that nearly every domain of H3K27me-marked chromatin is co-marked with ASH1-catalyzed H3K36me and ectopically-induced H3K27me is preferably deposited over ASH1-catalyzed H3K36me-marked chromatin[65]. It is possible the *kyn-1*/*iad-1* locus sports a chromatin environment conducive for the formation of H3K27me, and H3K27me has little functional impact on the overall regulation of these genes. How H3K27me might regulate this locus or how robust expression occurs, in spite of H3K27me2/3 enrichment, will require further study.

Materials and Methods

N. crassa Strains and Molecular Analysis

All *N. crassa* strains and primers used in this study are listed in Appendices C and D, respectively. Strains were grown, crossed, and maintained according to standard procedure[56]. Deletion strains were FLAG-tagged strains were built as previously described[58]. Induction of *kyn-1-3xFLAG* and *iad-1-3xFLAG* was carried out by spiking tryptophan (T0254; Sigma) into the growth medium to a final concentration of 1 mM and incubating for 1 hour prior to cell lysis. DNA isolation and western blotting were performed as previously described[27]. anti-FLAG-conjugated peroxidase (anti-FLAG-HRP) (A8592; Sigma) was used for the western blot analysis. Chemiluminescence from treatment with SuperSignal West Pico Substrate (34080; Thermo Fisher Scientific) was used for anti-FLAG-HRP and visualized using a LI-COR Odyssey Fc imaging system.

Whole Genome Sequencing, Mapping, and Identification of *tah-2*^{W735*}

Identification of *tah-2*^{W735*} was carried out through bulk-segregant analysis, as previously described[113]. Briefly, the *tah-2* mutant was crossed to a "Mauriceville" wild-type strain[114] and progeny that did not exhibit anthranilic acid fluorescence were pooled together for whole genome sequencing. Mapping of mutations was performed as previously described[110,113] using the programs FreeBayes and VCFtools[115,116].

Anthranilic Acid Fluorescence Assay

Approximately $8x10^6$ fresh conidia were inoculated into 250 mL Erlenmeyer flasks containing 100 mL of Vogel's medium supplemented with 1.5% sucrose and grown at 32˚C with shaking at 175 rpm for 18 hrs. Tryptophan was spiked in to a final concentration of 1 mM, and a 1 mL aliquot of the growth medium was sampled every 20 minutes for the duration of the time course. An additional 250 µL of 50 µM tryptophan was spiked in every 20 minutes in noted experiments. To maintain a relatively constant volume, 1 mL of fresh Vogel's with 1.5% sucrose was added to each culture after sampling. Sampling aliquots were filter sterilized, and anthranilic acid fluorescence (λ_{ex}: 336 nm; λ_{em}: 400 nm)[105] was assayed in technical triplicates using a solid-black 96-well plate (07-200-590; Corning) and a SpectraMax M5e microplate reader. Anthranilic acid fluorescence was normalized to dry mycelial mass of each culture.

ChIP-qPCR

ChIP was performed as previously described[35] using anti-H3K27me3 (9733; Cell Signaling Technology). For qPCR experiments, experimental replicates were performed in triplicate using PerfeCTa SYBR Green Fastmix ROX (Quantabio) with the listed primers (Table S2). Relative enrichment was determined by measuring enrichment as a percent of total input. The enrichment of H3K27me3 at each indicated locus was then scaled to relative enrichment to H3K27me3 at TelVIIL.

CHAPTER V

CONCLUDING SUMMARY

In Chapter II, I explored the heterochromatin spreading phenotype observed in Neurospora strains deficient in the Lysine-Specific Demethylase Complex (LSDC). Shinji Honda identified that the LSDC consists of LSD1, PHF1, and BDP-1 by immunoprecipitation followed by mass spectrometry. Both he and I confirmed association between complex members through co-immunoprecipitation and yeast two-hybrid experiments. I performed the DNA methylation-sensitive Southern hybridizations characterizing the spreading of DNA methylation and concomitant H3K9me3 observed in LSDC member deletion strains. I also built strains with catalytic-null alleles of *lsd1* and found that LSD1 catalytic activity was necessary to prevent heterochromatin spreading. I discovered the DNA methylation spreading observed in Δ*lsd1* strains is variable and is subject to change through sexual crossing and asexual propagation. I found the observed heterochromatin spreading is dependent on both the presence of DNA methylation and the histone deacetylation activity of the HCHC complex. Tereza Ormsby performed poly-A RNA-sequencing on a Δ*lsd1* strain and identified up- and down-regulated genes, which I used to analyze the correlation between heterochromatin spreading and misregulated gene expression. Interestingly, the observed gene changes do not appear to be driven by the spreading of H3K9me3 and DNA methylation over these genes.

These results implicate LSD1 in heterochromatin spreading in *N. crassa*, consistent with its conserved role as a regulator of heterochromatin spreading in other models. The requirement of DNA methylation of Δ*lsd1*-induced heterochromatin

spreading has been observed previously in instances with heterochromatin establishment outside of "canonical" domains of AT-rich retrotransposon relics brought on through RIP, such as at disiRNA locus DNA methylation (DLDM) and *dmm* mutants. Normally, the loss of DNA methylation has no effect on the presence of H3K9me3 at "canonical" domains. It appears certain as heterochromatin spread outside of these AT-rich domains, additional requirements arise for effective spreading. Though whether HCHC is required for DLDM or heterochromatin spreading in *dmm* mutants has not been tested, it seems likely, as heterochromatin is lost at the edges of domains where AT-richness is rapidly depleted, suggesting HCHC is required for propagation in chromatin contexts with 50% or more GC-content. In future studies, it will be important to explore the contributions of the other LSDC members in complex function as well as LSDC, as well as to investigate how LSDC is recruited to its chromosomal targets

In Chapter III, I characterized a histone turnover reporter strain using 3xFLAG-tagged histone H3 (H3-3xFLAG) under the control of the light-inducible *vvd* promoter that was built by Michael Rountree, Vincent Bicocca, and Sabrina Abdulla, and developed a protocol for replication-independent histone turnover profiling. I showed that H3-3xFLAG is robustly induced in response to a two-minute pulse of blue light, for at least two hours post induction. H3-3xFLAG is readily incorporated into chromatin and does not seem to affect histone concentration within chromatin, at least within 30 minutes of incorporation. By performing ChIP-seq on induced H3-3xFLAG, I created histone turnover enrichment profiles for wild-type and various heterochromatin mutant strains. I performed a meta-analysis of histone turnover at Neurospora genes with respect to expression. Extent of turnover appears to correlate with gene expression with the most

turnover present at promoters and the 5' and 3' ends of genes, and relatively low turnover within the middle of the gene body, consistent with previously examined models.

These results revealed that the trends in histone turnover in Neurospora appear consistent with observations from other models, with heterochromatin domains largely refractory towards histone exchange and increasing turnover within genes correlating with level of transcription. Overall, the work presented establishes this light-inducible histone turnover reporter as a simple yet powerful tool for investigating histone dynamics genome-wide.

In Chapter IV, I investigated the regulation of *kyn-1*/*iad-1*, a divergently expressed gene pair that is inducible by exposure to extracellular tryptophan. These two genes are involved in the initial steps of the kynurenine pathway, a highly conserved tryptophan catabolism pathway. The activation of this locus requires the transcription factor, TAH-2, which was previously identified by Kevin McNaught. Activity of the kynurenine pathway can be assayed through the fluorescent accumulation of anthranilic acid, which is rapidly produced though conversion of tryptophan. I performed initial time course characterizations of anthranilic acid accumulation in wild-type and Δ*tah-2* strains. I found that the loss of H3K27me3, a conserved histone mark involved in gene repression, does not result in increased kynurenine pathway activity. Further, I performed H3K27me3 ChIP-qPCR on wild-type strains grown under inducing conditions and observed a slight reduction only over the promoter region. I also found that chromatin remodeler knockout strains, Δ*crf4-1* and Δ*crf6-1*, had an increased anthranilic acid response to tryptophan exposure. This led me to investigate the anthranilic acid response in H3K36 methyltransferase mutants as H3K36 methylation has been implicated in the

localization of these chromatin remodeler proteins. I found that SET-2 is required for effective induction of *kyn-1*/*iad-1* and loss of ASH1 catalytic activity leads to increased anthranilic acid accumulation. Interestingly, I found that the anthranilic acid response from Δ*set-2*; *ash1** and Δ*set-2*; Δ*crf4-1* strains to be comparable to *ash1** or Δ*crf4-1* single mutants.

Altogether, these results describe a regulatory paradigm where H3K36 methyltransferases regulate the repression and activation of an inducible gene locus. My results suggest that repression is due to ASH1-mediated methylation of H3K36, which likely recruits chromatin remodeling activities to maintain a repressive environment. In response to tryptophan exposure, this repression is overcome in a SET-2-dependent manner. In the absence of the CRF4-1 chromatin remodeler or ASH1 catalytic activity, SET-2 is no longer necessary for effective induction. These findings provide insight on H3K36 methylation-mediated regulation of a gene pair locus with inducible activity, as well as an opportunity to investigate how gene expression may occur in the presence of repressive H3K27me3. How SET-2 overcomes ASH1-mediated repression is mysterious. It is not clear whether SET-2 catalytic activity is required for induction, or whether its recruitment involves its conserved mechanism of association with RNA pol II. Future studies investigating SET-2 recruitment and involvement will be important for uncovering the full repressive mechanism regulating this locus.

APPENDIX A

FIGURES

Figures for Chapter II

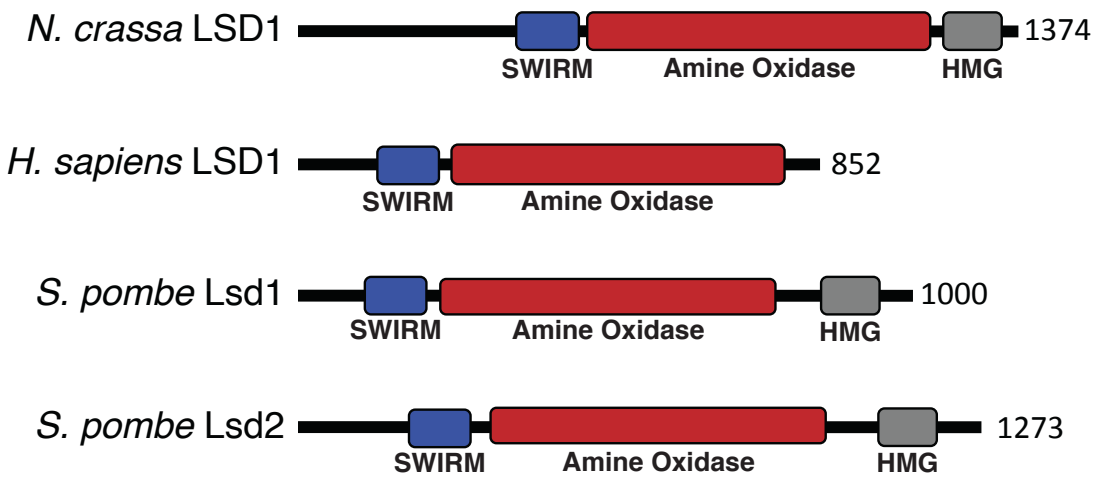

Fig. 1. Schematic representation of human, *S. pombe,* and Neurospora LSD1 homologs with predicted domains and amino acid lengths.

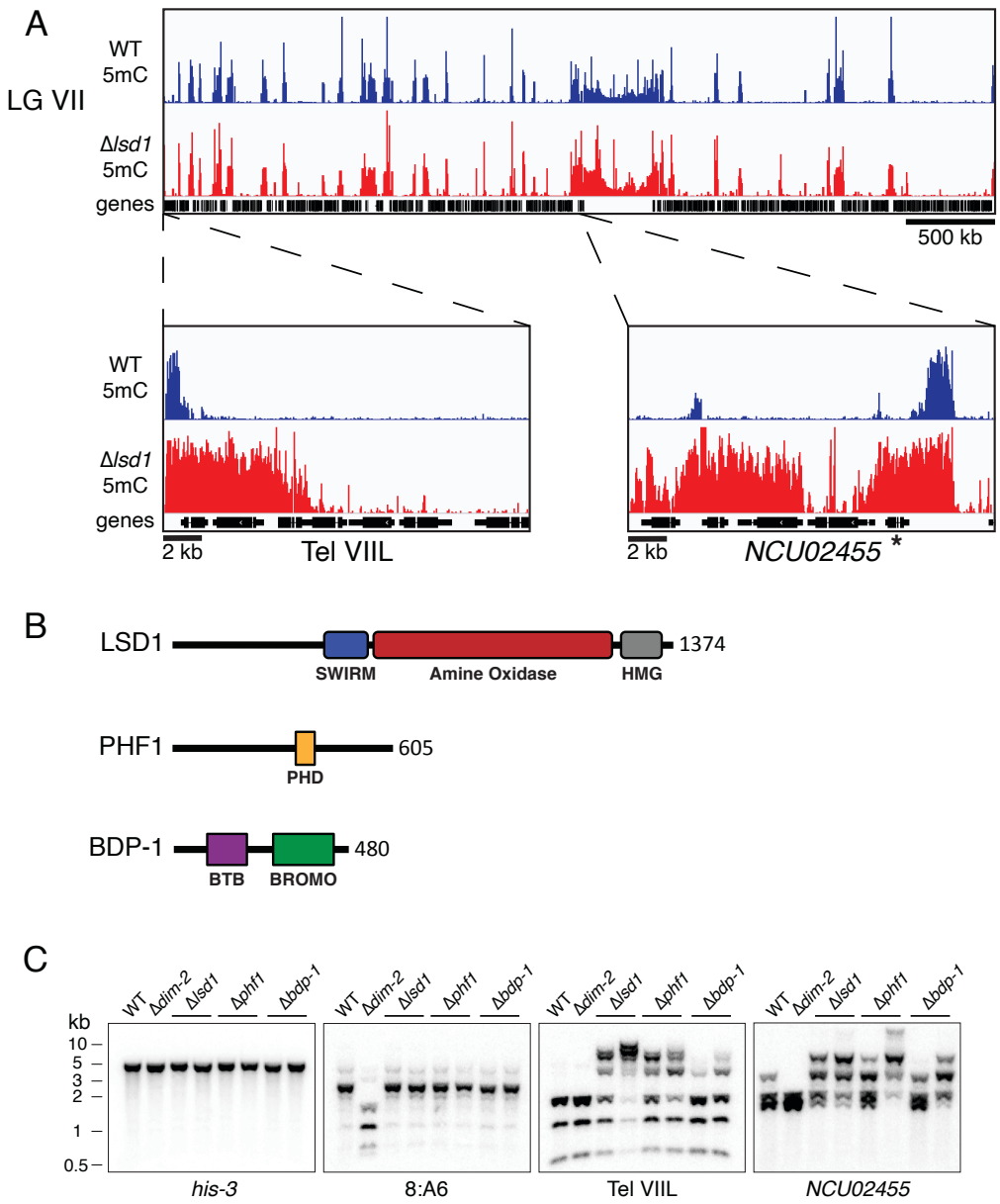

Fig. 2. Identification of LSDC in *Neurospora crassa*. (A) WGBS tracks displaying DNA methylation in WT (blue) and Δ*lsd1* (red) strains over LG VIIL (additional tracks for other chromosomes can be found in Supplemental Figure 2). *NCU02455* is indicated with an asterisk. (B) Schematic representation of the identified members of LSDC with their predicted domains and length (amino acids) indicated. (C) LSDC knockouts exhibit hypermethylation. Genomic DNA from WT, a strain lacking DNA methylation (Δ*dim-2*), and LSDC knockouts (Δ*lsd1,* Δ*phf1,* and Δ*bdp-1*) were digested with the 5mC-sensitive restriction enzyme AvaII and used for Southern hybridizations with the indicated probes for a euchromatin control (*his-3*), an unaffected heterochromatin control (8:A6), and two Δ*lsd1*-sensitive regions (Tel VIIL and NCU02455). Strains (left to right): N3753, N4711, N5555, N6411, N6221, N6414, N6220, and N6416.

Fig. 3 (see next page). Δ*lsd1* strains exhibit hyper DNA methylation at select loci genome-wide. WGBS tracks displaying DNA methylation in WT (blue) and Δ*lsd1* (red) strains across all Neurospora linkage groups.

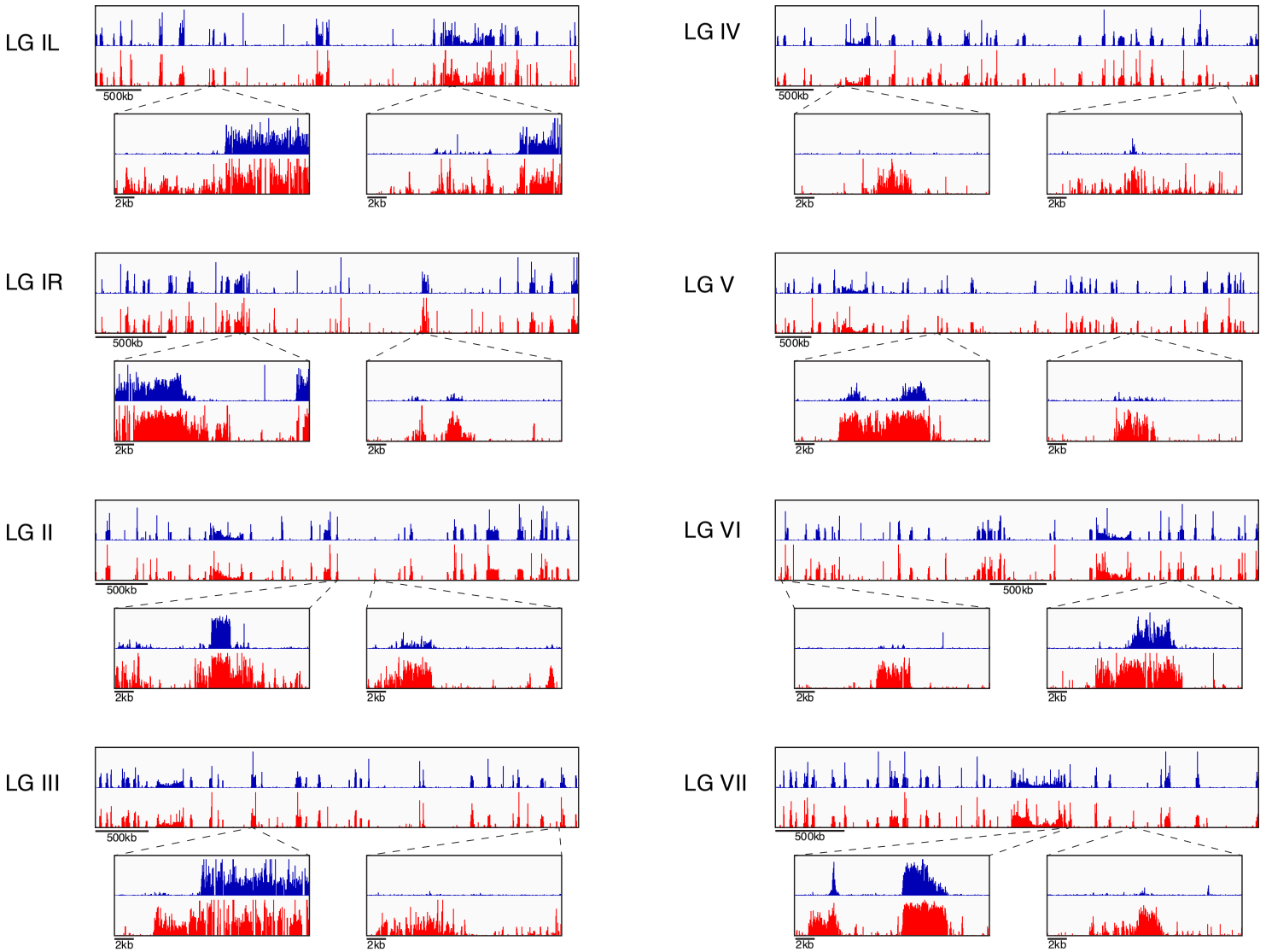
LG IL
500kb
2kb
2kb
LG IV
500kb
2kb
2kb
LG IR
500kb
2kb
2kb
LG V
500kb
2kb
2kb
LG II
500kb
2kb
2kb
LG VI
500kb
2kb
2kb
LG III
500kb
2kb
2kb
LG VII
500kb
2kb
2kb

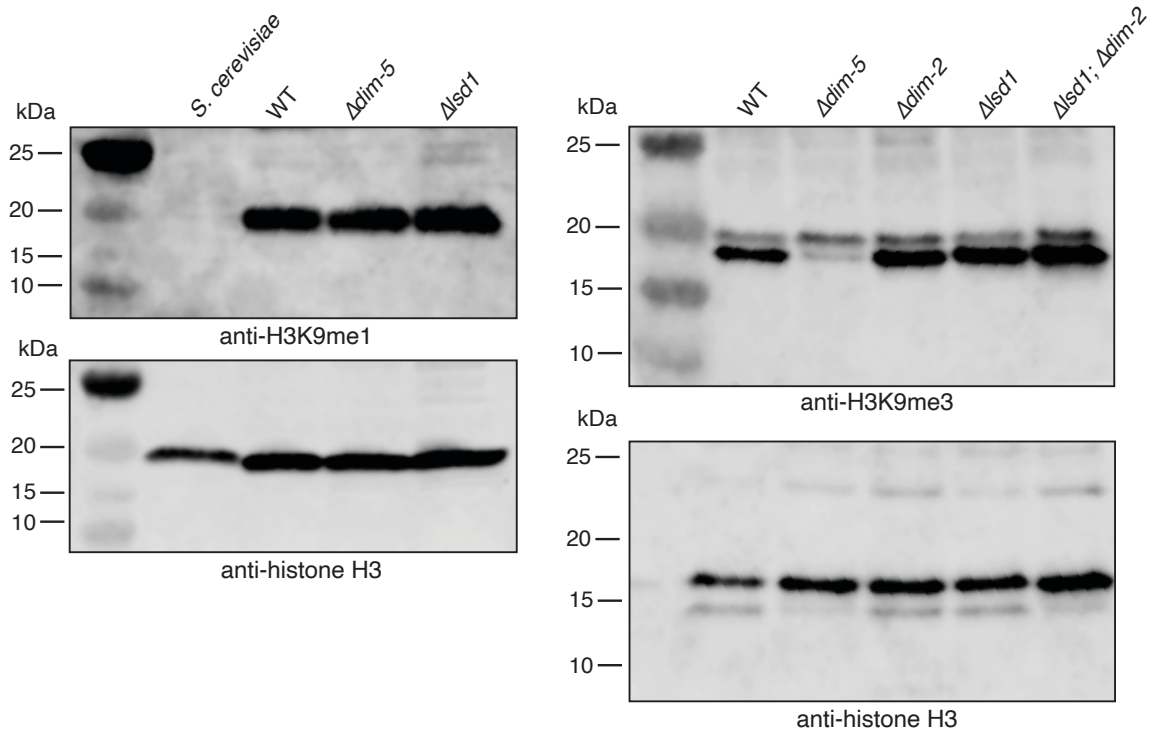

Fig. 4. H3K9me1 and -me3 in Δ*lsd1* strains. Western blot analysis of H3K9me1 in WT, Δ*dim-5*, and Δ*lsd1* cell extracts (left panel) and H3K9me3 in WT, Δ*dim-5*, Δ*dim-2*, Δ*lsd1*, and Δ*lsd1; Δdim-2* cell extracts (right panel). Cell extract from *S. cerevisiae*, which possesses no methylation on lysine 9 of histone H3, is included a negative control for H3K9me1. hH3 levels are included as a loading control for both blots.

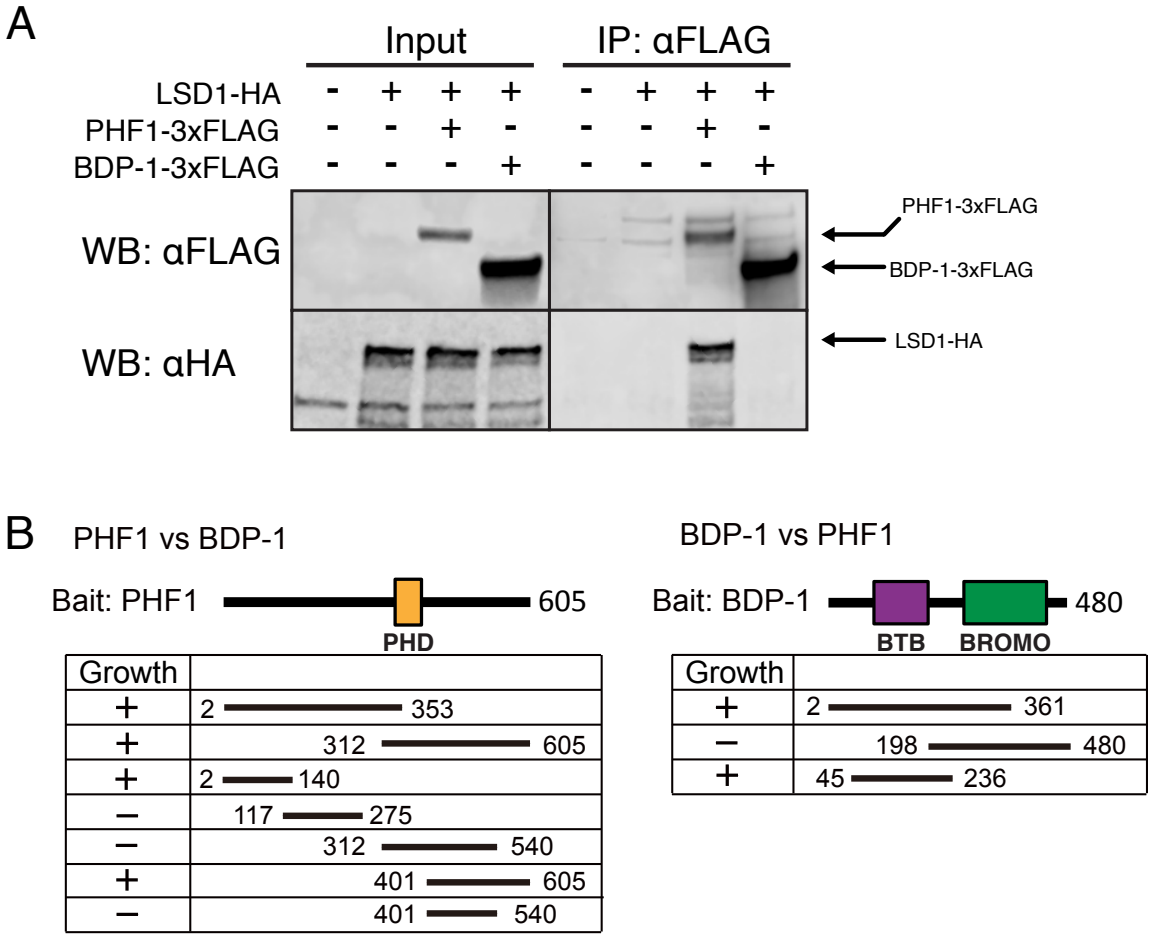

Fig. 5. Coimmunoprecipitation and yeast two-hybrid analysis of LSDC members. (A) Coimmunoprecipitation analysis of LSDC members. Pull downs were performed with antibodies to epitopes on indicated proteins. (B) Summary of results of yeast two-hybrid analysis of PHF1 and BDP-1. PHF1 fragments were fused to the GAL4 DNA binding domain and co-expressed with full length BDP-1 fused to the GAL4 activation domain (left), or full length PHF1 was fused to the GAL4 DNA binding domain and co-expressed with BDP-1 fragments fused to GAL4-activating domain (right). All constructs were co-transformed into PJ69-4A yeast, and transformants were tested on SD agar plates without Ade, His, Leu, and Ura. Growth results are at the left of each fragment schematic.

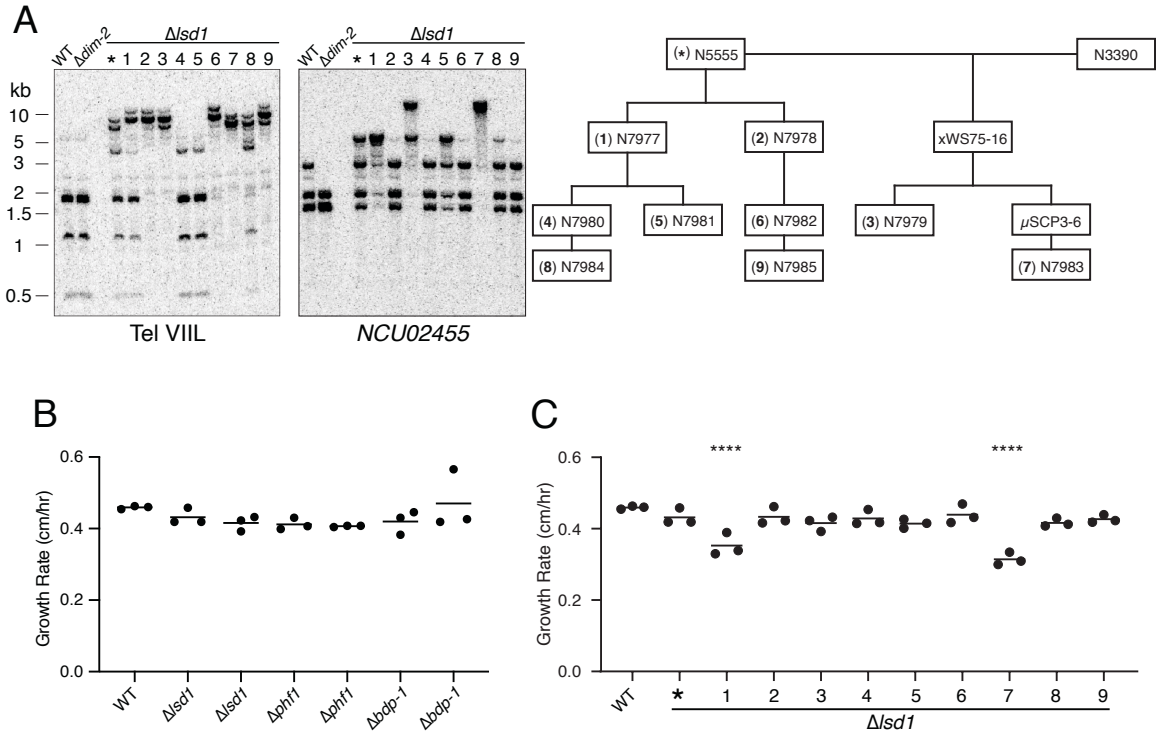

Fig. 6. Variable hypermethylation and growth rates in strains with knockouts of LSDC members. (A) DNA from asexually-propagated Δ*lsd1* strains exhibit variable hypermethylation. Genomic DNA from the FGSC knockout of *lsd1* and nine asexually-propagated strains was tested for DNA methylation by Southern hybridization, as in Figure 1C. The pedigree for these strains, relative to the initial strain (marked with an asterisk), is displayed on the right, and the pedigree provides a key to the numbers above the lanes in the Southern hybridization and to the strains in panel C. WT strain: N3753; Δ*dim-2* strain: N4711. (B) Linear growth rates of strains with LSDC member knockouts at 32˚C. Strains (left to right): N3753, N5555, N7979, N6221, N6222, N6219, and N6220. (C) Linear growth rates of asexually-propagated Δ*lsd1* strains, relative to the initial "parental" strain (N5555; indicated by an asterisk) at 32˚C. The quadruple asterisks indicate strains that grew significantly slower than the other strains ($p<0.0001$).

Fig. 7 (see next page). Δ*lsd1* strains exhibit variable extents of hyper DNA methylation. (A) WGBS tracks showing variable hyper DNA methylation in replicate bisulfite sequencing of the same Δ*lsd1* strain (red) and three different asexually-propagated Δ*lsd1* strains (black). DNA methylation-sensitive Southern hybridization analysis of Tel VIIL and NCU02455. The pedigree of the Δ*lsd1* strains is presented in Figure 6B. (B) DNA methylation-sensitive Southern hybridization analysis of LSD complex double knockouts with the indicated probes. Strains (left to right): N3753, N4711, N5555, N6414, N6416, N6272, N8109, N8110, N8111, N8112, N6271, N8105, N8106, N8107, and N8108.

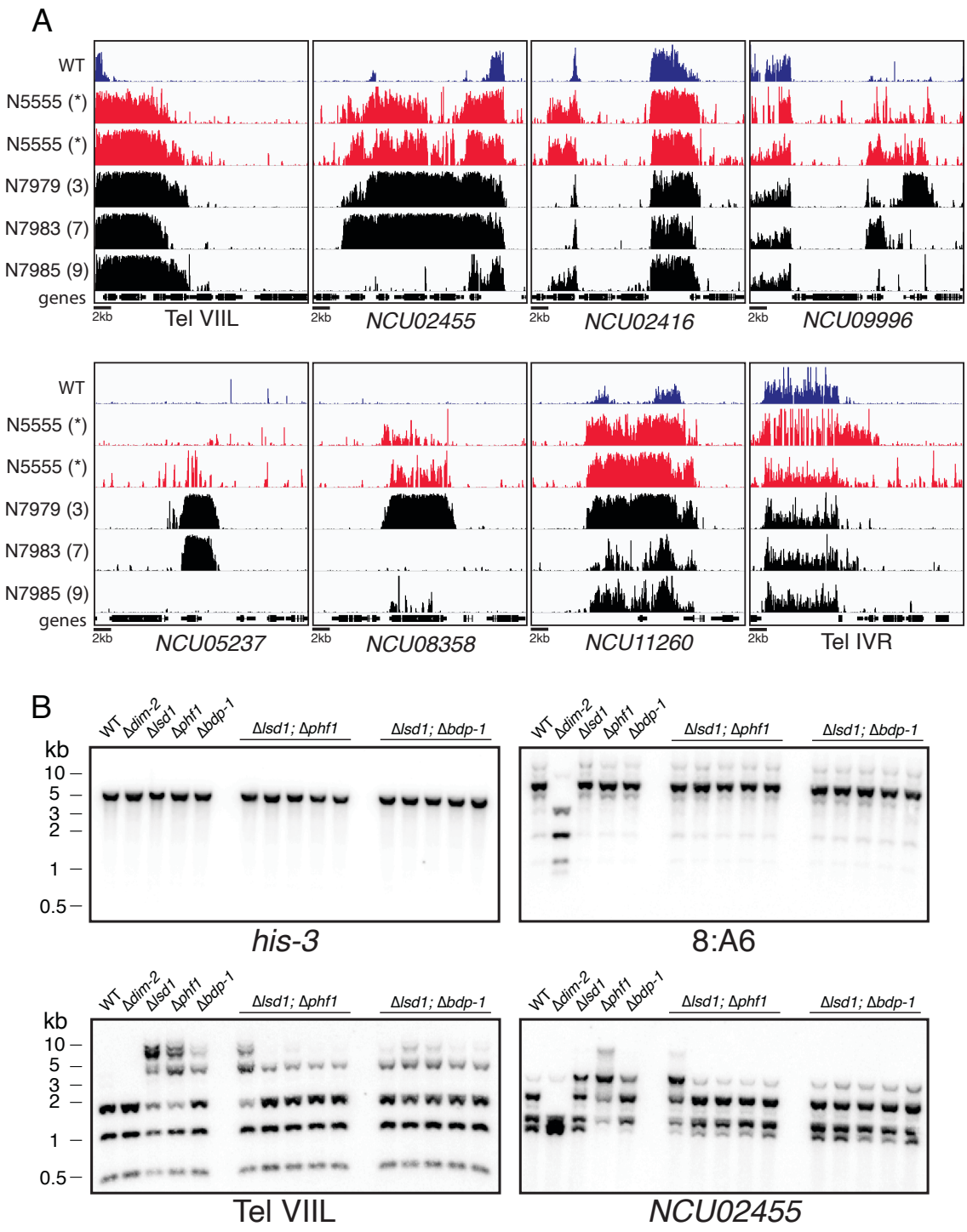
A
WT
N5555 (*)
N5555 (*)
N7979 (3)
N7983 (7)
N7985 (9)
genes
2kb
Tel VIIL
NCU02455
NCU02416
NCU09996
NCU05237
NCU08358
NCU11260
Tel IVR
B
WT
Δdim-2
Δlsd1
Δphf1
Δbdp-1
Δlsd1; Δphf1
Δlsd1; Δbdp-1
kb
10
5
3
2
1
0.5
his-3
8:A6
Tel VIIL
NCU02455

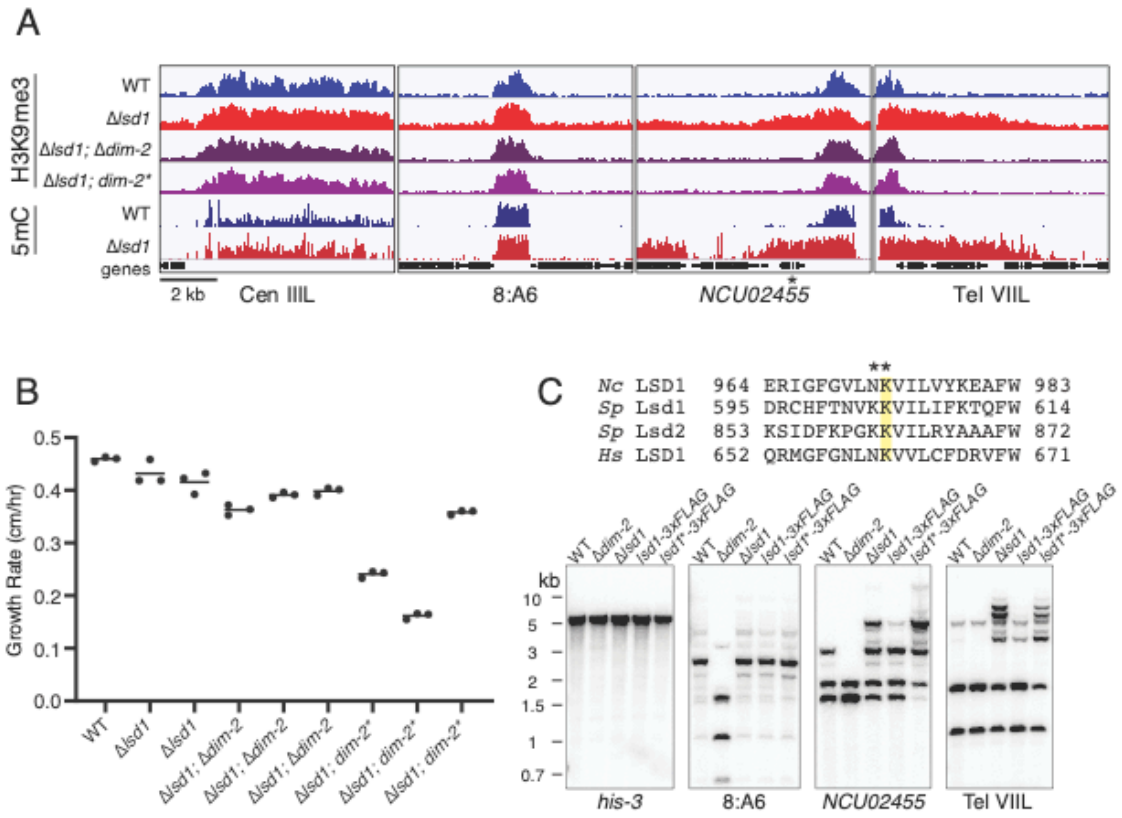

Fig. 8. LSD1 prevents DNA methylation-dependent hyper H3K9me3. (A) H3K9me3 ChIP-seq and WGBS tracks showing H3K9me3 enrichment and DNA methylation respectively at two unaffected heterochromatin regions (Cen IIIL and 8:A6) and two Δ*lsd1*-sensitive regions (NCU02455 and Tel VIIL) in the indicated strains. *dim-2** denotes the C926A catalytic-null mutation in *dim-2* (42). *NCU02455* is indicated with an asterisk. (B) Linear growth rates in WT, Δ*lsd1*, and Δ*lsd1* bearing a deletion (Δ) or catalytic-null (*) mutation in *dim-2*. Strains (left to right): N3753, N5555, N7979, N6337, N8081, N6679, N8083, and N8084. (C) Loss of LSD1 catalytic activity causes hyper DNA methylation. (Top panel) Sequence alignments of human, *S. pombe*, and Neurospora LSD1 homologs centered on a lysine essential for catalytic activity (highlighted). The NK982,983AA mutation introduced to create the presumptive catalytic-null *lsd1* Neurospora strains is displayed above. (Bottom panel) DNA methylation-sensitive Southern hybridization analysis (as in Figure 1C) on 3xFLAG-tagged and catalytic-null (indicated by *) 3xFLAG-tagged LSD1 strains. Strains (left to right): N3753, N4711, N5555, N6300, and N7899.

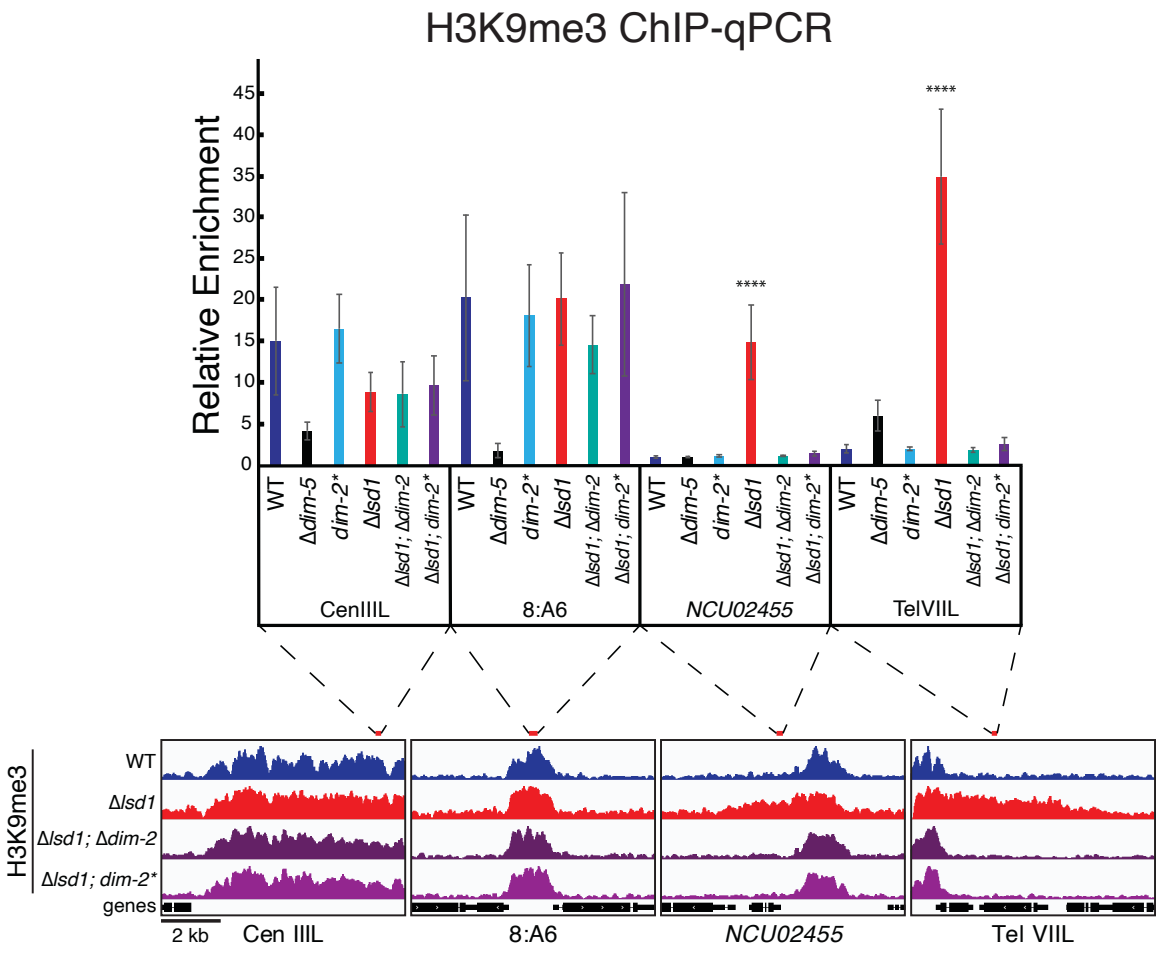

Fig. 9. Δ*lsd1* strains exhibit DNA methylation-dependent hyper H3K9me3. ChIP-qPCR validation of H3K9me3 ChIP-seq from Figure 3A. qPCR amplicons are displayed as red bars above H3K9me3 ChIP-seq tracks from Figure 3A. H3K9me3 enrichment was normalized to antibody-specific background levels at the histone H4 gene, *hH4*. Quadruple asterisks indicate p<0.0001.

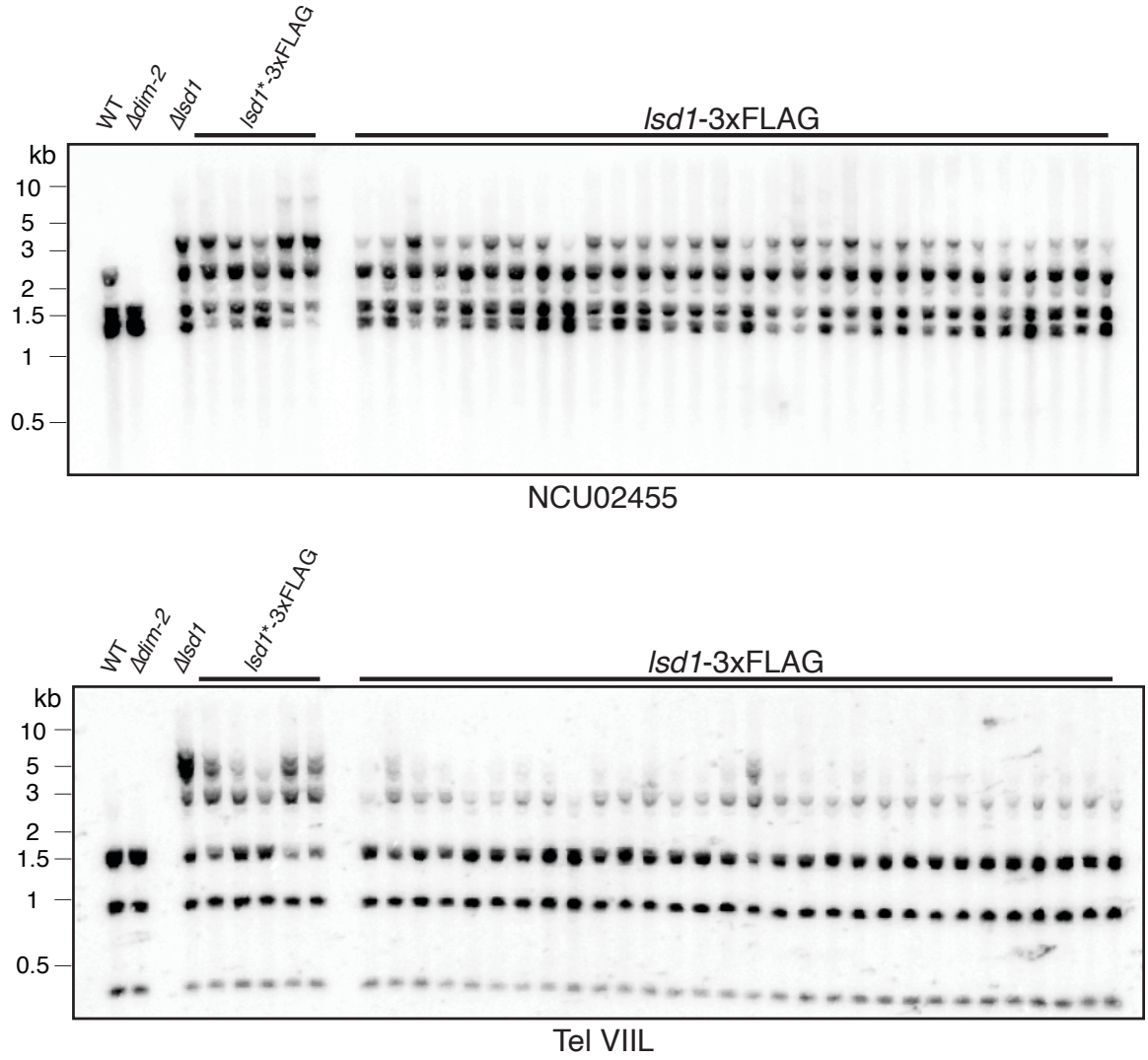

Fig. 10. *lsd1-3xFLAG* Neurospora strains exhibit slight hyper DNA methylation, but less so than catalytic-null *lsd-3xFLAG* strains. DNA methylation-sensitive Southern hybridization analysis comparing DNA methylation levels in catalytic-null LSD1-3xFLAG strains (indicated by an asterisk) and WT LSD1-3xFLAG siblings at two Δ*lsd1*-sensitive regions. Strains (left to right): N3753, N4711, N5555, N7943, N7944, N7945, N7946, N7899, N6300, N8040, N8041, N8042, N8043, N8044, N8045, N8046, N8047, N8048, N8049, N8050, N8051, N8052, N8053, N8054, N8055, N8056, N8057, N8058, N8059, N8060, N8061, N8062, N8063, N8064, N8065, N8066, N8067, and N8068.

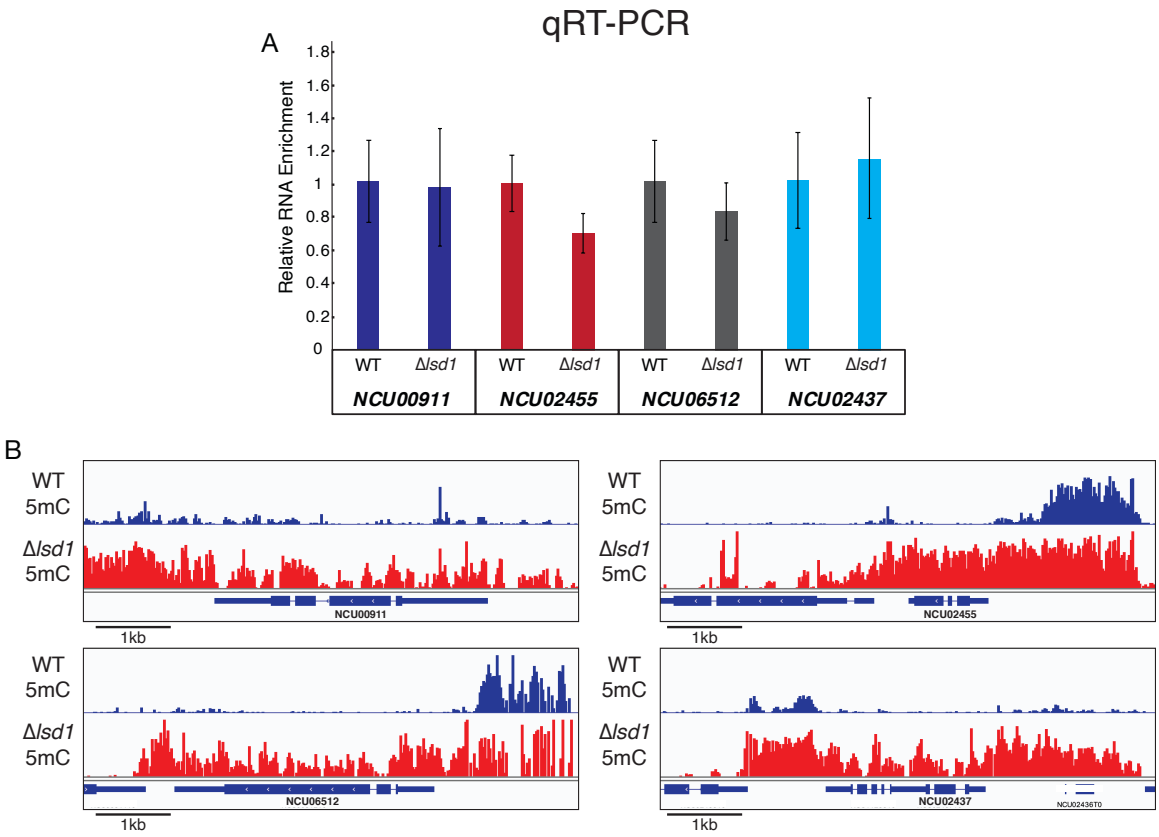

Fig. 11. Modest changes in gene expression in regions hypermethylated in Δ*lsd1* strains. (A) RT-qPCR results showing mRNA levels of indicated genes that become methylated in Δ*lsd1* methylated strains. (B) WGBS tracks showing Δ*lsd1* hyper DNA methylation (red) over the selected genes in illustrated in panel A.

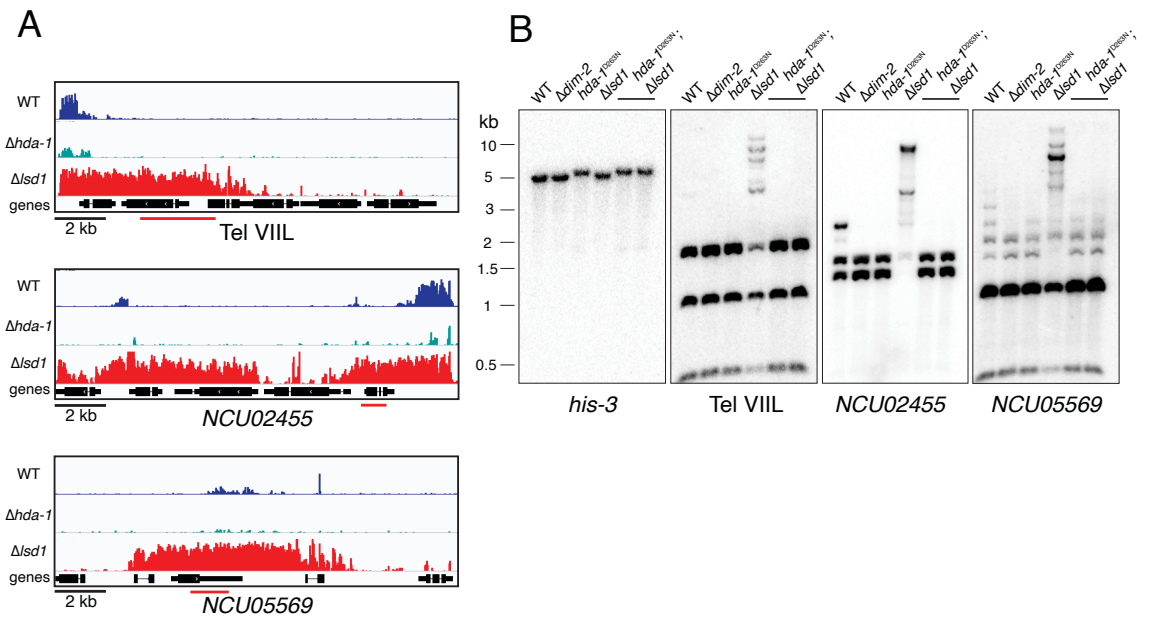

Fig. 12. HCHC catalytic activity is necessary for Δ*lsd1*-induced hyper DNA methylation. (A) WGBS tracks displaying DNA methylation in wild-type (WT), Δ*hda-1*, and Δ*lsd1* strains at selected Δ*lsd1*-sensitive regions. (B) DNA methylation-sensitive Southern hybridizations probing the regions illustrated in panel A showing the loss of Δ*lsd1*-induced hypermethylation in a *hda-1* catalytic-null background. The Southern probes used are indicated by a red bar in panel A. Strains (left to right): N3753, N4711, N3998, N6412, N8089, and N8090.

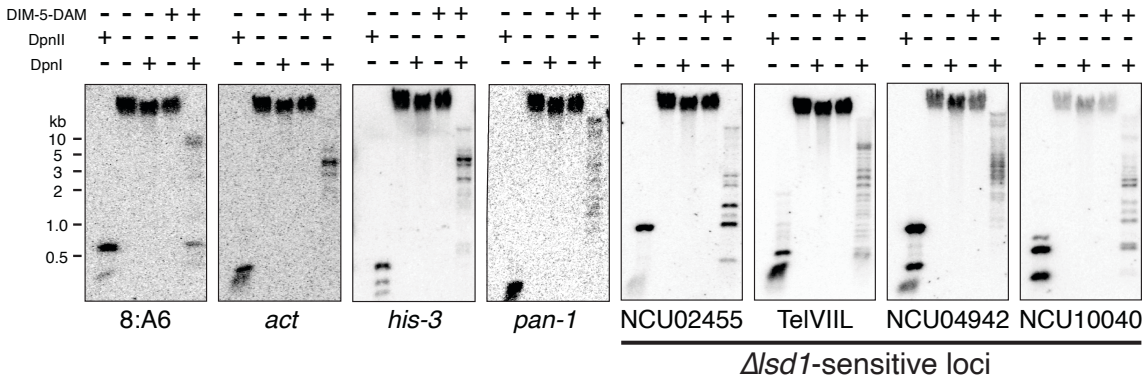

Fig. 13. DIM-5 appears constitutively localized over Δ*lsd1*-sensitive regions. Genomic DNA from strains expressing DIM-5 with or without a DNA adenine methyltransferase (Dam) moiety tag were incubated in the presence or absence of DpnI, which only cuts GATC sites when the adenine is methylated. To illustrate complete digestion, WT DNA was incubated with the adenine-methylation insensitive isoschizomer DpnII. Digested DNA was used in Southern hybridizations with probes for unaffected (8:A6, *act*, *his-3*, *pan-1*) and Δ*lsd1*-sensitive loci (NCU02455, Tel VIIL, NCU04942, NCU10040).

Fig. 14 (see next page). HCHC catalytic activity and DNA methylation become necessary for heterochromatin formation with increasingly GC-rich DNA. (A) Metaplot displaying the averaged profile of H3K9me3 enrichment in WT and Δ*hda-1* strains as determined by ChIP-seq and averaged %GC-content over all constitutive heterochromatin domains in wild-type. (B) Model showing interactions between factors involved in establishing heterochromatin with decreasing DNA AT-content. (Left) In the absence of HCHC catalytic activity, the significant AT-richness of the interior of heterochromatin domains is sufficient to recruit the histone lysine methyltransferase complex, DCDC, to establish H3K9me3 and subsequent methylation of underlying DNA. However, the abruptly decreasing AT content at heterochromatin borders is insufficient for DCDC-induced heterochromatin, and without HCHC, heterochromatin is unable to properly spread over the canonical domain. (Middle) In a wild-type scenario, HCHC is able to localize to heterochromatin boundaries through binding of H3K9me3 catalyzed by DCDC, as well as through AT-hook domains in the CHAP subunit. Histone deacetylation activity by HCHC is able to recruit DCDC to further mark H3K9me3 on neighboring chromatin and establish a propagating feedback loop capable of spreading heterochromatin across the entirety of the canonical domain. Here, factors such as LSD1 that limit heterochromatin spreading act to keep the expansion in check within proper limits of what should be heterochromatin. (Right) In the absence of such limiting factors where heterochromatin spreads over its boundary into euchromatin, or in DLDM where convergent transcription induces H3K9me3 and DNA methylation, heterochromatin is established over DNA with AT content well below the level for RIP-induced DNA methylation. Typically, DNA methylation is dependent on the H3K9me3 mark and loss of DNA methylation has no impact on H3K9me3 [5,27,28]. In instances of heterochromatin over low (~50%) AT-richness, DNA methylation now becomes essential for H3K9me3 and further spreading.

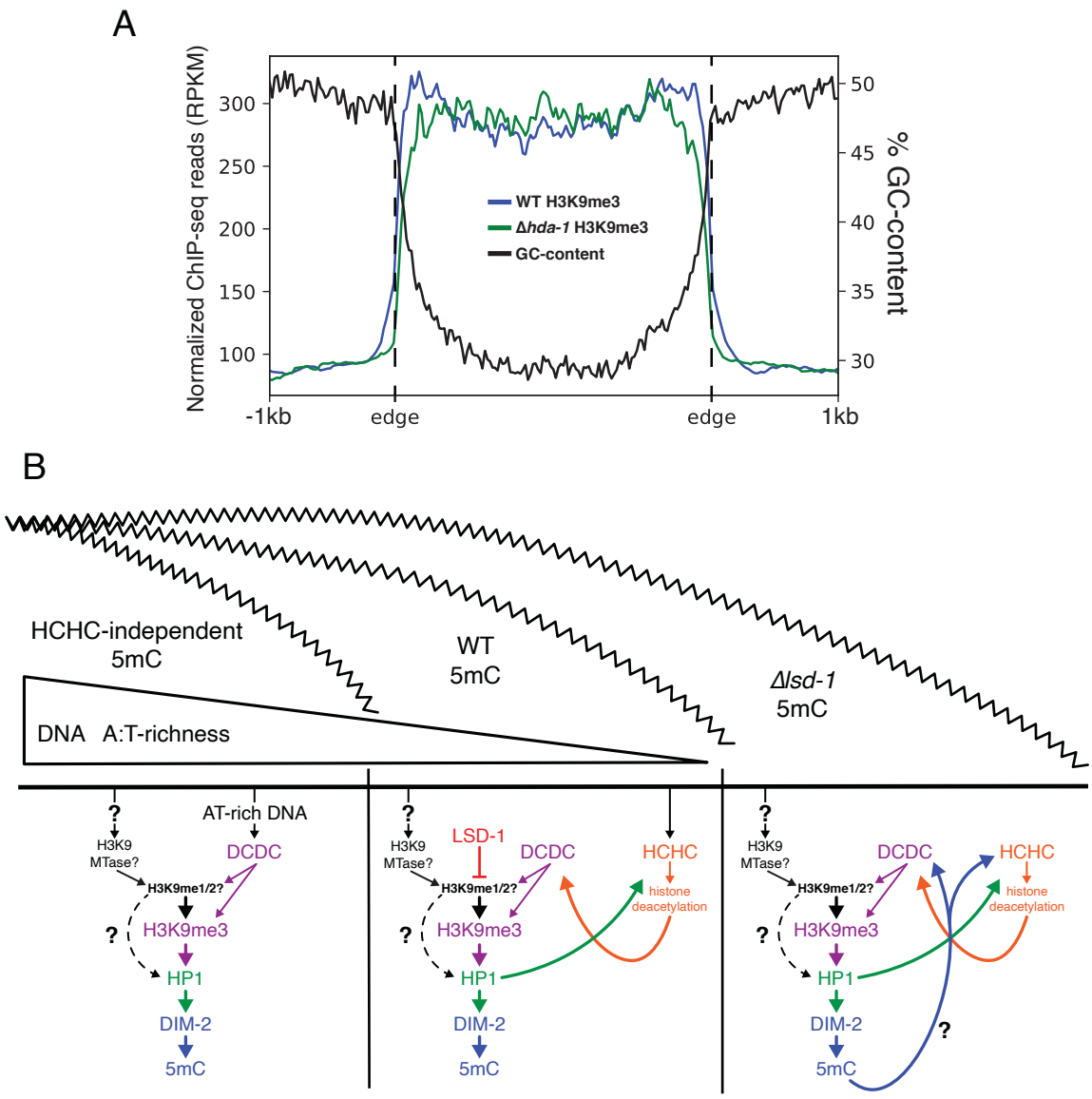
A
Normalized ChIP-seq reads (RPKM)
300
250
200
150
100
50
45
40
35
30
% GC-content
WT H3K9me3
Δhda-1 H3K9me3
GC-content
-1kb
edge
edge
1kb
B
HCHC-independent
5mC
WT
5mC
Δlsd-1
5mC
DNA A:T-richness
AT-rich DNA
H3K9
MTase?
DCDC
H3K9me1/2?
H3K9me3
HP1
DIM-2
5mC
LSD-1
HCHC
histone
deacetylation

Figures for Chapter III

Fig. 15 (see next page). A simple light-inducible system for assessing replication-independent histone turnover in *Neurospora crassa*. (A) Schematic overview of the light-inducible histone H3-3xFLAG reporter strain. (B) Expression time course analysis of H3-3xFLAG induction. H3-3xFLAG was induced with a two-minute pulse of blue light and H3-3xFLAG levels were examined at 20 minute intervals by immunoblotting. Uninduced H3-3xFLAG levels are indicated by "DD". Phosphoglycerate kinase 1 (PGK1) levels are included for each time point as a loading control.

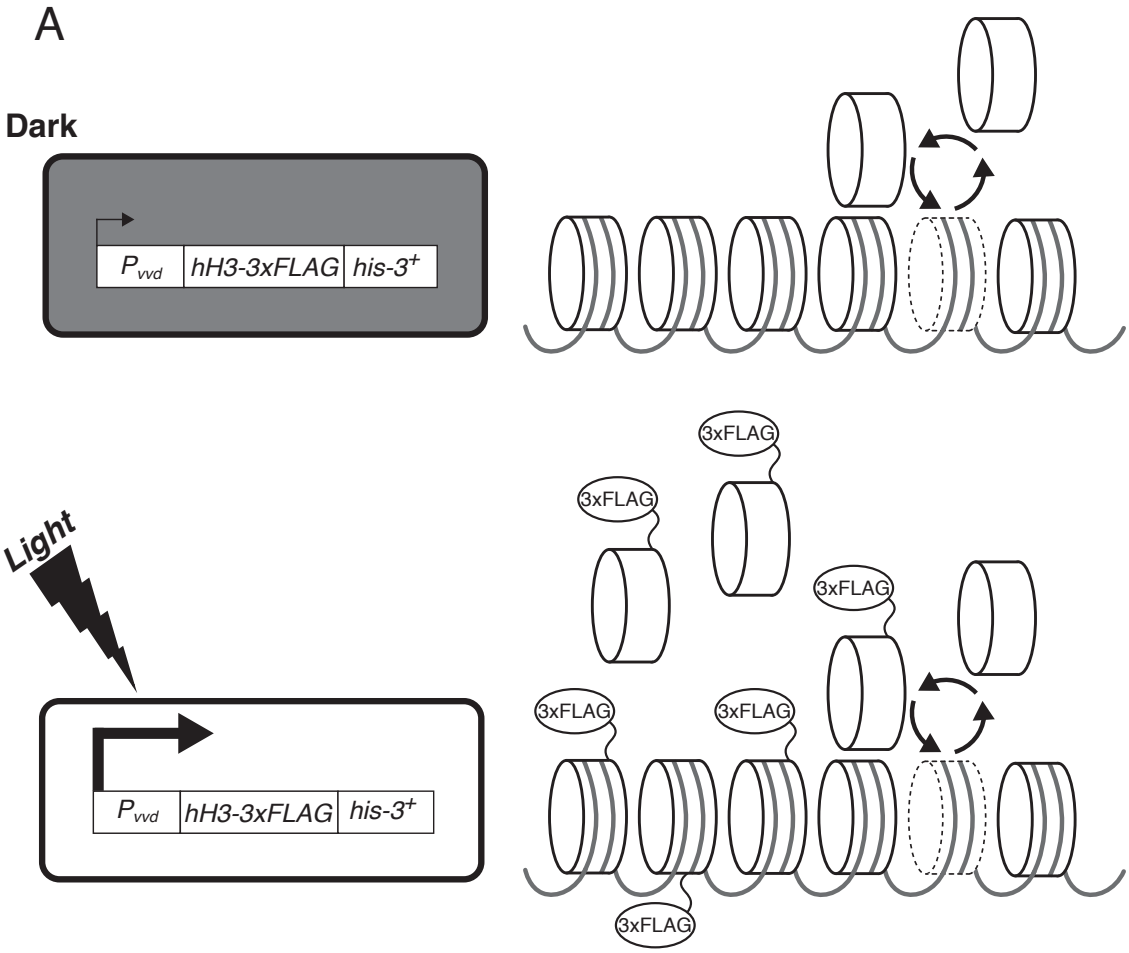
A
Dark
P_{vvd}
hH3-3xFLAG
his-3+
Light
3xFLAG
3xFLAG
3xFLAG
3xFLAG
3xFLAG
3xFLAG
P_{vvd}
hH3-3xFLAG
his-3+

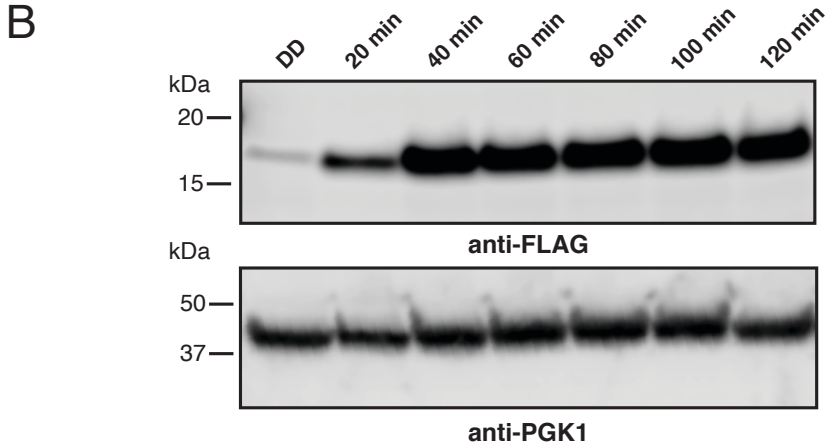
B
DD
20 min
40 min
60 min
80 min
100 min
120 min
kDa
20
15
anti-FLAG
kDa
50
37
anti-PGK1

Fig. 16 (see next page). Experimental schematic for genome-wide profiling of replication-independent histone turnover in *N. crassa*. 5 mL of Vogel's medium supplemented with 1.5% sucrose was innoculated with 5.0 x 10^6 conidia, and cultures were grown in complete darkness at 32˚C for 18 hours. To block DNA replication, cultures were treated with 100mM hydroxyurea (HU) and then induced with light, 3 hrs later. After 30 minutes to allow for incorporation of new H3-3xFLAG into chromatin, cultures were crosslinked, lysed, and the chromatin sheared. H3-3xFLAG was immunoprecipitated and the associated DNA isolated and analyzed by qPCR, or prepared for next-generation sequencing, and sequenced.

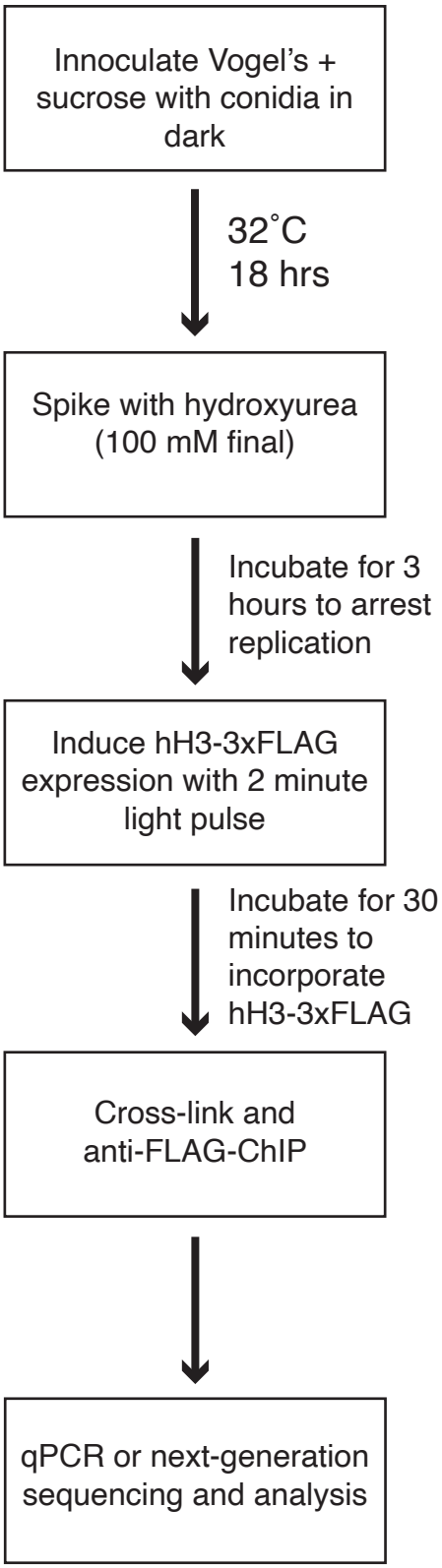
Innoculate Vogel's + sucrose with conidia in dark
32˚C
18 hrs
Spike with hydroxyurea (100 mM final)
Incubate for 3 hours to arrest replication
Induce hH3-3xFLAG expression with 2 minute light pulse
Incubate for 30 minutes to incorporate hH3-3xFLAG
Cross-link and anti-FLAG-ChIP
qPCR or next-generation sequencing and analysis

Fig. 17 (see next page). Histone turnover at representative genome regions. (A) H3-3xFLAG incorporation into chromatin increases with incubation time. qPCR analysis of FLAG ChIP (left) and hH3 ChIP (right) after 20 minutes or two hours of incorporation, at different chromatin contexts: active genes (*actin*, *fkr-5*, and *csr-1*), constitutive heterochromatin (Cen IIIL, 8:A6, and 8:F10), and facultative heterochromatin (Tel VIIL). Uninduced control levels are indicated by "DD". Data are presented as the mean and SD of three technical replicates. (B) Genome-wide profiling of histone turnover in *N. crassa*. Representative IGV tracks displaying H3-3xFLAG enrichment after 30 minutes of incorporation from replicate ChIP-seq experiments. Levels of DNA methylation (5mC), determined by bisulfite sequencing, is displayed to denote constitutive heterochromatin[3]. (C) Histone turnover meta-plot of gene expression level. Genes were divided into expression quartiles based on wild type expression levels, and H3-3xFLAG enrichment from two replicate experiments (denoted by a solid and dotted line) was aligned relative to their respective transcriptional start (TSS) and end (TES) sites, and scaled to 3 kb (number of genes in each quartile: Top 25% - 2433; 75-50% - 2432; 50-25% - 2431; Bottom 25% - 2433). H3-3xFLAG enrichment is displayed across the aligned gene bodies as well as 1 kb upstream regions for each quartile.

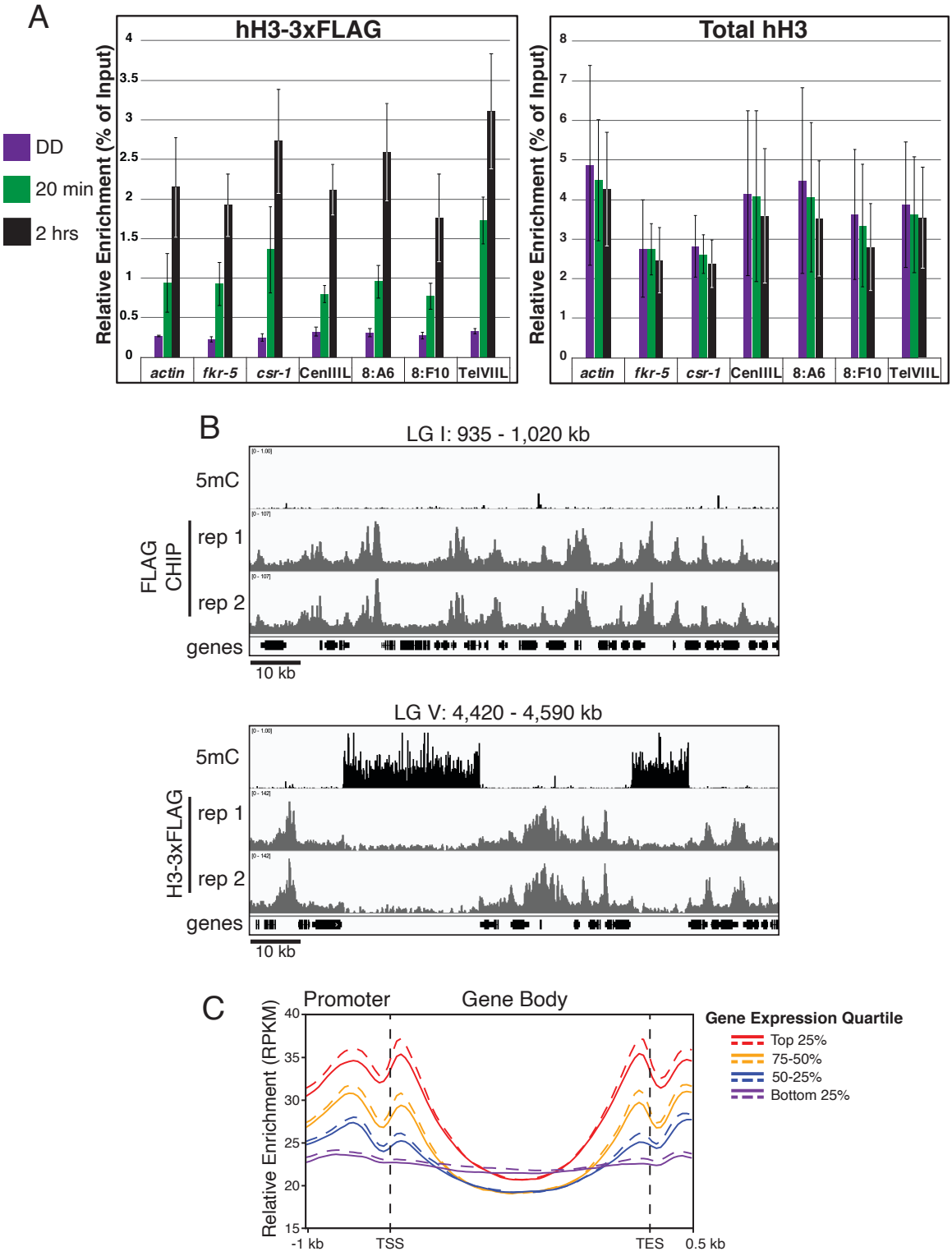
A
hH3-3xFLAG
Total hH3
Relative Enrichment (% of Input)
DD
20 min
2 hrs
actin
fkr-5
csr-1
CenIIIL
8:A6
8:F10
TelVIIL
B
LG I: 935 - 1,020 kb
5mC
FLAG CHIP
rep 1
rep 2
genes
10 kb
LG V: 4,420 - 4,590 kb
H3-3xFLAG
C
Promoter
Gene Body
Relative Enrichment (RPKM)
-1 kb
TSS
TES
0.5 kb
Gene Expression Quartile
Top 25%
75-50%
50-25%
Bottom 25%

Fig. 18 (see next page). Histone turnover at heterochromatin domains in heterochromatin mutants. (A) Representative IGV tracks displaying H3-3xFLAG enrichment in indicated heterochromatin mutants. Constitutive heterochromatin is marked by DNA methylation (5mC) and highlighted in yellow. (B) Metaplot of histone turnover at heterochromatin domains in heterochromatin mutants. Constitutive heterochromatin domains were aligned and scaled to 2.5 kb. Replicate H3-3xFLAG enrichment profiles for wild-type (black) and indicated heterochromatin mutant strains (red) are displayed over the scaled heterochromatin domains as well as 1 kb up- and down-stream from the domains.

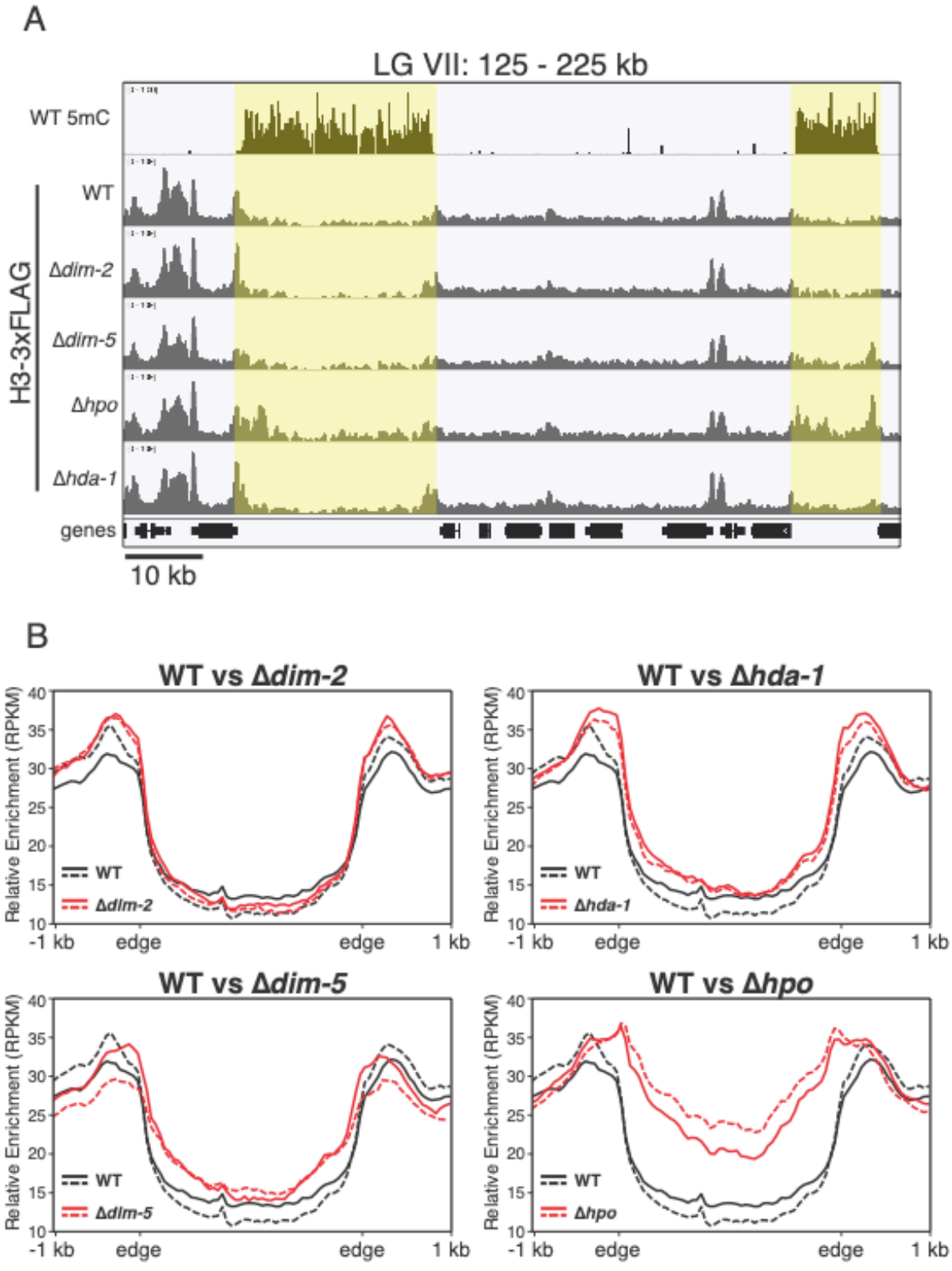
A
LG VII: 125 - 225 kb
WT 5mC
H3-3xFLAG
WT
Δdim-2
Δdim-5
Δhpo
Δhda-1
genes
10 kb
B
WT vs Δdim-2
WT vs Δhda-1
WT vs Δdim-5
WT vs Δhpo
Relative Enrichment (RPKM)
WT
-1 kb
edge
1 kb

Figures for Chapter IV

Fig. 19 (see next page). Induction of kynurenine pathway in Neurospora. (A) Kynurenine pathway with relevant Neurospora genes indicated. Activity of this pathway can be monitored by the fluorescent accumulation of anthranilic acid, which is indicated in magenta. (B) KYN-1 and IAD-1 are induced by extracelluar tryptophan. Primary transformants were cultured in the absence (Trp -) or presence (Trp +) of tryptophan, and cell lysates were probed for the indicated tagged protein by western blot. (C) Anthranilic acid accumulation is induced by supplemented tryptophan. Wild-type and Δ*tah-2* strain cultures were spiked with tryptophan, and the medium was sampled every 20 minutes from anthranilic acid fluorescence. Wild-type induction was also tested with additional tryptophan spiking every 20 minutes.

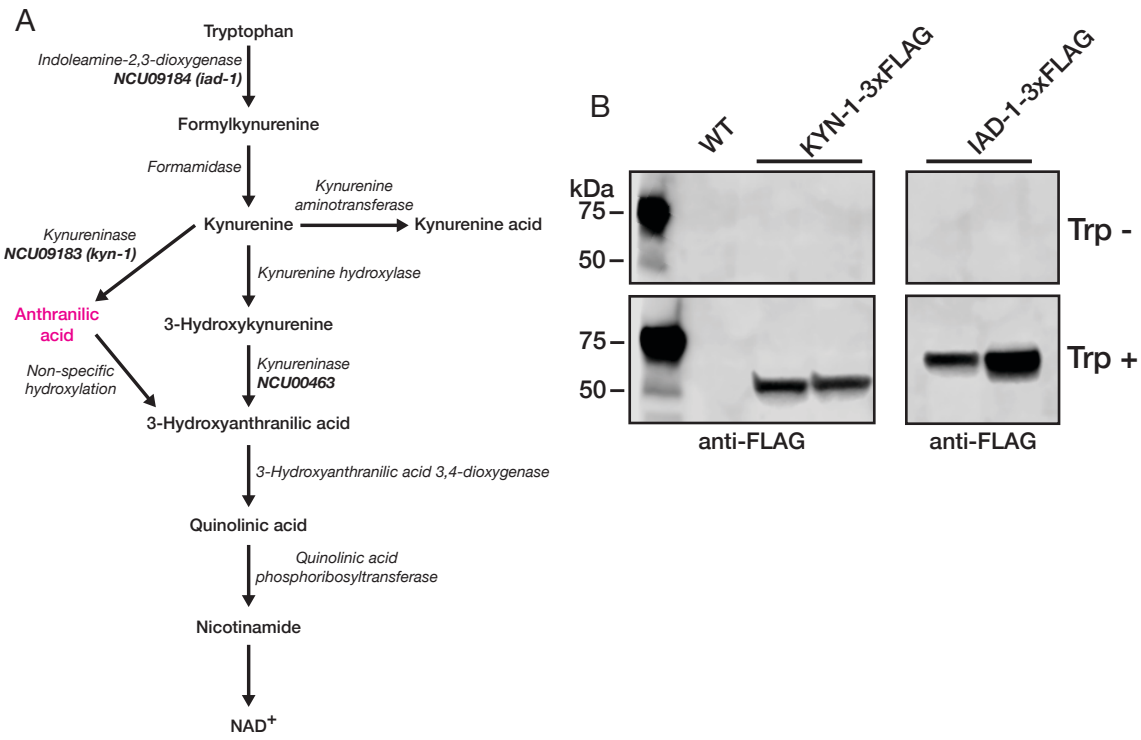
A
Tryptophan
Indoleamine-2,3-dioxygenase
NCU09184 (iad-1)
Formylkynurenine
Formamidase
Kynurenine
Kynurenine aminotransferase
Kynurenine acid
Kynureninase
NCU09183 (kyn-1)
Kynurenine hydroxylase
Anthranilic acid
3-Hydroxykynurenine
Non-specific hydroxylation
Kynureninase
NCU00463
3-Hydroxyanthranilic acid
3-Hydroxyanthranilic acid 3,4-dioxygenase
Quinolinic acid
Quinolinic acid phosphoribosyltransferase
Nicotinamide
NAD+
B
WT
KYN-1-3xFLAG
IAD-1-3xFLAG
kDa
75
50
Trp -
Trp +
anti-FLAG
anti-FLAG

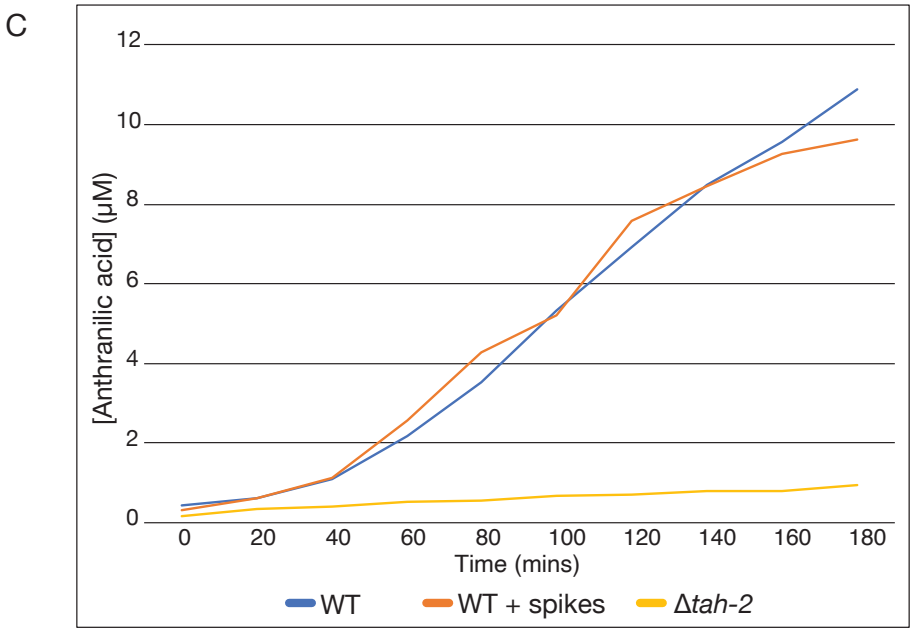
C
[Anthranilic acid] (μM)
12
10
8
6
4
2
0
0
20
40
60
80
100
120
140
160
180
Time (mins)
WT
WT + spikes
Δtah-2

Fig. 20 (see next page). Identification of *tah-2* by SNP mapping. Whole genome sequencing of non-inducible kynurenine pathway mutant genomic DNA identified a region within linkage group VII with an enrichment of Oakridge single nucleotide polymorphisms (SNPs). This region (indicated with a red asterisk) contained a premature stop codon in the putative transcription factor, TAH-2 (schematic below). Each point represents a running average of SNPs (window size = 10 SNPs; step size = 1 step).

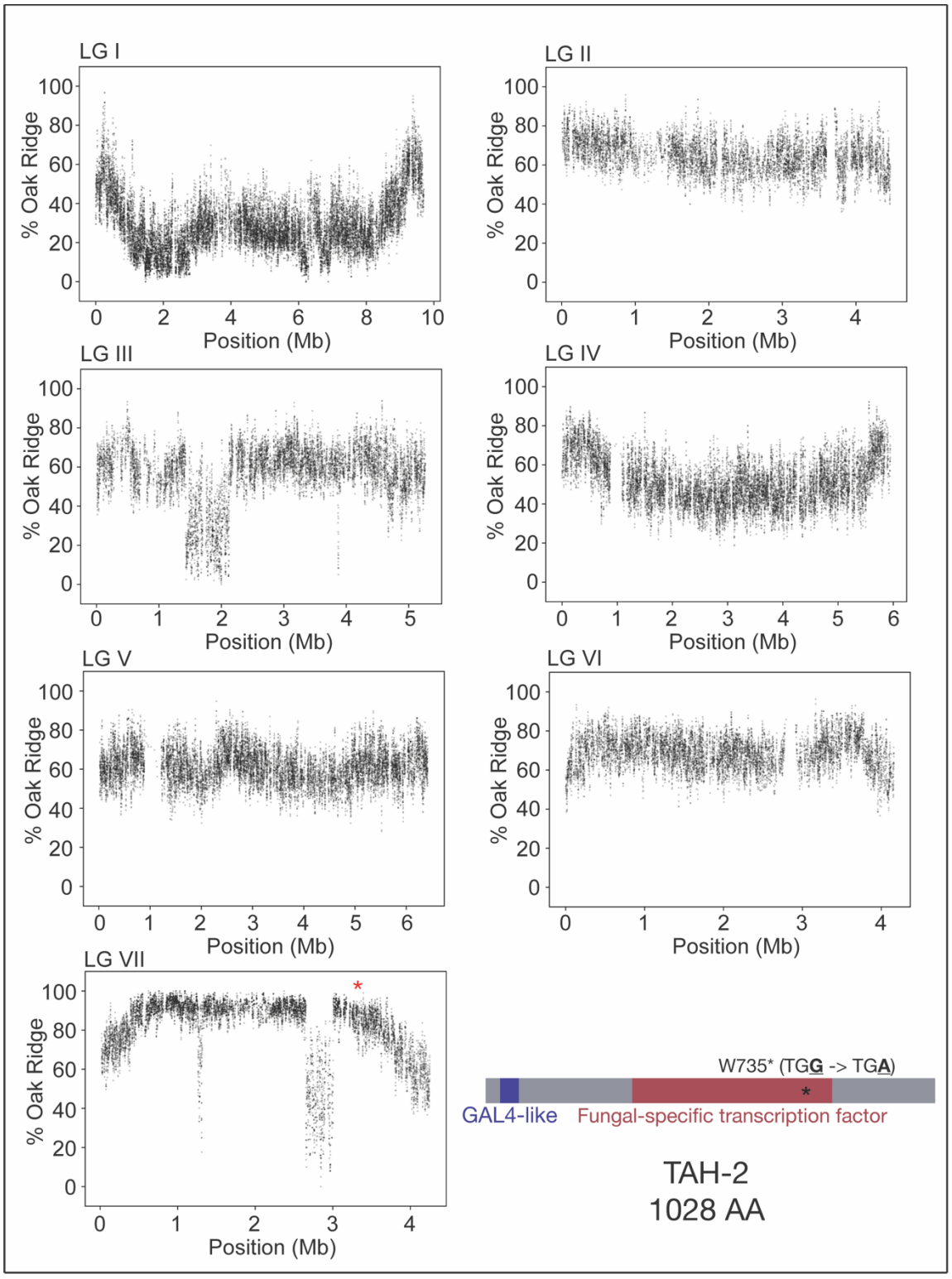
LG I
LG II
LG III
LG IV
LG V
LG VI
LG VII
% Oak Ridge
Position (Mb)
W735* (TGG -> TGA)
GAL4-like
Fungal-specific transcription factor
TAH-2
1028 AA

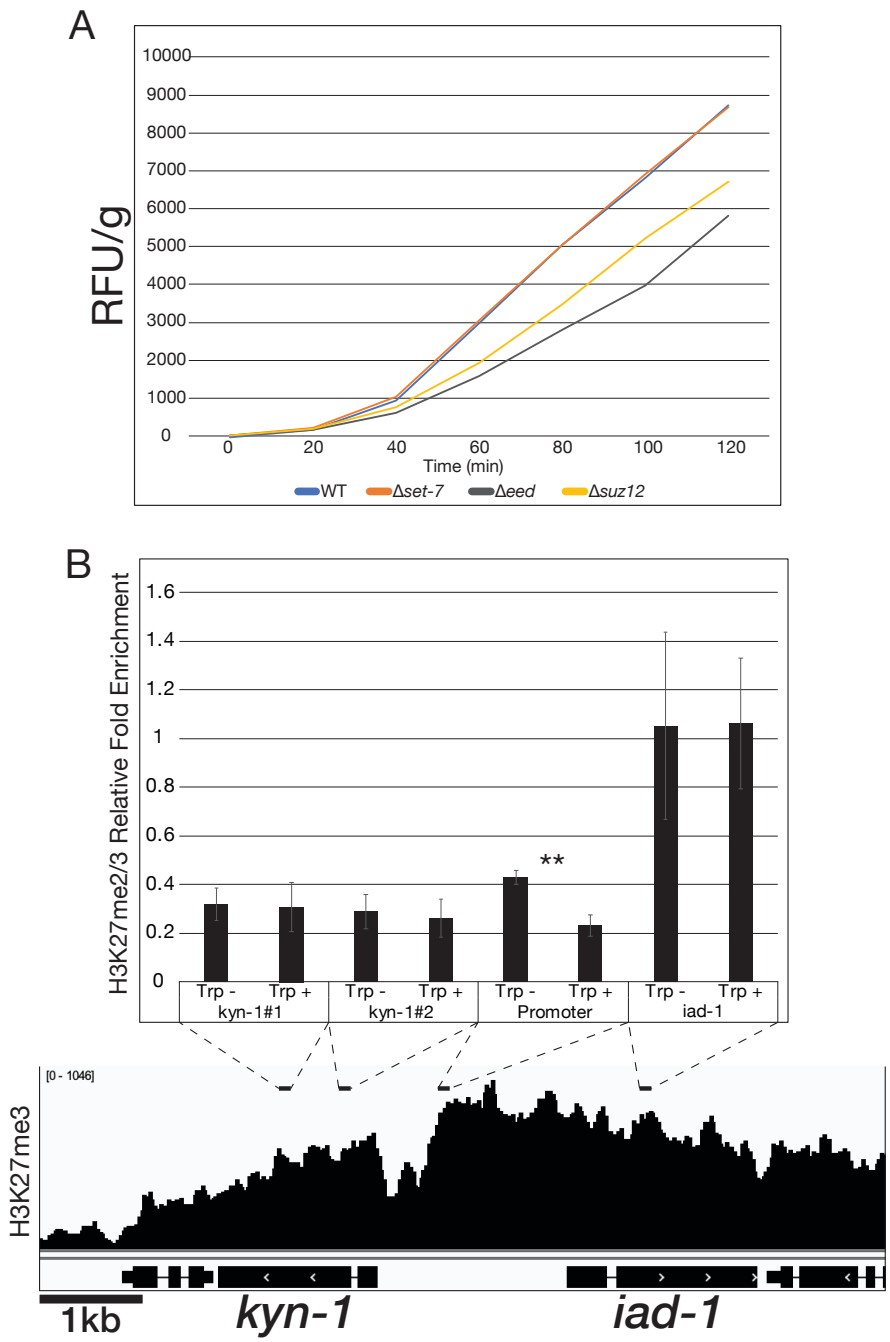

Fig. 21. Loss of H3K27me3 does not increase anthranilic acid accumulation. (A) Accumulation of anthranilic acid fluorescence does not increase in PRC2 knock out mutant strains. (B) H3K27me3 ChIP-qPCR of the *kyn-1*/*iad-1* locus in a wild-type strain under non-inducing (Trp -) or inducing (Trp +) conditions. Corresponding qPCR amplicons are indicated by a black bar above a H3K27me3 ChIP-seq track indicating H3K27me3 enrichment under non-inducting conditions. Double asterisk indicates significant reduction of H3K27me3 ($p<0.01$).

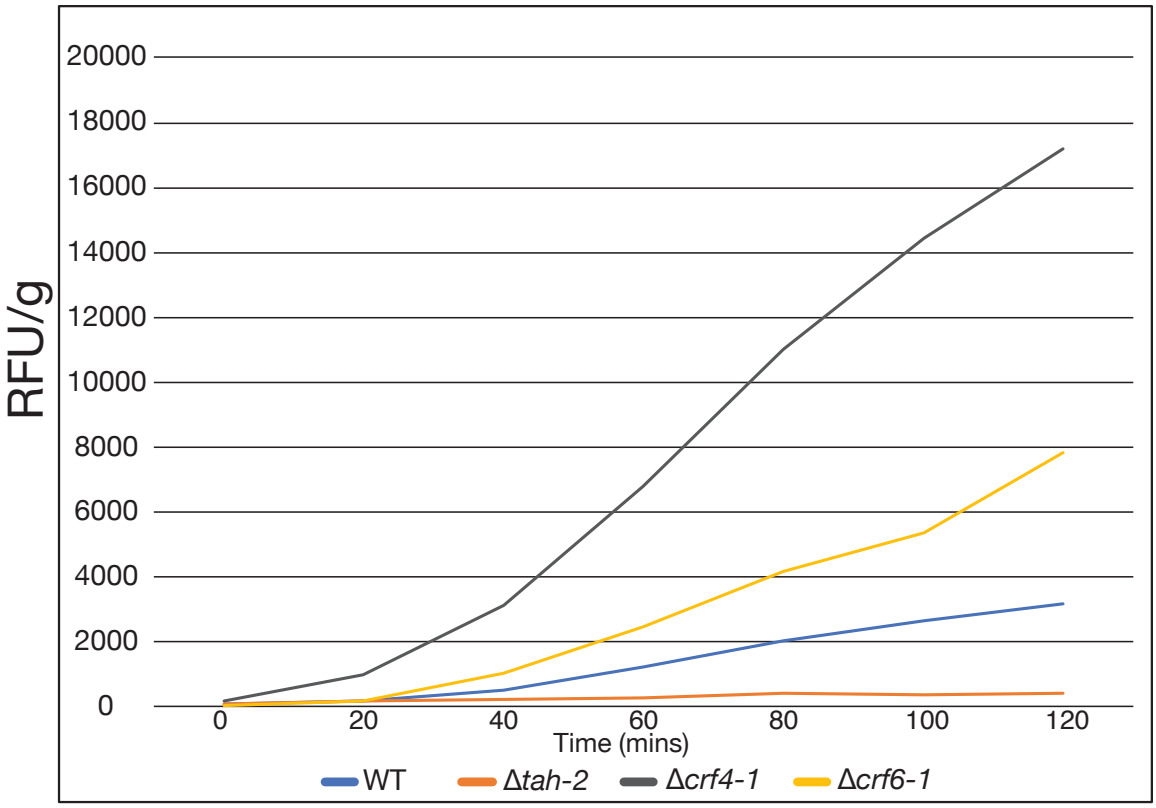

Fig. 22. Loss of chromatin remodelers increases anthranilic acid response. Accumulation of anthranilic acid fluorescence increases in chromatin remodeler knock out mutant strains.

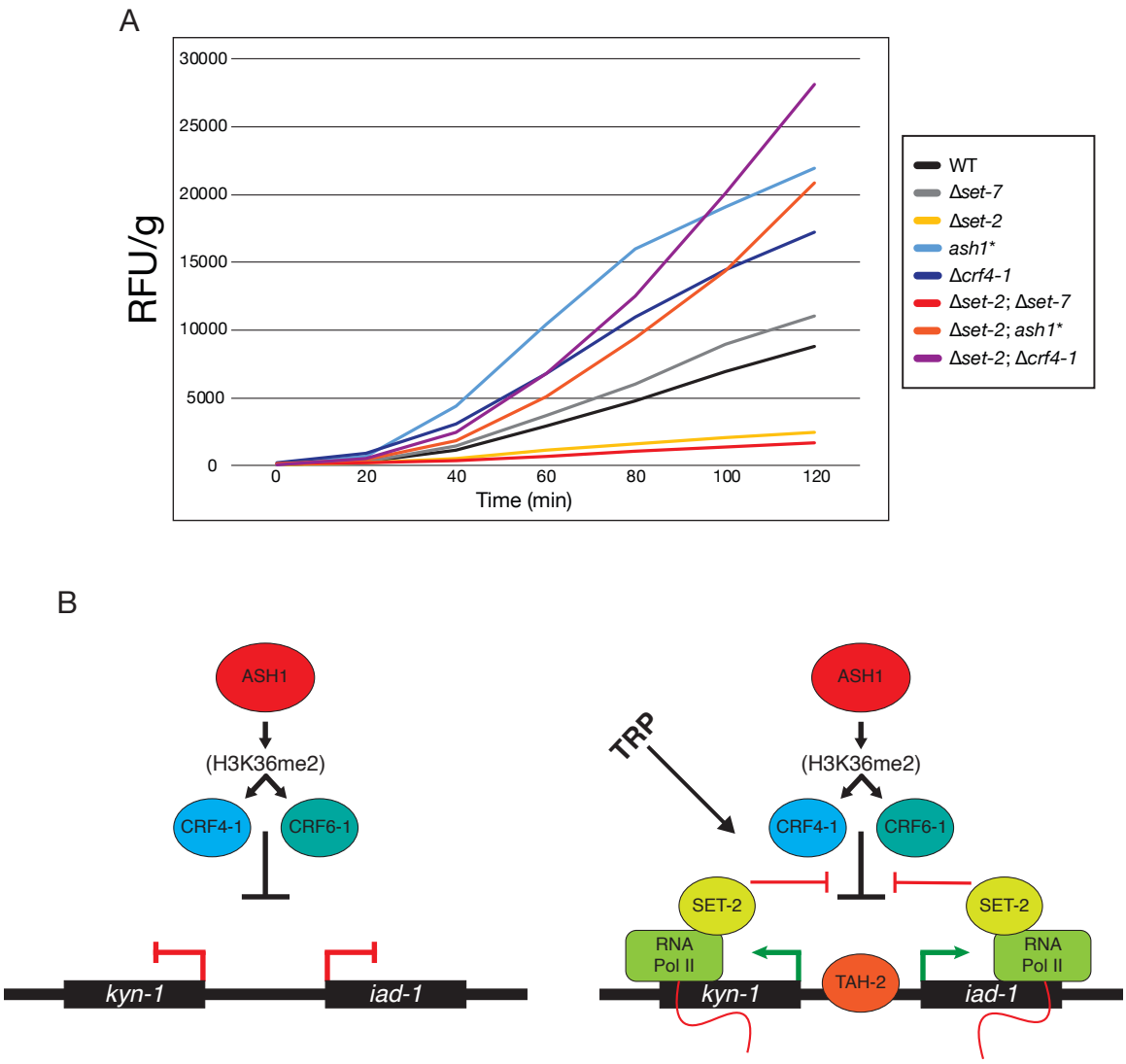

Fig. 23. Anthranilic acid response is regulated by H3K36 methyltransferases. (A) Anthranilic acid accumulation in H3K36 methyltransferase and chromatin remodeler knock out mutant strains. (B) Model for regulation of *kyn-1*/*iad-1* locus. Normally, this locus is silent in the absence of tryptophan, and ASH1 mediates silencing effected through the chromatin remodelers, CRF4-1 and CRF6-1 (left). In response to extracellular tryptophan, TAH-2 is recruited to this locus, and this repression is overcome through a SET-2-dependent manner (right). In the absence of ASH1 catalytic activity or either chromatin remodeler, SET-2 becomes dispensable for efficient induction of *kyn-1*/*iad-1*.

APPENDIX B

DATA TABLES

Table 1. LSD1-associated proteins.

Gene #	Predicted Protein	MW (kDa)	# Unique Peptides	Protein Coverage (%)
NCU01728	6-phosphofructo-2-kinase	90.463	412	64.3
NCU09602	Heat shock 70 kDa protein	70.553	37	48.3
NCU09120	**Lysine-specific histone demethylase**	**150.481**	**175**	**47.4**
NCU07830	40S ribosomal protein S14	16.019	6	47.3
NCU07297	**PHD Finger 1**	**63.895**	**76**	**46.8**
NCU06047	40S ribosomal protein S2	28.756	18	42.6
NCU08693	Hsp70-like protein	72.731	32	40.4
NCU03757	60S ribosomal protein L4-A	38.813	17	38.8
NCU02075	Heat shock protein 70	63.508	28	38.3
NCU02707	60S ribosomal protein L6	22.475	9	37.1
NCU07829	60S ribosomal protein L7	28.687	12	36.7
NCU03703	60S ribosomal protein L17	20.764	5	35.5
NCU01948	Ribosomal protein Srp1	18.214	4	34.4
NCU05554	60S ribosomal protein L13	23.876	9	33.6
NCU01827	60S ribosomal protein L27	15.722	3	32.6
NCU01452	40S ribosomal protein S1	29.068	8	32.4
NCU04173	Actin	41.607	10	31.5
NCU00489	Cytoplasmic ribosomal protein 10	28.666	8	30.5
NCU07014	40S ribosomal protein S17	16.942	4	29.5
NCU02295	Phosphatidylinositol-4-phosphate 5-kinase its3	111.877	35	29.5
NCU08620	40S ribosomal protein S16	15.723	3	28.9
NCU08500	40S ribosomal protein S8	23.011	5	28.7
NCU08809	**Bromodomain protein-1**	**53.227**	**13**	**27.3**
NCU06226	60S ribosomal protein L25	17.119	5	26.9
NCU05275	Ubiquitin-60S ribosomal protein L40	14.637	3	26.6
NCU08045	Phosphatidylethanolamine N-methyltransferase	109.551	30	26.1
NCU03102	40S ribosomal protein S11	18.428	4	26.1

NCU08389	60S ribosomal protein L20	20.343	4	25.9
NCU02003	Elongation factor 1-alpha	49.672	16	24.6
NCU02509	60S ribosomal protein L11	20.084	5	24.1
NCU06431	40S ribosomal protein S22	14.82	2	23.1
NCU08964	60S ribosomal protein L10	25.325	7	23.1
NCU04552	40S ribosomal protein S26E	13.546	2	22.7
NCU03982	Endoplasmic reticulum chaperone BiP	72.331	9	21.9
NCU03038	40S ribosomal protein S13	16.873	4	21.9
NCU01776	60S ribosomal protein L15	24.19	10	21.7
NCU03302	60S ribosomal protein L36	11.555	3	21.2
NCU01949	40S ribosomal protein S9	21.806	5	21.1
NCU02181	40S ribosomal protein S4	29.596	5	21.1
NCU06843	60S ribosomal protein L3	44.035	5	20.9
NCU02744	60S ribosomal protein L9	21.752	4	20.2
NCU07408	60S acidic ribosomal protein P0	33.534	5	20.1
NCU08269	Pyridoxamine 5'-phosphate oxidase	33.614	4	18.1
NCU03150	60S ribosomal protein L24	17.611	3	17.9
NCU01221	60S ribosomal protein L16	22.901	4	17.3
NCU00413	60S ribosomal protein L2	27.356	4	17.3
NCU06210	Uncharacterized protein	15.979	3	17.3
NCU08334	Uncharacterized protein	123.589	16	16.4
NCU08502	40S ribosomal protein S6	27.331	4	15.9
NCU09345	Thiamine biosynthesis protein NMT-1	38.198	7	15.5
NCU00634	Ribosomal protein L14	15.853	2	14.8
NCU06110	Thiamine thiazole synthase	36.864	3	14.2
NCU09468	Tubulin alpha-B chain	49.966	8	14
NCU00464	60S ribosomal protein L32	14.965	2	13.7
NCU06360	Histidinol-phosphate aminotransferase	43.583	3	13.7
NCU00294	60S ribosomal protein L10a	24.126	3	12.4
NCU04779	60S ribosomal protein L8	23.863	2	11.4
NCU05599	40S ribosomal protein S5	23.68	2	11.3
NCU04137	Vacuolar protein sorting-associated protein Vps5	64.1	6	11.2
NCU00475	40S ribosomal protein S18	17.768	2	10.9
NCU01589	Heat shock protein 60	60.489	4	10.1

Table 2. PHF1-associated proteins.

Gene #	Predicted Protein	MW (kDa)	# Unique Peptides	Protein Coverage (%)
NCU01728	6-phosphofructo-2-kinase	90.463	189	61.3
NCU09120	**Lysine-specific histone demethylase**	**150.481**	**177**	**42.1**
NCU07297	**PHD Finger 1**	**63.895**	**74**	**32.1**
NCU08693	Hsp70-like protein	72.731	16	31.6
NCU07014	40S ribosomal protein S17	16.942	4	29.5
NCU09602	Heat shock 70 kDa protein	70.553	17	28.9
NCU08809	**Bromodomain protein-1**	**53.227**	**15**	**24**
NCU01776	60S ribosomal protein L15	24.19	5	23.6
NCU07830	40S ribosomal protein S14	16.019	5	23.3
NCU03857	Isocitrate dehydrogenase [NADP]	51.848	8	20.6
NCU04173	Actin	41.607	5	19.5
NCU09345	Thiamine biosynthesis protein NMT-1, variant 2	38.198	3	19
NCU08389	60S ribosomal protein L20	20.343	4	19
NCU03150	60S ribosomal protein L24	17.611	3	18.6
NCU03757	60S ribosomal protein L4-A	38.813	5	17.7
NCU03982	Endoplasmic reticulum chaperone BiP	72.331	10	17.2
NCU03038	40S ribosomal protein S13	16.873	2	17.2
NCU03806	60S ribosomal protein L28	16.597	3	15.4
NCU05275	Ubiquitin-60S ribosomal protein L40	14.637	2	14.1
NCU07829	60S ribosomal protein L7	28.687	2	14.1
NCU02075	Heat shock protein 70	63.508	8	14
NCU02435	Histone H2B	14.841	2	13.9
NCU08045	Phosphatidylethanolamine N-methyltransferase	109.551	10	13.8
NCU02003	Elongation factor 1-alpha	49.672	10	10.9

Table 3. BDP-1-associated proteins.

Gene #	Predicted Protein	MW (kDa)	# Unique Peptides	Protein Coverage (%)
NCU08809	**Bromodomain protein-1**	**53.227**	**173**	**45.4**
NCU01728	6-phosphofructo-2-kinase	90.463	97	41.8
NCU11181	Small COPII coat GTPase sar1	21.583	4	27.5
NCU01249	Importin subunit alpha	59.696	25	25.7
NCU02003	Elongation factor 1-alpha	49.672	18	22.6
NCU02075	Heat shock protein 70	63.508	18	16.2
NCU09602	Heat shock 70 kDa protein	70.553	6	11.9

Table 4. Lysine methyltransferase KOs screened for loss of H3K9me1 in Δ*dim-5* background.

SET Domain Proteins - [117]	
NCU01206	set-1
NCU00269	set-2
NCU01932	ash1
NCU04389	set-4
NCU06119	set-5
NCU09495	set-6
NCU07496	set-7
NCU01973	set-8
NCU08733	set-9
NCU08551	hlm-1
NCU10039	set-11
NCU00970	
NCU02088	
NCU00089	
NCU06658	set-13
NCU09827	rkm-3
NCU09581	set-18
NCU02158	rkm-2
NCU04381	rkm-5
NCU02962	set-14
NCU00870	set-16
NCU08472	set-17
Non-SET Domain KMTs - [118]	
NCU06266	dot-1
NCU07459	PrmA
NCU01669	
NCU07132	PRKMT2
NCU02608	VC PKMT
NCU07181	EEF2 KMT
NCU03708	METTL21A
NCU04775	
NCU00487	METTL10
NCU02917	

NCU04602	Efm6
WRAD Complex - [119]	
NCU02104	RbBP5
NCU03037	DPY-30

Table 5. List of genes downregulated in Δ*lsd-1* (Methylated genes identified by bisulfite-seq are in yellow).

Gene#	WT FPKM	Δlsd1 FPKM	Fold Change (log_2)	P Value	Predicted Protein
NCU09968	1298.609113	1.628015575	-9.639637022	4.29E-118	Hypothetical protein
NCU05122	623.8966022	4.102681214	-7.248596084	1.67E-32	Hypothetical protein
NCU05788	754.7072016	9.963947109	-6.243055867	9.73E-32	Hypothetical protein
NCU09964	169.5522468	2.474665639	-6.098352481	7.17E-24	Hypothetical protein
NCU09969	87.48231749	1.628015575	-5.747805032	1.07E-12	Transposase of Sly1-1
NCU02919	114.8728848	3.321315703	-5.112139624	6.04E-11	cupin domain-containing protein
NCU08842	1165.895936	39.20294291	-4.894333255	1.87E-31	Hypothetical protein
NCU05852	81.2099852	4.167965767	-4.284241792	8.27E-10	glucuronan lyase-1
NCU16875	807.377254	41.67760855	-4.275898539	1.03E-22	Hypothetical protein
NCU00732	5847.188501	349.8500354	-4.062934559	1.03E-21	trichothecene C-15 hydroxylase
NCU02920	39.28880678	2.409381086	-4.027383849	9.41E-05	short-chain dehydrogenase/reductase SDR
NCU00607	4909.488324	311.8834007	-3.976493996	5.17E-67	Hypothetical protein
NCU01958	25.17856627	1.628015575	-3.951009728	0.003347461	mating-type protein A-1
NCU02061	59.5929699	4.037396661	-3.883644909	9.47E-07	Hypothetical protein
NCU09278	1080.307022	81.27225877	-3.732534581	3.44E-52	oxidoreductase
NCU09424	307.546009	26.11353375	-3.557932649	7.04E-24	Hypothetical protein
NCU07138	304.3823196	26.24410286	-3.535819375	1.27E-23	Hypothetical protein
NCU02918	46.56120666	4.102681214	-3.504489483	6.29E-05	polyketide synthase 6
NCU02022	101.0061937	9.182581598	-3.45940014	1.05E-09	Hypothetical protein
NCU04928	1154.74088	109.0790927	-3.404122643	3.12E-47	Hypothetical protein
NCU10040	4303.169207	419.1670244	-3.35980244	5.90E-28	Hypothetical protein
NCU09698	188.8680239	18.95067505	-3.317057323	2.79E-15	Hypothetical protein
NCU01957	123.8326353	12.95884005	-3.256383085	1.26E-10	AR2
NCU09639	83.66553563	9.963947109	-3.069844187	2.68E-07	Hypothetical protein
NCU02296	784.8286074	95.92234983	-3.032438723	1.06E-17	Allantoinase
NCU09357	772.8077392	94.75337525	-3.027860302	1.58E-33	stage V sporulation protein K
NCU09356	673.2386795	82.8349898	-3.022805865	3.09E-31	Hypothetical protein
NCU07767	25.26364323	3.25603115	-2.955876296	0.014934947	Hypothetical protein
NCU08037	38.19198066	4.949331278	-2.947964225	0.00131088	Hypothetical protein
NCU07736	964.0395692	127.6360113	-2.917056934	2.26E-34	Pep5 homolog
NCU05569	388.4156863	54.24474128	-2.840046278	9.84E-21	Hypothetical protein
NCU05980	34.92486542	4.949331278	-2.818949041	0.003377901	serine protease-13

NCU05948	181.5864496	27.34984201	-2.731052145	1.92E-11	Hypothetical protein
NCU08545	73.74908254	11.20025537	-2.719093476	1.33E-05	Hypothetical protein
NCU08535	958.0141475	146.3908327	-2.71022175	1.02E-09	acetyl-CoA carboxylase-1
NCU08674	1820.530339	281.2529381	-2.694418711	2.35E-37	Pentatricopeptide repeat protein
NCU09441	32.0164069	4.949331278	-2.693505892	0.007623791	Hypothetical protein
NCU07468	1446.764531	234.823901	-2.623178972	8.60E-34	NAD-epimerase/dehydratase-1
NCU00866	1356.289532	222.5790928	-2.607275199	1.12E-32	DUF1275 domain-containing protein
NCU07547	73.31703042	12.30804364	-2.574546889	3.06E-05	phosphoprotein P0-2
NCU09638	43.33078913	7.293427812	-2.570723585	0.002132984	polyketide synthase 5
NCU09640	66.37576398	11.39610903	-2.542115232	0.000129153	MFS toxin efflux pump
NCU08223	193.979309	33.86190431	-2.51816776	1.15E-06	Hypothetical protein
NCU00721	359.909944	63.03766468	-2.513349969	1.00E-16	proline-specific permease
NCU08191	73.54223091	12.8935555	-2.511922789	4.33E-05	Hypothetical protein
NCU06043	1115.716534	197.5712982	-2.497525251	9.59E-09	GPR/FUN34 family protein
NCU06341	199.5293136	35.49196901	-2.491036195	3.81E-11	MFS transporter
NCU03887	2343.042943	421.0746203	-2.476235569	1.29E-34	carbon catabolite regulation-3
NCU05723	1946.064513	356.7333137	-2.447641683	9.65E-33	kinetochore protein-11
NCU06468	302.8417598	55.87480598	-2.438294335	2.65E-14	midasin
NCU06666	2462.144605	455.7076446	-2.433735018	8.60E-34	inositol-3-phosphate synthase
NCU10610	55.73031591	10.48417441	-2.410249073	0.000691106	Hypothetical protein
NCU06140	60.49211881	11.52667813	-2.391770391	0.003469222	Hypothetical protein
NCU04435	317.6668066	60.56299904	-2.391005795	2.50E-14	general amino acid permease AGP3
NCU03257	3719.436454	719.048313	-2.370923436	2.44E-34	ammonium transporter MEP1
NCU01400	719.5671643	140.3969485	-2.357617775	1.14E-21	Hypothetical protein
NCU08968	29.5700309	5.795981342	-2.351010895	0.022199811	dimethyladenosine transferase
NCU03321	158.5623307	31.12814959	-2.34875835	2.88E-07	ribosome biogenesis-59
NCU04923	1065.752249	210.3383828	-2.341088055	1.88E-12	Gld1
NCU02802	377.1772067	74.88871646	-2.332422226	3.36E-15	mitochondrial ornithine carrier protein
NCU08595	131.7280972	26.17881831	-2.33109122	1.98E-07	ribosome biogenesis-49
NCU04656	6063.223324	1211.708776	-2.32304196	2.02E-35	MFS transporter
NCU10732	1056.940942	211.9623002	-2.318015173	2.05E-24	mitochondrial dicarboxylate transporter
NCU07307	3385.377427	681.9529179	-2.311572641	1.70E-12	fatty acid synthase beta subunit dehydratase
NCU16445	1169.802809	236.3377405	-2.307343424	3.58E-07	Hypothetical protein

NCU08793	1489.572378	304.8979535	-2.288499853	3.46E-27	Hypothetical protein
NCU05277	266.4130323	55.02815591	-2.27542277	5.81E-12	Hypothetical protein
NCU04058	316.0136466	65.31647666	-2.274467985	2.90E-13	bZip transcription factor, putative
NCU01209	46.7105046	9.702808898	-2.267272667	0.003351954	Hypothetical protein
NCU04880	66.44915938	13.80549011	-2.267008842	0.00033323	Hypothetical protein
NCU08137	5388.870434	1122.479999	-2.263293162	2.96E-33	Hypothetical protein
NCU02051	621.3293056	129.9801078	-2.257067252	6.09E-19	Hypothetical protein
NCU02850	50.63988671	10.68002807	-2.245358739	0.002181528	alcohol dehydrogenase-4
NCU03396	415.5301668	87.65375197	-2.245065467	2.78E-15	nucleolar protein nop-58
NCU07607	551.3903376	116.7601295	-2.23952627	1.70E-16	sugar transporter-16
NCU00821	194.8550948	41.35118578	-2.236401048	3.14E-09	sugar transporter-15
NCU03154	1124.758	238.922484	-2.235000098	1.45E-23	Pantothenate kinase
NCU04307	221.6109186	47.08188257	-2.234785051	4.25E-10	phenylalanine-7
NCU02369	12094.58684	2581.25601	-2.228216346	2.30E-06	Polygalacturonase
NCU00337	38.41051385	8.205362428	-2.226862301	0.010800571	nuclear export protein Noc3
NCU03646	3893.578696	839.8215372	-2.212942095	3.19E-23	Hypothetical protein
NCU08287	1465.328005	316.6266327	-2.210369123	8.65E-13	pyrABCN
NCU10895	403.1256258	87.39261376	-2.205646239	1.12E-14	mutS ortholog 4 protein
NCU09990	33.53611071	7.293427812	-2.201046459	0.019902591	Hypothetical protein
NCU07308	2147.106919	467.1792838	-2.200345827	5.02E-11	fatty acid synthase alpha subunit reductase
NCU07034	298.4177576	65.31852579	-2.191769252	8.65E-12	Hypothetical protein
NCU01595	37.35289257	8.205362428	-2.186581005	0.014009037	rRNA maturation-11
NCU04205	1214.158682	267.3944581	-2.182915514	9.67E-10	aspartyl protease-17
NCU01066	43.8112205	9.702808898	-2.174826043	0.0064656	L-amino acid oxidase
NCU05045	59.06415926	13.08940915	-2.173882977	0.001144557	MFS monocarboxylate transporter
NCU04931	2107.870596	468.8664365	-2.168537388	7.65E-27	Hypothetical protein
NCU07656	36.51129735	8.140077876	-2.165228431	0.015486455	Hypothetical protein
NCU08397	1219.390089	272.1397393	-2.163740178	2.87E-23	Hypothetical protein
NCU03963	141.1065653	31.84423054	-2.147681196	5.30E-07	5'-methylthioadenosine phosphorylase
NCU05089	256.2321739	58.0883334	-2.141131296	1.27E-10	MFS monocarboxylate transporter
NCU08358	521.3123521	118.3269588	-2.139369239	3.03E-07	Hypothetical protein
NCU06720	469.3179012	106.8655652	-2.134768435	2.59E-13	serine protease-11
NCU10009	703.2591114	161.432631	-2.123124113	4.52E-18	ATP-binding cassette transporter
NCU09267	2023.443583	466.3408302	-2.11735597	2.51E-12	copper radical oxidase
NCU06409	50.49976319	11.65724724	-2.115049474	0.018446542	ribosome biogenesis-51
NCU01070	187.5434901	43.49942866	-2.108156829	3.04E-08	Hypothetical protein

NCU12050	71.86154759	16.7350985	-2.102342963	0.000574717	Hypothetical protein
NCU02188	97.04928829	22.7269335	-2.094314596	4.50E-05	arabinose-proton symporter
NCU01195	3242.903706	762.0927989	-2.089247597	7.63E-27	Glu/Leu/Phe/Val dehydrogenase
NCU08976	2072.168412	490.1082183	-2.079969017	2.69E-12	fatty acid metabolism-1
NCU09045	279.1828973	66.03255762	-2.079961133	1.13E-10	heterokaryon incompatibility-16
NCU04583	148.8986014	35.2308308	-2.079419801	5.50E-07	acetyltransferase
NCU05235	143.932454	34.12304252	-2.076573735	1.11E-06	ribosome biogenesis protein RLP24
NCU07449	37.80580067	9.052012493	-2.062297128	0.017756085	Hypothetical protein
NCU05153	395.3702874	95.01451346	-2.056984648	4.40E-08	carbohydrate O-acetyltransferase
NCU00777	64.37312166	15.49879024	-2.054302821	0.001321596	Methyltransferase
NCU02653	40.55327969	9.833378004	-2.044059588	0.013287485	allantoate permease
NCU05629	54.86119741	13.35054737	-2.038887218	0.002660797	Hypothetical protein
NCU02729	86.84090661	21.29477158	-2.027875533	0.00017198	transducin family protein
NCU09465	59.03663598	14.58685562	-2.01694159	0.002660797	diphthamide biosynthesis protein 3
NCU09841	154.6512974	38.35629284	-2.011483742	8.75E-07	phosphotyrosine protein phosphatase
NCU01083	135.9585824	33.79866888	-2.00812889	2.52E-06	S-adenosylmethionine decarboxylase
NCU01611	977.4291351	243.0884006	-2.007511055	1.36E-18	carnitine-1

Table 6. List of genes upregulated in Δ*lsd1*.

Gene#	WT FPKM	Δ*lsd1* FPKM	Fold Change (log2)	P Value	Predicted Protein
NCU08570	2.020991173	26.89489927	3.73419766	0.000472711	Hypothetical protein
NCU07822	15.45061596	190.932765	3.627328438	9.84E-21	Hypothetical protein
NCU09685	8.603600908	86.34806091	3.32715127	1.92E-07	Hypothetical protein
NCU08271	56.29582425	458.4454975	3.025650409	2.01E-27	guanine triphosphate binding-15
NCU04697	9.585319651	72.6731399	2.922523792	1.95E-06	cyanide hydratase
NCU04407	54.69104348	338.0437769	2.627833595	3.96E-12	RNA methyltransferase-5
NCU07497	104.7078682	608.5493532	2.539004414	7.52E-24	Hypothetical protein
NCU07938	117.2199952	678.3786605	2.532872105	0.022071512	MFS transporter
NCU04823	528.4854863	2818.412899	2.414947226	0.000877967	alcohol dehydrogenase-12
NCU07111	166.2067219	840.9556766	2.339051034	3.01E-13	metallo-beta-lactamase-2
NCU00578	29.22054861	138.8995021	2.248986257	6.17E-06	peptidyl-prolyl cis-trans isomerase-like 1
NCU04237	565.7933057	2599.938824	2.200130665	5.93E-27	phosphopantothenoylcysteine decarboxylase
NCU03109	14.6574	65.57761488	2.161574216	0.002772376	Hypothetical protein
NCU06513	81.33175987	362.5925305	2.156458469	1.30E-13	Hypothetical protein
NCU06974	508.5207769	2236.773077	2.137040275	2.74E-17	histidinol-phosphatase
NCU01058	12.99506554	56.32974872	2.115933126	0.000997833	Hypothetical protein
NCU07995	8.074790268	33.79661976	2.065382266	0.014600114	Hypothetical protein

APPENDIX C

STRAIN TABLES

All strains are *N. crassa*

Chapter II

Strains	Genotype	Source
N150	*mat A*	FGSC#2489
N625	*mat a his-3*$^{-}$	FGSC#6524
N1909	*mat a his-3::*P_{qa}*::dim-2*^{C926A}*; Δdim-2::hph*	Kouzminova and Selker, 2001
N2930	*mat A his-3*$^{-}$*; Δmus-52::bar*$^{+}$	Honda et al., 2008
N3435	*mat A his-3*$^{-}$*; Δhda-1::hph*	Honda et al., 2016
N3752	*mat A*	FGSC#2489
N3753	*mat a*	FGSC#4200
N3944	*mat A; Δdim-5::bar*	Lewis et al., 2010
N3998	*mat A his-3::*P_{hda-1}*::hda-1*^{D263N}*-3xFLAG; Δhda-1::hph*	Honda et al., 2016
N4711	*mat A his-3*$^{-}$*; Δdim-2::hph*	This Study
N5555	*mat a Δlsd1::hph*	FGSC#11964
N5637	*mat A his-3*$^{-}$*; dim-5-Dam::hph*	This Study
N6220	*mat A; Δbdp-1::hph*	FGSC# 11957
N6221	*mat a; Δphf1::hph*	FGSC# 14344
N6271	*mat ? Δlsd1::hph; Δbdp-1::hph*	This Study
N6272	*mat ? Δlsd1::hph; Δphf1::hph*	This Study
N6300	*mat A his-3*$^{-}$ *lsd1-3xFLAG::hph*	This Study
N6301	*mat A his-3*$^{-}$ *lsd1-HA::hph*	This Study
N6307	*mat A his-3*$^{-}$ *lsd1-3xFLAG::hph*	This Study
N6308	*mat a his-3*$^{-}$*; phf1-3xFLAG::hph*	This Study
N6309	*mat A his-3*$^{-}$*; phf1-3xFLAG::hph*	This Study
N6310	*mat a his-3*$^{-}$*; bdp-1-3xFLAG::hph*	This Study
N6313	*mat A his-3*$^{-}$*; phf1-3xFLAG::hph*	This Study
N6314	*mat a his-3*$^{-}$*; phf1-3xFLAG::hph*	This Study
N6337	*mat a Δlsd1::hph; Δdim-2::hph*	This Study
N6395	*mat A his-3*$^{-}$*; lsd1-HA::hph; phf1-3xFLAG::hph*	This Study
N6396	*mat A his-3*$^{-}$ *lsd1-HA::hph; bdp-1-3xFLAG::hph*	This Study
N6411	*mat A his-3*$^{-}$ *Δlsd1::nat-1*	This Study
N6412	*mat a his-3*$^{-}$ *Δlsd1::nat-1*	This Study
N6414	*mat a his-3*$^{-}$*; Δphf1::nat-1*	This Study
N6416	*mat a his-3*$^{-}$*; Δbdp-1::nat-1*	This Study
N6679	*mat a his-3::dim-2*^{C926A} *Δlsd1::nat-1; Δdim-*	This Study

	2::hph	
N7899	*his-3⁻ lsd1^{NK972,973AA}-3xFLAG::nat-1*	This Study
N7943	*his-3⁻ lsd1^{NK972,973AA}-3xFLAG::nat-1*	This Study
N7944	*his-3⁻ lsd1^{NK972,973AA}-3xFLAG::nat-1*	This Study
N7945	*his-3⁻ lsd1^{NK972,973AA}-3xFLAG::nat-1*	This Study
N7946	*his-3⁻ lsd1^{NK972,973AA}-3xFLAG::nat-1*	This Study
N7977	*mat a Δlsd1::hph*	This Study
N7978	*mat a Δlsd1::hph*	This Study
N7979	*mat ? Δlsd1::hph*	This Study
N7980	*mat a Δlsd1::hph*	This Study
N7981	*mat a Δlsd1::hph*	This Study
N7982	*mat a Δlsd1::hph*	This Study
N7983	*mat ? Δlsd1::hph*	This Study
N7984	*mat a Δlsd1::hph*	This Study
N7985	*mat a Δlsd1::hph*	This Study
N8040	*his-3⁻? lsd1-3xFLAG::hph*	This Study
N8041	*his-3⁻? lsd1-3xFLAG::hph*	This Study
N8042	*his-3⁻? lsd1-3xFLAG::hph*	This Study
N8043	*his-3⁻? lsd1-3xFLAG::hph*	This Study
N8044	*his-3⁻? lsd1-3xFLAG::hph*	This Study
N8045	*his-3⁻? lsd1-3xFLAG::hph*	This Study
N8046	*his-3⁻? lsd1-3xFLAG::hph*	This Study
N8047	*his-3⁻? lsd1-3xFLAG::hph*	This Study
N8048	*his-3⁻? lsd1-3xFLAG::hph*	This Study
N8049	*his-3⁻? lsd1-3xFLAG::hph*	This Study
N8050	*his-3⁻? lsd1-3xFLAG::hph*	This Study
N8051	*his-3⁻? lsd1-3xFLAG::hph*	This Study
N8052	*his-3⁻? lsd1-3xFLAG::hph*	This Study
N8053	*his-3⁻? lsd1-3xFLAG::hph*	This Study
N8054	*his-3⁻? lsd1-3xFLAG::hph*	This Study
N8055	*his-3⁻? lsd1-3xFLAG::hph*	This Study
N8056	*his-3⁻? lsd1-3xFLAG::hph*	This Study
N8057	*his-3⁻? lsd1-3xFLAG::hph*	This Study
N8058	*his-3⁻? lsd1-3xFLAG::hph*	This Study
N8059	*his-3⁻? lsd1-3xFLAG::hph*	This Study
N8060	*his-3⁻? lsd1-3xFLAG::hph*	This Study
N8061	*his-3⁻? lsd1-3xFLAG::hph*	This Study
N8062	*his-3⁻? lsd1-3xFLAG::hph*	This Study
N8063	*his-3⁻? lsd1-3xFLAG::hph*	This Study
N8064	*his-3⁻? lsd1-3xFLAG::hph*	This Study
N8065	*his-3⁻? lsd1-3xFLAG::hph*	This Study
N8066	*his-3⁻? lsd1-3xFLAG::hph*	This Study
N8067	*his-3⁻? lsd1-3xFLAG::hph*	This Study
N8068	*his-3⁻? lsd1-3xFLAG::hph*	This Study
N8081	*Δlsd1::hph; Δdim-2::hph*	This Study

N8082	Δ*lsd1::hph; Δdim-2::hph*	This Study
N8083	*his-3::dim-2*^{C926A} *Δlsd1::nat-1; Δdim-2::hph*	This Study
N8084	*his-3::dim-2*^{C926A} *Δlsd1::nat-1; Δdim-2::hph*	This Study
N8089	*his-3::Phda-1::hda-1D263N-3xFLAG Δlsd1::nat-1; Δhda-1::hph*	This Study
N8090	*his-3::Phda-1::hda-1D263N-3xFLAG Δlsd1::nat-1; Δhda-1::hph*	This Study
N8105	*mat ? Δlsd1::hph; Δbdp-1::hph*	This Study
N8106	*mat ? Δlsd1::hph; Δbdp-1::hph*	This Study
N8107	*mat ? Δlsd1::hph; Δbdp-1::hph*	This Study
N8108	*mat ? Δlsd1::hph; Δbdp-1::hph*	This Study
N8109	*mat ? Δlsd1::hph; Δphf1::hph*	This Study
N8110	*mat ? Δlsd1::hph; Δphf1::hph*	This Study
N8111	*mat ? Δlsd1::hph; Δphf1::hph*	This Study
N8112	*mat ? Δlsd1::hph; Δphf1::hph*	This Study

Chapter III

Strain	Genotype	Source
N2930	*mat A his-3⁻; Δmus-52::bar⁺*	Honda et al., 2008
N3012	*mat a his-3⁻; Δmus-52::bar⁺*	FGSC#9539
N3435	*mat A his-3⁻; Δhda-1::hph⁺*	Honda et al., 2016
N3752	*mat A*	FGSC#2489
N5948	*mat A Δset-7::bar⁺; Δhpo::hph⁺*	Jamieson et al., 2016
N6049	(*mat A his-3⁻; Δmus-52::bar⁺ + P_{vvd}::hH3-3xFLAG::his-3⁺*)	This study
N6054	(*mat a his-3⁻; Δmus-52::bar⁺ + P_{vvd}::hH3-3xFLAG::his-3⁺*)	This study
N6336	*mat A his-3⁻ Δlsd1::hph⁺; Δdim-2::hph⁺*	This study
N6338	*mat A Δlsd1::hph⁺; Δdim-5::bar⁺*	This study
N6340	*mat a Δlsd1::hph⁺; Tel IIIL::nat-1?; Δhpo::hph⁺*	This study
N6684	*mat a P_{vvd}::hH3-3xFLAG::his-3⁺; Δdim-2::hph⁺*	This study
N6685	*mat ? P_{vvd}::hH3-3xFLAG::his-3⁺; Δdim-5::bar⁺*	This study
N6687	*mat a P_{vvd}::hH3-3xFLAG::his-3⁺*	This study
N6690	*mat ? P_{vvd}::hH3-3xFLAG::his-3⁺; Δhpo::hph⁺*	This study
N6732	*mat a P_{vvd}::hH3-3xFLAG::his-3⁺; Δhda-1::hph⁺*	This study

Chapter IV

Strains	Genotype	Source
N3752	*mat a*	FGSC#2489
N4718	Δ*set-7::hph mat a*	Jaimeson et al., 2013
N4719	*mat A*; Δ*eed::hph*	Jaimeson et al., 2013
N4720	*mat a*; Δ*suz12::hph*	Jaimeson et al., 2013
N5761	*mat a*; Δ*set-2::hph*	FGSC#15504
N6157	*mat a*; Δ*tah-2::hph*	This Study
N6171	*mat a*; Δ*crf4-1::hph*	This Study
N6172	*mat a*; Δ*crf6-1::hph*	FGSC#14805
N6267	Δ*set-7::hph mat A ash1*^{Y888F}*-3xFLAG::hph*; Δ*set-2::nat-1*	Bicocca et al., 2019
N6334	Δ*set-7::bar mat?*; Δ*set-2::hph*	This Study
N6553	*mat a*; Δ*mus52::bar*; Δ*crf4-1::hph*	This Study
N6764	*mat a*; Δ*set-2::nat-1*; Δ*crf4-1::hph*; Δ*mus52::bar?*	This Study
N6875	*mat a*; *ash1*^{Y888F}*-3xFLAG::nat-1*	This Study
N8181	(*mat a*; Δ*mus52::bar* + *kyn-1-3xFLAG::nat-1*)	This Study
N8182	(*mat a*; Δ*mus52::bar* + *kyn-1-3xFLAG::nat-1*)	This Study
N8183	(*mat a*; Δ*mus52::bar* + *iad-1-3xFLAG::nat-1*)	This Study
N8184	(*mat a*; Δ*mus52::bar* + *iad-1-3xFLAG::nat-1*)	This Study

APPENDIX D

PRIMER TABLES

Chapter II

Primer	Sequence
For 3xFLAG-tagging LSD1	
LSD1 KI FP1	5'-TAGCTCTTATGGCTGGCGAC-3'
LSD1 KI RP2	5'-CCGCCTCCGCCTCCGCCGCCTCCGCCCCCAGTCATCGCAACATCA-3'
LSD1 KI FP3	5'-TATACGAAGTTATGGATCCGAGCTCGAGGTTAAGACGTTATCAAG-3'
LSD1 KI RP4	5'-TTGTTTGGGGCGCTTGATGG-3'
For 3xFLAG-tagging PHF1	
NCU07297(Phf1) KI FP1	5'-GTCACAGACGGAAACGCATC-3'
NCU07297(Phf1) KI RP2	5'-TCCGCCTCCGCCTCCGCCGCCTCCGCCTACCCTCAAGCCATTCTC-3'
NCU07297(Phf1) KI FP3	5'-CTATACGAAGTTATGGATCCGAGCTCGGAAGACTTTGAGCGTGTC-3'
NCU07297(Phf1) KI RP4	5'-ACCTAGTACTGGCATTTATC-3'
For 3xFLAG-tagging BDP-1	
Bdf1(NCU08809) KI FP1	5'-CGACTACGAGGTTCTCATCG-3'
Bdf1(NCU08809) KI RP2	5'-TCCGCCTCCGCCTCCGCCGCCTCCGCCGTTAGATCCCTCTTGGCC-3'
Bdf1(NCU08809) KI FP3	5'-CTATACGAAGTTATGGATCCGAGCTCGCGCTCTGTCCAAATGGAC-3'
Bdf1(NCU08809) KI RP4	5'-GTTGCAGTGCTATTCCATCG-3'
For Δlsd1::nat-1 KO	
6696	5'-TGGGGCAACGGGAACGAAGA-3'
6697	5'-GCTCCAGCCAAGCCCAAAAAACGTGAGGCGCAGAGAGAGG-3'
6698	5'-TGAGCATGCCCTGCCCCTGAGCATAGATGCAAACGTCGCC-3'
6699	5'-CCAAGAACGCCGGCGAGATG-3'
For Δphf1::nat-1 KO	
5284	5'-GGCCGCGATCGAGAATGGGA-3'
6694	5'-GCTCCAGCCAAGCCCAAAAAGCGACAGCATTGACCACGTG-3'
6695	5'-TGAGCATGCCCTGCCCCTGAGGCTCCCTCCTCCTCTCTCC-3'
5285	5'-CTGGGCTCTCTGCGAGGGTC-3'
For Δbdp-1::nat-1 KO	

6700	5'-CGGAGTTGTGCGGTGATGGC-3'
6701	5'-GCTCCAGCCAAGCCCAAAAAAAGCTCCCGCAGAACCAAGC-3'
6702	5'-TGAGCATGCCCTGCCCCTGACGTGCGATGCTAAGCCTCCA-3'
5289	5'-CGCCGTCCAGCAAACGTTCA-3'
4883	5'-AACCCCATCCGCCGGTACGCG-3'
4884	5'-TCCTTCACCACCGACACCGTCTTCC-3'
For catalytic-null LSD1-3xFLAG	
6716	5’-GCCACGCCCAAGTAACAACG-3’
6717	5’-TGACGGCCGCGAGAACACCAAAGCCTATACGTTCG-3’
6718	5’-TCTCGCGGCCGTCATCCTCGTGTACAAGGAGGCAT-3’
6720	5’-CCTCCGCCTCCGCCTCCGCCGCCTCC GCCCCCAGTCATCGCAACATCAA-3’
6721	5’-GAGCTCGGTACCAAGCTTGATGCATAGC GGTTAAGACGTTATCAAGTAAGTGAG-3’
6722	5’-AAATAAAAGCCGCAGACGGG-3’
Southern Hybridization Probes	
Tel VIIL (2391bp)	
5272	5'-GGCATCCGTGGGTGTCCCAG-3'
5273	5'-TTCCCGTCCCTACCAGGCAT-3'
NCU02455 (910bp)	
5440	5'-GCTGCCAGGTGTCCAACTAC-3'
5442	5'-CAGCTCATTGTGCTCCTGGA-3'
NCU10040 (1071bp)	
5446	5'-TCCGCCTTCAACTCTTCCGC-3'
5448	5'-GCCAGCGTGTGACGGTCATC-3'
NCU04942 (1056bp)	
5449	5'-CCTGTGGCGGTTAGCGACAA-3'
5451	5'-TGACACCAGCGCTGTCACCG-3'
NCU05569 (1172bp)	
6692	5'-ACCAGTGTCGTCCAACCCAG-3'
6693	5'-GGTGGTCTTGGTCGAGGCCT-3'
his-3 (2631bp)	
1665	5'-GACGGGGTAGCTTGGCCCTAATTAACC-3'
3128	5'-CGATTTAGGTGACACTATAG-3'
8:A6 (605bp)	
1877	5’-TGGTTGGTCGATTGTGGTGG-3'
1878	5’-TTTTGAGGATCCGCCATCCG-3'
actin (717bp)	
3211	5'-CACGGTGTCGTTACCAACTG-3'
3212	5'-GTCGGAGAGACCAGGGTACA-3'
pan-1 (1007bp)	

3181	5’-CGATAAGCTTGATATCGAATTCAGGTT GTCCGGCCATCTCAGTCTGATCC-3’
3182	5’-TCGCATACGCCAACCCATGC-3’
qPCR	
ChIP-qPCR	
hH4 (102bp)	
4082	5'-CATCAAGGGGTCATTCAC-3'
4083	5'-TTTGGAATCACCCTCCAG-3'
Cen IIIL (169bp)	
5250	5'-CGACTATCCGAACCGGAAGGAG-3'
5251	5'-CCGAATCCGGCTCAGTACAGC-3'
8:A6 (302bp)	
1823	5'-GGATGGCGGATCCTCAAAAATA-3'
1824	5'-TAACCGCCGCTTTTTAAAATTAGGA-3'
NCU02455 (158bp)	
5440	5'-GCTGCCAGGTGTCCAACTAC-3'
5441	5'-GAGGCTAGTAGCGACAGCGA-3'
Tel VIIL (208bp)	
5272	5'-TTCCCGTCCCTACCAGGCAT-3'
5273	5’-GAGCGGAGGTGGACTTTGCG-3'
RT-qPCR	
NCU02840 (104bp)	
6271	5'-CCCTCTCAGACGAGGATATTCA-3'
6272	5'-GCTCTGCTGCTTCTCCTTTAT-3'
NCU00911 (207bp)	
6636	5'-GACAACAAAGGCCAAGGACG-3'
6637	5'-ACCTGGATCCAGTATGAGCC-3'
NCU02455 (228bp)	
6638	5'-TTGATAACCTGACCACCGCC-3'
6639	5'-TTTCCTGTCGCTGTCGCTAC-3'
NCU06512 (219bp)	
6640	5'-GAGGGGATGATGTCGACACC-3'
6641	5'-CCCCCCTAATCTCCGTTTGT-3'
NCU02437 (196bp)	
6642	5'-AGGAGACGATGGACACGACC-3'
6643	5'-TACGTCAACCGAAACGACGC-3'
Yeast two-hybrid	
PHF1 constructs	
418 MfeI-Phf1(NCU07297) 2aa FP	5'-ATCCAATTGGCAGACCAGACACCAAACGT-3'
419	5'-CGGGATCCTATACCCTCAAGCCATTCT-3'

Phf1(NCU07297) 605aa BamHI RP	
513 Phf1(NCU07297) 353aa BamHI RP	5'-CGGGATCCTAGGCTTGCTCGGCTGTGCGCT-3'
610 MfeI-Phf1(NCU07297) 117aa FP	5'-ATCCAATTGCCCCTGGTCCAGCCGAGCAT-3'
611 Phf1(NCU07297) 275aa BamHI RP	5'-CGGGATCCTATTCGTCCGCGTCTTGTTGTT-3'
612 EcoRI-Phf1(NCU07297) 312aa FP	5'-CGAATTCACCAAATCCGGCCGTCAAGT-3'
695 EcoRI-Phf1(NCU07297) 401aa FP	5'-CGAATTCGTATGTTCGCTGTGTGTGGC-3'
696 Phf1(NCU07932) 540aa BamHI RP	5'-CGGGATCCTAGCCTTGGTTCTCTTGGCTCG-3'
710 Phf1140aa BamHI RP	5'-CGGGATCCTACAAAGAAAGGTTCTTCTTGA-3'
711 EcoRI-Phf1 401aa FP	5'-CGAATTCGTATGTTCGCTGTGTGTGGC-3'
BDP-1 constructs	
420 MfeI-Bdp1(NCU08809) 2aa FP	5'-ATCCAATTGGACATGAGTGCCTCGCCTAC-3'
421 Bdp1(NCU08809) 478aa BamHI RP	5'-CGGGATCCTAGTTAGATCCCTCTTGGC-3'
514 MfeI-Bdp1(NCU08809) 198aa FP	5'-ATCCAATTGGAGTACCGCCGAATCACAAA-3'
515 Bdp1(NCU08809) 236aa BanHI RP	5'-CGGGATCCTAGTAATCGGCCGCCCAGGAAA-3'
615 Bdp1(NCU08809) 361aa BamHI RP	5'-CGGGATCCTACAGTTTCTTGGAGGTGGTAA-3'
691 EcoRI-Bdp1(NCU08809) 45aa FP	5'-CGAATTCAACGAGACACACGATGACCA-3'
707 EcoRI-Bdp1 45aa FP	5'-CGAATTCAACGAGACACACGATGACCA-3'
708 Bdp1 236aa BamHI RP	5'-CGGGATCCTAGTAATCGGCCGCCCAGGAAA-3'

Chapter III

Primer	Sequence
For building P_{vvd}::3xFLAG *tagging vector*	
VVD-3000F_EcoRI\NotI	5'-GGCTAGAATTCGCGGCCGCTTATTCACGCCAGCACTGTGATTC-3'
VVD-R1_XbaI	5'-GGCTAGTCTAGAGGTGCTGGTTATGAGACAGTGTG-3'
qPCR	
Actin (146bp)	
3210	5'-CTTCTGGCCCATACCGATCAT-3'
3216	5'-ATGTCGCGATAGCTTCCATC-3'
fkr-5 (158bp)	
5440	5'-GCTGCCAGGTGTCCAACTAC-3'
5441	5'-GAGGCTAGTAGCGACAGCGA-3'
csr-1 (101bp)	
5351	5'-TTTGGTCCCTACCCCAGACA-3'
5352	5'-CCATTGACGACATTGCGGAG-3'
Cen IIIL (169bp)	
5250	5'-CGACTATCCGAACCGGAAGGAG-3'
5251	5'-CCGAATCCGGCTCAGTACAGC-3'
8:A6 (302bp)	
1823	5'-GGATGGCGGATCCTCAAAAATA-3'
1824	5'-TAACCGCCGCTTTTTAAAATTAGGA-3'
8:F10 (316bp)	
1827	5'-GTAACGCAAATTCTAAAATTGCAATAC-3'
1828	5'-CTTAGTAATTAATTTAATACGTGCGCC-3'
Tel VIIL (208bp)	
5272	5'-TTCCCGTCCCTACCAGGCAT-3'
5273	5'-GAGCGGAGGTGGACTTTGCG-3'

Chapter IV

Primer	Sequence
For 3xFLAG-tagging KYN-1	
pWS185	5'-GCGGACCCTTCCGAAGTGGT-3'
pWS186	5'-CCTCCGCCTCCGCCTCCGCCGCCTCCGCCACCCCTGATAGCCGCCTC-3'
pWS187	5'-GAGCTCGGTACCAAGCTTGATGCATAGCCACGGGTCGTAGCACGTGGG-3'
pWS188	5'-CACCATCACGCACACCACAC-3'
For 3xFLAG-tagging IAD-1	
pWS189	*5'-GCCCAAGGGGCATACATCAT-3'*
pWS190	*5'-CCTCCGCCTCCGCCTCCGCCGCCTCCGCCCCTTCCAACTTCCCCCGCCT-3'*
pWS191	*5'-GAGCTCGGTACCAAGCTTGATGCATAGCGTTGGGGTGCTGGGAGGGAA-3'*
pWS192	*5'-GAGGGAGACGAGGAGCGTAG-3'*
ChIP-qPCR	
kyn-1 #1 (148bp)	
4838	5'-GTACCTCAACGGTGGTCCTG-3'
4839	5'-GTCCATATTGAACCGCACGC-3'
kyn-1 #2 (182bp)	
4840	5'-TCCTCACTTTCCAACTCGCC-3'
4841	5'-ATCTTGTGTCGCTTGTCGGT-3'
promoter (158bp)	
4842	5'-TTCACCATCCGTCGTTTCGT-3'
4843	5'-ACCGACAGATCGAATGACCG-3'
iad-1 (180bp)	
4844	5'-AATGTACGGCTGCTGTGTCA-3'
4845	5'-AGACGGTACGTGTTGGAACC-3'

REFERENCES CITED

1. Allshire, R. C. & Madhani, H. D. Ten principles of heterochromatin formation and function. *Nat. Rev. Mol. Cell Biol.* **19**, 229–244 (2018).

2. Sharma, S., Kelly, T. K. & Jones, P. A. Epigenetics in cancer. *Carcinogenesis* **31**, 27–36 (2009).

3. Aramayo, R. & Selker, E. U. *Neurospora crassa*, a model system for epigenetics research. *Cold Spring Harb. Perspect. Biol.* **5**, a017921–a017921 (2013).

4. Jamieson, K., Rountree, M. R., Lewis, Z. A., Stajich, J. E. & Selker, E. U. Regional control of histone H3 lysine 27 methylation in Neurospora. *Proc. Natl. Acad. Sci.* **110**, 6027–6032 (2013).

5. Tamaru, H. *et al.* Trimethylated lysine 9 of histone H3 is a mark for DNA methylation in *Neurospora crassa*. *Nat. Genet.* **34**, 75–9 (2003).

6. Dodge, J. E., Kang, Y.-K., Beppu, H., Lei, H. & Li, E. Histone H3-K9 Methyltransferase ESET Is Essential for Early Development. *Mol. Cell. Biol.* **24**, 2478–2486 (2004).

7. Okano, M., Bell, D. W., Haber, D. A. & Li, E. DNA methyltransferases Dnmt3a and Dnmt3b are essential for de novo methylation and mammalian development. *Cell* **99**, 247–257 (1999).

8. Peters, A. H. F. M. *et al.* Loss of the Suv39h histone methyltransferases impairs mammalian heterochromatin and genome stability. **107**, 323–337 (2001).

9. Ronemus, M. J., Galbiati, M., Ticknor, C., Chen, J. & Dellaporta, S. L. Demethylation-induced developmental pleiotropy in Arabidopsis. *Science* (1996). doi:10.1126/science.273.5275.654

10. Tachibana, M. *et al.* G9a histone methyltransferase plays a dominant role in euchromatic histone H3 lysine 9 methylation and is essential for early embryogenesis. *Genes Dev.* **16**, 1779–1791 (2002).

11. Zhang, K., Mosch, K., Fischle, W. & Grewal, S. I. S. Roles of the Clr4 methyltransferase complex in nucleation, spreading and maintenance of heterochromatin. *Nat. Struct. Mol. Biol.* **15**, 381–388 (2008).

12. Al-Sady, B., Madhani, H. D. & Narlikar, G. J. Division of labor between the chromodomains of HP1 and Suv39 methylase enables coordination of heterochromatin spread. *Mol. Cell* **51**, 80–91 (2013).

13. Coveney, J. & Woodland, H. R. The DNase I sensitivity of *Xenopus laevis* genes transcribed by RNA polymerase III. *Nature* **298**, 578–580 (1982).

14. DeLotto, R. & Schedl, P. Internal promoter elements of transfer RNA genes are preferentially exposed in chromatin. *J. Mol. Biol.* **179**, 607–628 (1984).

15. Aygün, O., Mehta, S. & Grewal, S. I. S. HDAC-mediated suppression of histone turnover promotes epigenetic stability of heterochromatin. *Nat. Struct. Mol. Biol.* **20**, 547–54 (2013).

16. Scott, K. C., Merrett, S. L. & Willard, H. F. A heterochromatin barrier partitions the fission yeast centromere into discrete chromatin domains. *Curr. Biol.* **16**, 119–129 (2006).

17. Raab, J. R. *et al.* Human tRNA genes function as chromatin insulators. *EMBO J.* **31**, 330–350 (2012).

18. Ayoub, N. *et al.* A novel jmjC domain protein modulates heterochromatization in fission yeast. *Mol. Cell. Biol.* **23**, 4356–4370 (2003).

19. Honda, S. *et al.* The DMM complex prevents spreading of DNA methylation from transposons to nearby genes in *Neurospora crassa*. *Genes Dev.* 443–454 (2010). doi:10.1101/gad.1893210.populations

20. Metzger, E. *et al.* LSD1 demethylates repressive histone marks to promote androgen-receptor-dependent transcription. *Nature* **437**, 436–439 (2005).

21. Lan, F. *et al. S. pombe* LSD1 homologs regulate heterochromatin propagation and euchromatic gene transcription. *Mol. Cell* **26**, 89–101 (2007).

22. Rudolph, T. *et al.* Heterochromatin formation in Drosophila is initiated through active removal of H3K4 methylation by the LSD1 homolog SU(VAR)3-3. *Mol. Cell* **26**, 103–115 (2007).

23. Laurent, B. *et al.* A specific LSD1/KDM1A isoform regulates neuronal differentiation through H3K9 demethylation. *Mol. Cell* **57**, 957–970 (2015).

24. Shi, Y. *et al.* Histone demethylation mediated by the nuclear amine oxidase homolog LSD1. *Cell* **119**, 941–953 (2004).

25. Wissmann, M. *et al.* Cooperative demethylation by JMJD2C and LSD1 promotes androgen receptor-dependent gene expression. *Nat. Cell Biol.* **9**, 347–353 (2007).

26. Wang, J. *et al.* The lysine demethylase LSD1 (KDM1) is required for maintenance of global DNA methylation. *Nat. Genet.* **41**, 125–9 (2009).

27. Honda, S. & Selker, E. U. Direct interaction between DNA methyltransferase DIM-2 and HP1 is required for DNA methylation in *Neurospora crassa*. *Mol. Cell. Biol.* **28**, 6044–55 (2008).

28. Lewis, Z. A. *et al.* Relics of repeat-induced point mutation direct heterochromatin formation in *Neurospora crassa*. *Genome Res.* **19**, 427–437 (2008).

29. Colot, H. V. *et al.* A high-throughput gene knockout procedure for Neurospora reveals functions for multiple transcription factors. *Proc. Natl. Acad. Sci. U. S. A.* **103**, 10352–7 (2006).

30. McCluskey, K., Wiest, A. & Plamann, M. The fungal genetics stock center: A repository for 50 years of fungal genetics research. *Journal of Biosciences* **35**, 119–126 (2010).

31. Ebbole, D. & Sachs, M. S. A rapid and simple method for isolation of *Neurospora crassa* homokaryons using microconidia. *Fungal Genet. Rep.* **37**, (1990).

32. Kouzminova, E. & Selker, E. U. Dim-2 encodes a DNA methyltransferase responsible for all known cytosine methylation in Neurospora. *EMBO J.* **20**, 4309–4323 (2001).

33. Dang, Y., Li, L., Guo, W., Xue, Z. & Liu, Y. Convergent transcription induces dynamic DNA methylation at disiRNA loci. *PLoS Genet.* **9**, e1003761 (2013).

34. Lee, M. G., Wynder, C., Cooch, N. & Shiekhattar, R. An essential role for CoREST in nucleosomal histone 3 lysine 4 demethylation. *Nature* **437**, 432–435 (2005).

35. Jamieson, K. *et al.* Loss of HP1 causes depletion of H3K27me3 from facultative heterochromatin and gain of H3K27me2 at constitutive heterochromatin. *Genome Res.* **26**, 97–107 (2016).

36. Rusche, L. N., Kirchmaier, A. L. & Rine, J. The establishment, inheritance, and function of silenced chromatin in *Saccharomyces cerevisiae*. *Annu. Rev. Biochem.* **72**, 481–516 (2003).

37. Jih, G. *et al.* Unique roles for histone H3K9me states in RNAi and heritable silencing of transcription. *Nature* **547**, 1–26 (2017).

38. Irelan, J. T. & Selker, E. U. Cytosine methylation associated with repeat-induced point mutation causes epigenetic gene silencing in *Neurospora crassa*. *Genetics* **146**, 509–523 (1997).

39. Rountree, M. R. & Selker, E. U. DNA methylation inhibits elongation but not initiation of transcription in *Neurospora crassa*. *Genes Dev.* **11**, 2383–2395 (1997).

40. Honda, S. *et al.* Heterochromatin protein 1 forms distinct complexes to direct histone deacetylation and DNA methylation. *Nat. Struct. Mol. Biol.* **19**, 471–7, S1 (2012).

41. Honda, S. *et al.* Dual chromatin recognition by the histone deacetylase complex HCHC is required for proper DNA methylation in *Neurospora crassa*. *Proc. Natl. Acad. Sci.* 201621475 (2016). doi:10.1073/pnas.1621475114

42. Yamada, T., Fischle, W., Sugiyama, T., Allis, C. D. & Grewal, S. I. S. The nucleation and maintenance of heterochromatin by a histone deacetylase in fission yeast. *Mol. Cell* **20**, 173–85 (2005).

43. Fischer, T. *et al.* Diverse roles of HP1 proteins in heterochromatin assembly and functions in fission yeast. *Proc. Natl. Acad. Sci. U. S. A.* **106**, 8998–9003 (2009).

44. Gessaman, J. D. & Selker, E. U. Induction of H3K9me3 and DNA methylation by tethered heterochromatin factors in *Neurospora crassa*. *Proc. Natl. Acad. Sci.* 201715049 (2017). doi:10.1073/pnas.1715049114

45. Lewis, Z. A., Adhvaryu, K. K., Honda, S., Shiver, A. L. & Selker, E. U. Identification of DIM-7, a protein required to target the DIM-5 H3 methyltransferase to chromatin. *Proc. Natl. Acad. Sci. U. S. A.* **107**, 8310–5 (2010).

46. Lewis, Z. A. *et al.* DNA methylation and normal chromosome behavior in Neurospora depend on five components of a histone methyltransferase complex, DCDC. *PLoS Genet.* **6**, e1001196 (2010).

47. Zhang, X. *et al.* Structure of the Neurospora SET domain protein DIM-5, a histone H3 lysine methyltransferase. *Cell* **111**, 117–127 (2002).

48. Klose, R. J., Kallin, E. M. & Zhang, Y. JmjC-domain-containing proteins and histone demethylation. *Nat. Rev. Genet.* **7**, 715–727 (2006).

49. Yun, M., Wu, J., Workman, J. L. & Li, B. Readers of histone modifications. *Cell Res.* **21**, 564–578 (2011).

50. Qian, C. *et al.* Structure and chromosomal DNA binding of the SWIRM domain. *Nat. Struct. Mol. Biol.* **12**, 1078–1085 (2005).

51. Pinheiro, I. *et al.* Prdm3 and Prdm16 are H3K9me1 methyltransferases required for mammalian heterochromatin integrity. *Cell* **150**, 948–960 (2012).

52. Galazka, J. M. *et al.* Neurospora chromosomes are organized by blocks of importin alpha-dependent heterochromatin that are largely independent of H3K9me3. *Genome Res.* **26**, 1069–1080 (2016).

53. Schultz, J. Variegation in Drosophila and the inert chromosome regions. *Proc. Natl. Acad. Sci.* **22**, 27–33 (1936).

54. Dimitri, P. & Pisano, C. Position effect variegation in *Drosophila melanogaster*: relationship between suppression effect and the amount of Y chromosome. *Genetics* (1989).

55. Tamaru, H. & Selker, E. U. A histone H3 methyltransferase controls DNA methylation in *Neurospora crassa*. *Nature* **414**, 277–283 (2001).

56. Davis, R. *Neurospora: Contributions of a Model Organism*. (Oxford Univ. Press, 2000).

57. Davis, R. H. & de Serres, F. J. Genetic and microbiological research techniques for *Neurospora crassa*. in *Methods in Enzymology* **17**, 79–143 (1970).

58. Honda, S. & Selker, E. U. Tools for fungal proteomics: multifunctional Neurospora vectors for gene replacement, protein expression and protein purification. *Genetics* **182**, 11–23 (2009).

59. Klocko, A. D. *et al.* Neurospora Importin α is required for normal heterochromatic formation and DNA Methylation. *PLoS Genet.* **11**, 1–24 (2015).

60. Afgan, E. *et al.* The Galaxy platform for accessible, reproducible and collaborative biomedical analyses: 2016 update. *Nucleic Acids Res.* **44**, W3–W10 (2016).

61. Langmead, B. & Salzberg, S. L. Fast gapped-read alignment with Bowtie 2. *Nat. Methods* **9**, 357–359 (2012).

62. Ramírez, F. *et al.* deepTools2: a next generation web server for deep-sequencing data analysis. *Nucleic Acids Res.* **44**, W160–W165 (2016).

63. Thorvaldsdóttir, H., Robinson, J. T. & Mesirov, J. P. Integrative Genomics Viewer (IGV): High-performance genomics data visualization and exploration. *Brief. Bioinform.* **14**, 178–192 (2013).

64. Song, Q. *et al.* A reference methylome database and analysis pipeline to facilitate integrative and comparative epigenomics. *PLoS One* **8**, (2013).

65. Bicocca, V. T., Ormsby, T., Adhvaryu, K. K., Honda, S. & Selker, E. U. ASH1-catalyzed H3K36 methylation drives gene repression and marks H3K27me2/3-competent chromatin. *Elife* **7**, 1–19 (2018).

66. Hurley, J. H. *et al.* A tool set for the genome-wide analysis of *Neurospora crassa* by RT-PCR. *G3 (Bethesda)*. **5**, 2043–9 (2015).

67. Vogel, M. J., Peric-Hupkes, D. & van Steensel, B. Detection of in vivo protein-DNA interactions using DamID in mammalian cells. *Nat. Protoc.* **2**, 1467–78 (2007).

68. Venkatesh, S. & Workman, J. L. Histone exchange, chromatin structure and the regulation of transcription. *Nat. Rev. Mol. Cell Biol.* **16**, 178–189 (2015).

69. Choi, E. S., Shin, J. A., Kim, H. S. & Jang, Y. K. Dynamic regulation of replication independent deposition of histone H3 in fission yeast. *Nucleic Acids Res.* **33**, 7102–7110 (2005).

70. Rufiange, A., Jacques, P. É., Bhat, W., Robert, F. & Nourani, A. Genome-wide replication-independent histone H3 exchange occurs predominantly at promoters and implicates H3 K56 Acetylation and Asf1. *Mol. Cell* **27**, 393–405 (2007).

71. Dion, M. F. *et al.* Dynamics of replication-independent histone turnover in budding yeast. *Science (80-.).* **315**, 1405–1408 (2007).

72. Kraushaar, D. C. *et al.* Genome-wide incorporation dynamics reveal distinct categories of turnover for the histone variant H3.3. *Genome Biol.* **14**, (2013).

73. Ahmad, K. & Henikoff, S. The histone variant H3.3 marks active chromatin by replication-independent nucleosome assembly. *Mol. Cell* **9**, 1191–1200 (2002).

74. Chen, C. H. & Loros, J. J. Neurospora sees the light: Light signaling components in a model system. *Commun. Integr. Biol.* **2**, 448–451 (2009).

75. Elvin, M., Loros, J. J., Dunlap, J. C. & Heintzen, C. The PAS/LOV protein VIVID supports a rapidly dampened daytime oscillator that facilitates entrainment of the Neurospora circadian clock. *Genes Dev.* **19**, 2593–2605 (2005).

76. Heintzen, C., Loros, J. J. & Dunlap, J. C. The PAS protein VIVID defines a clock-associated feedback loop that represses light input, modulates gating, and regulates clock resetting. *Cell* **104**, 453–464 (2001).

77. Hurley, J. M., Chen, C. H., Loros, J. J. & Dunlap, J. C. Light-inducible system for tunable protein expression in *Neurospora crassa*. *G3 Genes, Genomes, Genet.* **2**, 1207–1212 (2012).

78. Luger, K., Dechassa, M. L. & Tremethick, D. J. New insights into nucleosome and chromatin structure: An ordered state or a disordered affair? *Nat. Rev. Mol. Cell Biol.* **13**, 436–447 (2012).

79. E. Martegani, F. Tome, F. T. Timing of nuclear division cycle in *Neurospora crassa*. *J. Cell Sci.* **136**, 127–136 (1981).

80. Kaplan, T. *et al.* Cell cycle- and chaperone-mediated regulation of H3K56ac incorporation in yeast. *PLoS Genet.* **4**, (2008).

81. Gossett, A. J. & Lieb, J. D. In vivo effects of histone H3 depletion on nucleosome occupancy and position in *Saccharomyces cerevisiae*. *PLoS Genet.* **8**, (2012).

82. Jin, C. *et al.* H3.3/H2A.Z double variant-containing nucleosomes mark 'nucleosome-free regions' of active promoters and other regulatory regions. *Nat. Genet.* **41**, 941–945 (2009).

83. Goldberg, A. D. *et al.* Distinct factors control histone variant H3.3 localization at specific genomic regions. *Cell* **140**, 678–691 (2010).

84. Ooi, S. L., Henikoff, J. G. & Henikoff, S. A native chromatin purification system for epigenomic profiling in *Caenorhabditis elegans*. *Nucleic Acids Res.* **38**, 1–14 (2009).

85. Chow, C. M. *et al.* Variant histone H3.3 marks promoters of transcriptionally active genes during mammalian cell division. *EMBO Rep.* **6**, 354–360 (2005).

86. Mito, Y., Henikoff, J. G. & Henikoff, S. Genome-scale profiling of histone H3.3 replacement patterns. *Nat. Genet.* **37**, 1090–1097 (2005).

87. Deal, R. B., Henikoff, J. G. & Henikoff, S. Genome-wide kinetics of nucleosome turnover determined by metabolic labeling of histones. *Science (80-.).* **328**, 1161–1165 (2010).

88. Shivaswamy, S. *et al.* Dynamic remodeling of individual nucleosomes across a eukaryotic genome in response to transcriptional perturbation. *PLoS Biol.* **6**, 0618–0630 (2008).

89. Albert, I. *et al.* Translational and rotational settings of H2A.Z nucleosomes across the *Saccharomyces cerevisiae* genome. *Nature* **446**, 572–576 (2007).

90. Kaplan, N. *et al.* The DNA-encoded nucleosome organization of a eukaryotic genome. *Nature* **458**, 362–366 (2009).

91. Mavrich, T. N. *et al.* A barrier nucleosome model for statistical positioning of nucleosomes throughout the yeast genome. *Genome Res.* **18**, 1073–1083 (2008).

92. Whitehouse, I., Rando, O. J., Delrow, J. & Tsukiyama, T. Chromatin remodelling at promoters suppresses antisense transcription. *Nature* **450**, 1031–1035 (2007).

93. Yuan, G.-C. *et al.* Genome-scale identification of nucleosome positions in S. cerevisiae. *Science* **309**, 626–30 (2005).

94. Johnson, S. M., Tan, F. J., McCullough, H. L., Riordan, D. P. & Fire, A. Z. Flexibility and constraint in the nucleosome core landscape of *Caenorhabditis elegans* chromatin. *Genome Res.* **16**, 1505–1516 (2006).

95. Valouev, A. *et al.* A high-resolution, nucleosome position map of *C. elegans* reveals a lack of universal sequence-dictated positioning. *Genome Res.* **18**, 1051–1063 (2008).

96. Mavrich, T. N. *et al.* Nucleosome organization in the Drosophila genome. *Nature* **453**, 358–362 (2008).

97. Sasaki, S. *et al.* Chromatin-associated periodicity in genetic variation downstream of transcriptional start sites. *Science (80-.).* **323**, 401–404 (2009).

98. Ozsolak, F., Song, J. S., Liu, X. S. & Fisher, D. E. High-throughput mapping of the chromatin structure of human promoters. *Nat. Biotechnol.* **25**, 244–248 (2007).

99. Schones, D. E. *et al.* Dynamic regulation of nucleosome positioning in the human genome. *Cell* **132**, 887–898 (2008).

100. Freitag, M., Hickey, P. C., Khlafallah, T. K., Read, N. D. & Selker, E. U. HP1 is essential for DNA methylation in *Neurospora*. *Mol. Cell* **13**, 427–34 (2004).

101. Aronson, B. D., Johnson, K. A., Loros, J. J. & Dunlap, J. C. Negative feedback defining a circadian clock: Autoregulation of the clock gene frequency. *Science (80-.).* (1994). doi:10.1126/science.8128244

102. Heinz, S. *et al.* Simple combinations of lineage-determining transcription factors prime cis-regulatory elements required for macrophage and B cell identities. *Mol. Cell* (2010). doi:10.1016/j.molcel.2010.05.004

103. Savitz, J. The kynurenine pathway: a finger in every pie. *Mol. Psychiatry* **25**, 131–147 (2020).

104. Kolodziej, L. R., Paleolog, E. M. & Williams, R. O. Kynurenine metabolism in health and disease. *Amino Acids* **41**, 1173–1183 (2011).

105. Turner, J. R., Sorsoli, W. A. & Matchett, W. H. Induction of kynureninase in *Neurospora*. *J. Bacteriol.* **103**, 364–369 (1970).

106. Schlitt, S; Lester, G; Russell, P. Isolation and characterization of low-kynureninase mutants of *Neurospora crassa*. *J. Bacteriol.* **117**, 1117–1120 (1974).

107. Tanizawa, K. & Soda, K. Comparison of inducible and constitutive kynureninases of *Neurospora crassa*. **85**, 1367–1375 (1979).

108. Gaertner, F. H., Cole, K. W. & Welch, G. R. Evidence for distinct kynureninase and hydroxykynureninase activities in *Neurospora crassa*. *J. Bacteriol.* **108**, 902–909 (1971).

109. Badawy, A. A. B. Kynurenine pathway of tryptophan metabolism: Regulatory and functional aspects. *Int. J. Tryptophan Res.* **10**, (2017).

110. Pomraning, K. R., Smith, K. M. & Freitag, M. Bulk segregant analysis followed by high-throughput sequencing reveals the Neurospora cell cycle gene, ndc-1, to be allelic with the gene for ornithine decarboxylase, spe-1. *Eukaryot. Cell* **10**, 724–733 (2011).

111. Schuettengruber, B., Bourbon, H. M., Di Croce, L. & Cavalli, G. Genome Regulation by Polycomb and Trithorax: 70 Years and Counting. *Cell* **171**, 34–57 (2017).

112. Smolle, M. *et al.* Chromatin remodelers Isw1 and Chd1 maintain chromatin structure during transcription by preventing histone exchange. *Nat. Struct. Mol. Biol.* **19**, 884–892 (2012).

113. Wiles, E. T. *et al.* Evolutionarily ancient BAH-PHD protein mediates Polycomb silencing. *bioRxiv* (2019). doi:10.1101/868117

114. Metzenberg, R. L., Stevens, J. N., Selker, E. U. & Morzycka-Wroblewska, E. Identification and chromosomal distribution of 5S rRNA genes in *Neurospora crassa*. *Proc. Natl. Acad. Sci. U. S. A.* **82**, 2067–2071 (1985).

115. Garrison, E. & Marth, G. Haplotype-based variant detection from short-read sequencing -- Free bayes -- Variant Calling -- Longranger. *arXiv Prepr. arXiv1207.3907* (2012). doi:arXiv:1207.3907 [q-bio.GN]

116. Danecek, P. *et al.* The variant call format and VCFtools. *Bioinformatics* (2011). doi:10.1093/bioinformatics/btr330

117. Freitag, M. Histone Methylation by SET Domain Proteins in Fungi. *Annu. Rev. Microbiol.* **71**, 413–439 (2017).

118. Falnes, P. O., Jakobsson, M. E., Davydova, E., Ho, A. & Ma ecki, J. Protein lysine methylation by seven-ß-strand methyltransferases. *Biochem. J.* **473**, 1995–2009 (2016).

119. Patel, A., Vought, V. E., Dharmarajan, V. & Cosgrove, M. S. A novel non-SET domain multi-subunit methyltransferase required for sequential nucleosomal histone H3 methylation by the mixed lineage leukemia protein-1 (MLL1) core complex. *J. Biol. Chem.* **286**, 3359–3369 (2011).